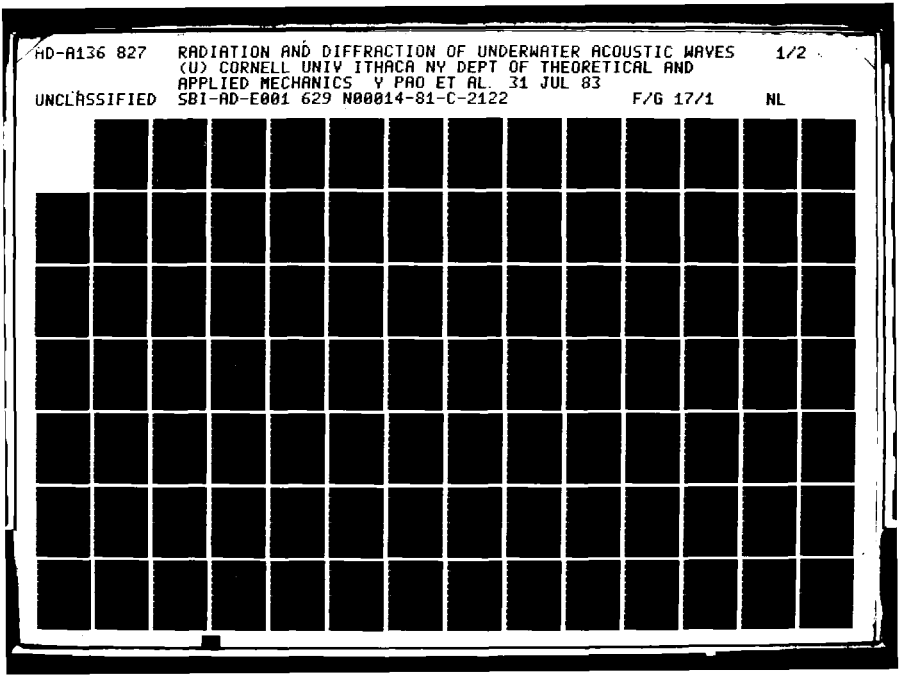
AD-A136 827 RADIATION AND DIFFRACTION OF UNDERWATER ACOUSTIC WAVES 1/2
(U) CORNELL UNIV ITHACA NY DEPT OF THEORETICAL AND
APPLIED MECHANICS Y PAO ET AL. 31 JUL 83
UNCLASSIFIED SBI-AD-E001 629 N00014-81-C-2122 F/G 17/1 NL

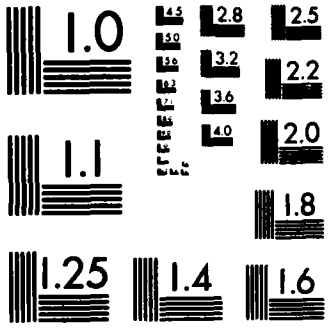

MICROCOPY RESOLUTION TEST CHART
NATIONAL BUREAU OF STANDARDS-1963-A

Final Report*

to

NAVAL RESEARCH LABORATORY

RADIATION AND DIFFRACTION OF UNDERWATER ACOUSTIC WAVES

by

Yih-Hsing Pao
Department of Theoretical and Applied Mechanics
Cornell University, Ithaca, New York 14853

Summary

The above-named project was sponsored by the Naval Research Laboratory for a period of two years, beginning on March 1, 1981, and ending on March 1, 1983, and was subsequently given a without-cost extension to July 31, 1983. The greater part of the research was conducted by Professor Yih-Hsing Pao and Dr. George C.C. Ku of Cornell University.

Research results are shown in the three technical reports included herein, the titles of which are:

1. Acoustic Radiations of a Summerged Cylindrical Shell
2. Acoustic Radiation from a Submerged Finite Circular Cylindrical Shell Driven by a Harmonic Force
3. Attenuation Constants and Phase Velocities of Eighteen Polymeric Materials

Reference should be made to each abstract, which summarizes the results of each investigation.

*NRL Contract No. N00014-81-C-2122

Forward

The project entitled "Radiation and Diffraction of Underwater Acoustic Waves" was proposed by Professor Yih-Hsing Pao of Cornell University in November of 1980 after consultation with Dr. Lawrence Flax of the Naval Research Laboratory. Through the Office of Naval Research, the project was funded, beginning on March 1, 1981, for a two-year period. It was extended (without addition of funds) for seven months, ending on July 31, 1983.

The Statement of Work of the original proposal was revised in the contract, with the following two topics receiving focus:

(1) Radiation of Transient Pulse from an Elastic Body

(2) Generalized Ray and Geometric Theory of Diffraction.

To maintain close collaboration with Naval personnel, Dr. George C.C. Ku of Cornell University was assigned to work at the Physical Acoustics Branch of the Naval Research Laboratory under the supervision of Dr. Flax. Dr. Flax left NRL in July 1981, and the research work has changed to concentrate on the analysis of radiation of a submerged circular cylindrical shell, under the supervision of Dr. L.R. Dragnette who also directed the experimental investigation.

The analysis was based on a mathematical theory closely representing the experimental model, and the objective was to determine the radiation pressure of the acoustic wave field near the shell (one to ten radius from the central axis of the shell), under the excitation of a point force with a harmonic time function. Analysis of the motion of the shell was based on Donnell's equation for circular cylindrical shells, and that of the acoustic radiation was based on the scalar wave equation.

The shell vibration is coupled to the fluid particle motion through the reactive fluid pressure on the surface of the shell.

Both shells of infinite length (neglecting the reflections of waves from both ends of the shell) and finite length have been investigated. The results for an infinite shell are presented in Technical Report No. 1, which is included with this report. The analysis follows the previous work by W. Voger and D. Feit, "Response of Point-Excited Infinitely Long Cylindrical Shell Immersed in Acoustic Medium (NSRDC Report 80-061, 1980). Dertailed angular variations of the radiation pressure near the shell are calculated at several axial locations. These results were compared with experimental measurements which are not included in this report.

Analysis of the radiation for a finite cylindrical shell is discussed in Technical Report No. 2. The problem is far more complicated than that for an infinite shell, and numerical calculations have not yet been completed.

During the second year, in collaboration with other personnel of the Physical Acoustics Branch of NRL, George Ku also worked in another research project on the deformation of optical fibers under the radiation pressure. One phase of the research, the measurement of phase velocities and attenuation constants of eighteen polymeric materials was conducted at the Ultrasonics Laboratory of Cornell University by Mr. C.P. Chen. The results are compiled in Technical Report No. 3, prepared by Mr. Chen.

Each technical report contains an abstract which summarizes the results of each investigation.

Technical Report No. 1*

ACOUSTIC RADIATIONS OF A SUBMERGED CYLINDRICAL SHELL

George C. C. Ku and Yih-Hsing Pao
Department of Theoretical and Applied Mechanics
Cornell University, Ithaca, New York 14853

Abstract

The acoustic radiation of an infinitely long cylindrical shell submerged in water is analyzed on the basis of the Donnell's equation for thin shell coupled with the wave equation for the fluid pressure field. The shell is excited into steady vibration by a concentrated harmonic force applied normal to the shell surface. Dispersion of waves in the shell is analyzed and confirmed with the Pochhammer's theory for thick-walled circular cylinders. The comparison establishes the upper limit of frequencies for which the analysis is applicable. Radiated pressure fields around the shell are calculated for a few receivers at various locations in the fluid.

*NRL Contract No. N00014-81-C-2122

ACOUSTIC RADIATIONS OF A SUBMERGED CYLINDRICAL SHELL

Table of Contents

1. INTRODUCTION

The acoustic radiation of a submerged infinitely long cylindrical shell has been investigated by many researchers [1-9]. The practical importance of these investigations for the design of underwater vehicles is well documented, but the approach has been approximate in many cases. One approach is to apply Green's function of the wave equation for acoustic pressure and an assumed vibrational mode of the submerged object [2-4]. Another approach is to couple the wave equation for an infinite acoustic medium to the thin shell theory through the acoustic pressure on the shell surface [5-9]. The mathematical complexity of the second approach arises from the fluid reaction, which affects the vibration of the shell, being itself determined by the amplitude of the modes of vibration. A general treatment of the interaction of acoustic waves with a structure is given in Ref. 10.

The problem treated in this report is an infinitely long cylindrical shell, freely suspended in the fluid medium and vacuous inside. The shell is subjected to a harmonic point force on the cylindrical surface. The wave propagation in the surrounding fluid medium is governed by a simplified wave equation. The material of the shell is assumed to be isotropic, homogeneous, and linearly elastic. The shell thickness and deflections are sufficiently small that Donnell's equation for thin shells can be applied. The dynamic effect of the hydrostatic pressure is neglected. Through the condition of continuity for the radial velocity of the vibrating shell and the radial particle velocity of the fluid medium, the acoustic pressure can be treated as a reactive force acting on the submerged cylindrical shell.

The deflection of the shell and the radiating acoustic pressure are described in the cylindrical coordinate (r, θ, z). Due to azimuthal symmetry of the loading and the shell geometry, the displacements are conveniently decomposed into the Fourier series in the angular coordinates θ. The axial dependence (in the z coordinate) is eliminated by using the integral Fourier transformation. Through the condition of continuity, the acoustically radiated pressure is derived in terms of the radial deflection of the vibrating thin shell. To calculate the radiated pressure field, a special numerical integration scheme is developed to evaluate the inverse Fourier transform.

In Donnell's theory, the extensional, torsional, and radial vibrational modes of a cylindrical thin shell are all coupled in a system of three equations. To show the coupling effect of these modes, the dispersion curves for each circumferential mode are calculated. Three branches of the dispersion curves are formed and each one can be identified as one vibrational mode with its distinct group and phase velocities. By comparing these dispersion curves with those derived from the exact theory of elasticity for thick-walled cylinders [11, 12], the validity of Donnell's equations is established. The agreement for the fundamental modes is excellent, but the situation is somewhat different for the higher modes. Furthermore, the dispersion curves based on Donnell's equation do not exhibit the overtones above the first three modes. This indicates that Donnell's equations of motion are not adequate for evaluating the response of a cylindrical shell at high frequencies.

Numerical examples are shown for the radiated acoustic pressure

around a circumference of radius equal to ten times the mean shell radius. The perturbed pressure field (the perturbation over the ambient pressure) decreases rapidly from the point of application of the harmonic force in both circumferential and axial directions. The pressure varies in the forcing frequency, and it is higher at 100 KHz than that at 10 KHz because the radial modes of the shell are strongly excited at high frequencies.

2. EQUATIONS OF MOTION FOR A SUBMERGED CYLINDRICAL SHELL

Consider an infinitely long circular cylindrical shell submerged in a fluid medium as shown in Fig. 1. The center line of the cylindrical shell coincides with the z axis of the cylindrical coordinate (r, θ, z). An oscillatory point force of circular frequency ω is driven in the radial direction against the cylindrical shell. It generates a steady-state motion in the shell which radiates acoustic energy into the surrounding fluid medium at the same frequency.

For a thin cylindrical shell of mean radius a, the equations of motion (Donnell's equations) for the three components of a displacement vector $\underline{u}(\theta, z, t)$ are

$$\frac{\partial^2 u}{\partial z^2} + \frac{1-\nu}{2a^2}\frac{\partial^2 u}{\partial \theta^2} + \frac{1+\nu}{2a}\frac{\partial^2 v}{\partial z \partial \theta} + \frac{\nu}{a}\frac{\partial w}{\partial z} = \frac{\ddot{u}}{C_p^2} \tag{1a}$$

$$\frac{1+\nu}{2a}\frac{\partial^2 u}{\partial z \partial \theta} + \frac{1-\nu}{2}\frac{\partial^2 v}{\partial z^2} + \frac{1}{a^2}\frac{\partial^2 v}{\partial \theta^2} + \frac{1}{a^2}\frac{\partial w}{\partial \theta} = \frac{\ddot{v}}{C_p^2} \tag{1b}$$

$$\frac{\nu}{a}\frac{\partial u}{\partial z} + \frac{1}{a^2}\frac{\partial v}{\partial \theta} + \frac{w^2}{a^2} + \frac{h^2}{12}\left(\frac{\partial^2}{\partial z^2} + \frac{1}{a^2}\frac{\partial^2}{\partial \theta^2}\right)^2 w$$
$$= -\frac{\ddot{w}}{C_p^2} + \frac{1-\nu^2}{Eh}\left[\frac{F\delta(\theta)\delta(z)}{a} - P_0(a,\theta,z)\right] e^{-i\omega t} \tag{1c}$$

where u, v and w are the longitudinal, tangential, and radial displacements of the cylindrical shell [13, 14]. The parameter E is Young's modulus, ν the Poisson ratio, ρ_s the mass density of the shell and $C_p^2 = E/\rho_s(1-\nu^2)$ where C_p is the extensional wave speed in a thin plate. The last term on the right-hand side of Eq. (1c) represents the harmonic point force placed at $z=0$, and $\theta=0$ plus the

reacting acoustic pressure $p(r,\theta,z,t) = p_0(r,\theta,z)\exp(-i\omega t)$ at the interface between the shell and the fluid medium. Due to the symmetry about a diametral plane, the displacements can be expressed in the following forms:

$$u(\theta,z,t) = \sum_{n=0}^{\infty} U_n(z)\cos n\theta e^{-i\omega t} \tag{2a}$$

$$v(\theta,z,t) = \sum_{n=0}^{\infty} V_n(z)\sin n\theta e^{-i\omega t} \tag{2b}$$

$$w(\theta,z,t) = \sum_{n=0}^{\infty} W_n(z)\cos n\theta e^{-i\omega t} \tag{2c}$$

The index n is called the circumferential modal number which indicates a mode of $2n$ nodal points along the circumference. Similarly, the delta function in θ is expanded into a cosine series

$$\delta(\theta) = \frac{1}{2\pi}\sum_{n=0}^{\infty} \varepsilon_n \cos n\theta \tag{3}$$

where

$$\varepsilon_n = \begin{cases} 1, & n = 0 \\ 2, & n \geq 1 \end{cases} \tag{4}$$

Substituting Eqs. (2) - (4) into Eq. (1) and applying the orthogonality conditions for $\cos n\theta$ and $\sin n\theta$, we obtain the following ordinary differential equations for $U_n(z)$, $V_n(z)$ and $W_n(z)$:

$$\begin{aligned} &\frac{d^2U_n}{dz^2} - \frac{1-\nu}{2a^2} n^2 U_n + \frac{1+\nu}{2a} n \frac{dV_n}{dz} + \frac{\nu}{a}\frac{dW_n}{dz} = -\frac{\omega^2}{C_p^2} U_n \\ &-\frac{1+\nu}{2a} n \frac{dU_n}{dz} + \frac{1-\nu}{2}\frac{d^2V_n}{dz^2} - \frac{n^2}{a^2} V_n - \frac{n}{a^2} W_n = -\frac{\omega^2}{C_p^2} V_n \\ &\frac{\nu}{a}\frac{dU_n}{dz} + \frac{n}{a^2} V_n + \frac{W_n}{a^2} + \frac{h^2}{12}\left(\frac{d^2}{dz^2} - \frac{n^2}{a^2}\right)^2 W_n = \frac{\omega^2}{C_p^2} W_n + \frac{1-\nu}{Eh}\frac{\bar{r}}{a}\frac{\varepsilon_n}{2\pi}\delta(z) \\ &- \frac{1-\nu}{Eh}\frac{\varepsilon_n}{2\pi}\int_0^{2\pi} P_0(a,\theta,z)\cos n\theta d\theta \end{aligned} \tag{5}$$

These equations are solved by applying the Fourier transform, which is defined as

$$\bar{U}_n(k) = \int_{-\infty}^{\infty} e^{-ikz} U_n(z)\,dz \ , \text{ etc.} \tag{6}$$

The inverse transform of $\bar{U}_n(k)$ is

$$U_n(z) = \frac{1}{2\pi} \int_{-\infty}^{\infty} e^{ikz} \bar{U}_n(k)\,dk \ . \tag{7}$$

where k is physically the wave number along the z-axis. The transformed equations are:

$$[k^2a^2 + \frac{1-\nu}{2} n^2 - \Omega^2]\bar{U}_n(k) - ikan \frac{1+\nu}{2} \bar{V}_n(k) - ika\nu\bar{W}_n(k) = 0 \tag{8a}$$

$$ikan \frac{1+\nu}{2} \bar{U}_n(k) + [k^2a^2 \frac{1-\nu}{2} + n^2 - \Omega^2]\bar{V}_n(k) + n\bar{W}_n(k) = 0 \tag{8b}$$

$$ika\nu\bar{U}_n(k) + n\bar{V}_n(k) + [\frac{h^2}{12a^2} (k^2a^2 + n^2)^2 + 1 - \Omega^2]\bar{W}_n(k) =$$

$$= \frac{1-\nu^2}{Eh} Fa^2 \frac{\varepsilon_n}{2\pi} - \frac{1-\nu^2}{Eh} \frac{\varepsilon_n a^2}{2\pi} \int_0^{2\pi} \bar{P}_0(a,\theta,k)\cos n\theta\,d\theta \tag{8c}$$

where $\Omega = \omega a/C_p$ is a dimensionless frequency.

3. EQUATION FOR ACOUSTIC WAVES IN A FLUID MEDIUM

The perturbing pressure field $P(r, \theta, z, t)$ in an ideal fluid medium caused by the vibrating shell is governed by the wave equation

$$\nabla^2 P(r,\theta,z,t) = \frac{1}{c^2} \ddot{P}(r,\theta,z,t) \tag{9}$$

where ∇^2 is the Laplacian operator and c is the wave speed in the fluid. For a harmonic time dependent wave motion, Eq. (9) reduces to

$$(\nabla^2 + k_o^2) P_o(r,\theta,z) = 0 \tag{10}$$

where $k_o = \omega/c$ is the wave number in the infinitely extended fluid medium. Applying again the Fourier transform, Eq. (6), to the z-variable, we obtain

$$\left(\frac{\partial^2}{\partial r^2} + \frac{1}{r} \frac{\partial}{\partial r} + \frac{1}{r^2} \frac{\partial^2}{\partial \theta^2} - k^2 + k_o^2 \right) \bar{P}_o(r,\theta,k) = 0 \tag{11}$$

This homogeneous differential equation has a solution

$$\bar{P}_o(r,\theta,k) = \sum_{n=0}^{\infty} A_n H_n(\kappa r) \cos n\theta \tag{12}$$

where $\kappa = (k_o^2 - k^2)^{1/2}$. The Hankel function of the first kind, $H_n(\kappa r)$, is used to represent outgoing waves in the infinitely extended fluid medium. The conventional superscript (1) for H_n is omitted throughout this report.

The unknown coefficients A_n of Eq. (12) can be determined from the continuity conditions at the shell-fluid interface. For an ideal fluid the normal velocity must be continuous.

$$\frac{\partial \underset{\sim}{u}(\theta,z,t)}{\partial t} \cdot \underset{\sim}{n} = \underset{\sim}{v}_f(a,\theta,z,t) \cdot \underset{\sim}{n} \tag{13}$$

The fluid particle velocity $\underset{\sim}{v}_f(a, \theta, z, t)$ is related to the perturbed pressure $P(a, \theta, z, t)$ by the momentum relation

$$\nabla P(r,\theta,z,t) = -\rho \frac{\partial \underset{\sim}{v}_f}{\partial t} (r,\theta,z,t) \quad . \tag{14}$$

Under the assumption of infinitesimal displacement of the vibrating shell, the surface normal $\underset{\sim}{n}$ of the cylindrical shell still orients in the radial direction, and the radial component of Eq. (14) is

$$\frac{\partial p}{\partial r} (a,\theta,z,t) = -\rho \frac{\partial v_f}{\partial t} (r,\theta,z)\Big|_{r=a} = -\rho \frac{\partial^2 w}{\partial t^2} (\theta,z,t) \quad . \tag{15}$$

Substituting Eqs. (2) and (12) into (15), the coefficient A_n is obtained as

$$A_n = \frac{\rho\omega^2 \overline{W}_n(k)}{\kappa H_n'(\kappa a)} \quad . \tag{16}$$

Consequently, the Fourier transformed pressure field, Eq. (12), may be written as

$$\overline{p}_0(r,\theta,k) = \sum_{n=0}^{\infty} Z_{nr}(k) \dot{\overline{W}}_n(k) \cos n\theta \tag{17}$$

where

$$Z_{nr}(k) = \frac{i\rho c k_0 H_n(\kappa r)}{\kappa H_n'(\kappa a)} \quad . \tag{18}$$

On the surface of the cylindrical shell, the reacting acoustic pressure is written as

$$\overline{p}_0(a,\theta,k) = \sum_{n=0}^{\infty} Z_{na}(k) \dot{\overline{W}}_n(k) \cos n\theta \tag{19}$$

where

$$Z_{na}(k) = Z_{nr}(k)\Big|_{r=a} \quad . \tag{20}$$

It is the Fourier transform of the acoustic impedance for the surrounding fluid medium at the surface of the cylindrical shell.

4. RESPONSE OF THE CYLINDRICAL SHELL

Replacing $\bar{P}_o(a, \theta, k)$ in Eq. (8c) by that given in Eq. (19), we arrive at the following relation:

$$ika\nu\bar{U}_n(k) + n\bar{V}_n(k) + \left[\frac{h^2}{12a^2}(k^2a^2+n^2)^2+1-\Omega^2-\frac{1-\nu^2}{Eh}\, i\omega a^2 Z_{na}(k)\right]\bar{W}_n(k) = \frac{a}{Eh}(1-\nu^2)\frac{F\varepsilon_n}{2\pi} \quad . \tag{21}$$

From Eqs. (8a), (8b) and (21), the radial displacement $\bar{W}_n(k)$ is determined by using Cramer's rule,

$$\bar{W}_n(k) = \frac{\varepsilon_n F}{-i\omega 2\pi a[Z_{np}(k)+Z_{nm}(k)+Z_{na}(k)]} \tag{22}$$

where

$$Z_{np}(k) = \frac{iC_p\rho_s h}{\Omega a}\left[\frac{h^2}{12a^2}(a^2k^2+n^2)^2+1-\Omega^2\right]$$

$$Z_{nm}(k) = \frac{iC_p\rho_s h}{\Omega a}\frac{1}{\Delta}\left\{k^2a^2\nu\left[n^2(1+\nu)+\nu\left(\Omega^2-k^2a^2\frac{1-\nu}{2}-n^2\right)\right] + n^2\left[\Omega^2-\frac{(1-\nu)n^2}{2}-k^2a^2\right]\right\} \tag{23}$$

$$\Delta = \left[\Omega^2-\frac{1-\nu}{2}n^2-k^2a^2\right]\left[\Omega^2-\frac{1-\nu}{2}k^2a^2-n^2\right] - k^2a^2n^2\frac{(1+\nu)^2}{4} \quad .$$

Note that Eq. (22) describes the relation between the Fourier transformed radial displacement $\bar{W}_n(k)$ of the cylindrical shell for each circumferential mode n and the harmonic driving force $F\exp(-i\omega t)\,\delta(\theta)\,\delta(z)$. Therefore, $Z_{np}(k) + Z_{nm}(k) + Z_{na}(k)$ is the total impedance of the submerged cylindrical shell per unit circumference. Of

the three terms, $Z_{na}(k)$ is due to the reacting fluid medium, $Z_{np}(k)$ is due to the flexural vibration of the shell, and $Z_{nm}(k)$ is due to the extensional vibration.

To determine the radial displacement $W_n(z)$ from $\bar{W}_n(k)$ of Eq. (22), the inverse integral Fourier transform (7) is used. From Eq. (2c), we obtain finally the radial velocity of the submerged cylindrical shell

$$\dot{w}(\theta,z,t) = \frac{F}{2\pi^2 a} \sum_{n=0}^{\infty} \varepsilon_n \cos n\theta e^{-i\omega t} \int_0^{\infty} \frac{\cos kz}{Z_n(k)}\, dk \tag{24}$$

where

$$Z_n(k) = Z_{np}(k) + Z_{nm}(k) + Z_{na}(k) \ . \tag{25}$$

Similarly, the axial and tangental velocities $\dot{u}$ and $\dot{v}$ are obtained:

$$\dot{u}(\theta,z,t) = \frac{F}{2\pi^2 a} \sum_{n=0}^{\infty} \varepsilon_n \cos n\theta e^{-i\omega t} \int_0^{\infty} \frac{\sin kz}{Z_n(k)} Z_u(k)\, dk \tag{26}$$

$$\dot{v}(\theta,z,t) = \frac{F}{\pi^2 a} \sum_{n=1}^{\infty} \sin n\theta e^{-i\omega t} \int_0^{\infty} \frac{\cos kz}{Z_n(k)} Z_v(k)\, dk \tag{27}$$

where

$$Z_u(k) = \frac{ka}{\Delta} \left[n^2 \frac{1+\nu}{2} + \nu\left(-k^2a^2 \frac{1-\nu}{2} - n^2 + \Omega^2\right)\right] \tag{28}$$

$$Z_v(k) = \frac{n}{\Delta} \left[k^2a^2\nu \frac{1+\nu}{2} + \left(-k^2a^2 - \frac{1-\nu}{2} n^2 + \Omega^2\right)\right] \ . \tag{29}$$

Note that the integrations in Equations (24), (26) and (27) contribute to the velocities of the submerged thin shell for each

particular circumferential mode n, and the total displacement is obtained by summing up all circumferential modes. For the case of $n=0$, Eqs. (24) and (26) show that the radial and longitudinal displacements are independent of θ. On the other hand, Eq. (27) indicates that the tangential displacement vanishes. This may be interpreted by the decomposition of a point force into an infinite series in Eq. (3). When $n=0$, the point driving force degenerates into a ring force at $Z=0$ of amplitude $F/2\pi a$. Furthermore, in Eqs. (24), (26) and (27), if the wave number k in the inverse Fourier transform degenerates to zero, the radial and tangential displacements will be independent of z and the longitudinal displacement vanishes identically. This corresponds to the case for a cylindrical shell with forces distributed along a line in the axial direction, normal to the surface of the shell.

5. PRESSURE FIELD OF RADIATION

The radial motion, $\dot{w}(\theta,z,t)$ in Eq. (24) was derived in a recent report by Voger and Fait [15]. They also calculated the radial displacements for various orders of n. In this report, we evaluate in detail the radiation pressure field in the fluid medium.

Substituting Eq. (22) into (17), the transformed acoustic field of radiation is obtained

$$\bar{p}_0(r,\theta,k) = \sum_{n=0}^{\infty} \frac{\varepsilon_n F}{2\pi a Z_n(k)} Z_{nr}(k)\cos n\theta \quad . \tag{30}$$

The pressure field is

$$p(r,\theta,z,t) = \frac{F}{2\pi^2 a} \sum_{n=0}^{\infty} \varepsilon_n \cos n\theta e^{-i\omega t} \int_0^{\infty} Z_{nr}(k) \frac{\cos kz}{Z_n(k)} dk \quad . \tag{31}$$

Note that, in the above equation, if the wave number $k < k_o$, the pressure field $P(r,\theta,z,t)$ is a progressive wave inasmuch as $Z_{nr}(k)$ in Eq. (18) acts as both resistive and reactive impedance. On the other hand, when $k > k_0$, the argument of the Hankel function, $\kappa r = (k_0^2 - k^2)^{1/2} r$ becomes purely imaginary. If the Hankel function of the first kind with the imaginary argument is replaced by the modified Bessel function of the second kind,

$$H_n(ix) = (2/\pi) i^{-(n+1)} K_n(x) \quad , \tag{32}$$

$Z_{nr}(k)$ in Eq. (31) is given by

$$Z_{nr}(k) = \frac{i\rho c k_0 K_n[(k^2-k_0^2)^{\frac{1}{2}}r]}{(k^2-k_0^2)^{\frac{1}{2}}K_n'[(k^2-k_0^2)^{\frac{1}{2}}a]} \tag{33}$$

It is a pure reactive impedance. Thus no acoustic energy is radiated from the cylindrical shell. Figure 2 shows the relation between the acoustic wave number k_o in the fluid medium and its projection along the z axis of the shell. It indicates that the radiation is possible only when $k < k_o$.

6. DISPERSION RELATIONS

Since the displacements u,v,w and the pressure field P are all related to a common factor $Z_n(k) = Z_{np}(k) + Z_{nm}(k) + Z_{na}(k)$, it is important to examine the characteristics of this impedance for a submerged cylindrical shell. We consider first a cylindrical shell in a vacuum driven by a point force.

Without the surrounding fluid medium, the radial displacement $\bar{W}_n(k)$ in Eq. (22) is reduced to:

$$\bar{W}_n(k) = \frac{\varepsilon_n F}{-i\omega 2\pi a [Z_{np}(k)+Z_{nm}(k)]} \tag{34}$$

The zeros of the impedance function are given by the roots of the following equation:

$$Z_n^0(k,\Omega) = Z_{np}(k,\Omega) + Z_{nm}(k,\Omega) = 0 \ . \tag{35}$$

When n=0. The above is simplified to:

$$Z_0^0(k,\Omega) = \frac{iC_p\rho_s h}{\Omega a}\left[\frac{h^2}{12a^2}(ka)^4 + 1 - \Omega^2 + \frac{k^2a^2\nu^2}{\Omega^2 - k^2a^2}\right] = 0 \tag{36}$$

It is a second order equation in Ω^2 except when $\Omega = \omega a/C_p = 0$ There are two roots for each value of ka, and the locus of the roots forms two branches of dispersion curves as shown in Fig. 3a. As ka approaches infinity, these two branches of dispersion curves approach the following asymptotes:

$$\begin{aligned} &\Omega/ka \to kh/\sqrt{12} \\ &\frac{\Omega}{ka} \to 1 + \frac{\nu^2/k^2a^2}{1-k^2h^2/12} \quad \text{as} \quad ka \to \infty \end{aligned} \tag{37}$$

On the other hand, when ka approaches zero, Eq. (36) is reduced to:

$$Z_0^*(k,\Omega)\Big|_{ka\to 0} = \frac{iC_p\rho_s h}{\Omega a}\left[1 - \Omega^2 + \frac{k^2a^2\nu^2}{\Omega^2 k^2 a^2}\right] = 0 \qquad (38)$$

The branches of dispersion curves start at the following values along the Ω-axis:

$$\Omega \to \sqrt{1-\nu^2}\ ka \approx 0 \qquad \text{as } ka \to 0 \qquad (39a)$$

$$\Omega \to 1 \qquad (39b)$$

By substituting the value of Ω in Eq. (39a) into the homogeneous equation (8), the eigenfunctions can be easily identified as:

$$\left|\frac{\bar{U}_0(k)}{\bar{W}_0(k)}\right| = \left|\frac{1}{\nu ka}\right| \quad , \quad \bar{V}_0(k) = 0 \quad \text{as } ka \to 0 \quad . \qquad (40)$$

This implies that the dispersion curve started at $\Omega = 0$ corresponds to the extensional mode of a cylindrical thin shell. Similarly, if the value of $\Omega = 1$, which corresponds to the ring frequency $f = C_p/(2\pi a)$ of the cylindrical shell, in Eq. (39b) is used, the eigenfunctions are:

$$\left|\frac{\bar{W}_0(k)}{\bar{U}_0(k)}\right| = \left|\frac{1}{\nu ka}\right| \quad , \quad \bar{V}_0(k) = 0 \quad \text{as } ka \to 0 \quad . \qquad (41)$$

Therefore the dispersion curve starting at $\Omega = 1$ corresponds to the radial mode of the cylindrical thin shell.

From these dispersion curves, the phase velocity and the group velocity for each vibrational mode are calculated as shown in Fig. 3b, 3c. Both the phase and group velocities of the radial mode approach C_p, the extensional wave speed in a thin plate, asymptotically. On the

other hand, the phase and group velocities of the extensional vibrational mode approach zero when ka is less than 10 and then increase gradually as ka increases.

For $n=1$ in Eq. (35), the dispersion relation is:

$$Z_1^0(k,\Omega) = \left[\frac{h^2}{12a^2}(a^2k^2+1)^2 + 1 - \Omega^2\right]\left\{\left[\Omega^2 - \frac{1-\nu}{2} - k^2a^2\right]\left[\Omega^2 - \frac{1-\nu}{2}k^2a^2 - 1\right] - k^2a^2\frac{(1+\nu)^2}{4}\right\} + \left[k^2a^2(1+\nu\Omega^2 - k^2a^2\nu) + \Omega^2 - \frac{1-\nu}{2} - k^2a^2\right] = 0 \quad . \tag{42}$$

It is a third order equation in Ω^2, and there are three distinct branches of dispersion curves for $n=1$ mode as shown in Fig. 4a. When ka approaches infinity, Eq. (42) becomes:

$$Z_1^0(k,\Omega)\Big|_{ka\to\infty} \cong -k^6a^6\left[-\frac{k^2h^2}{12} + \frac{\Omega^2}{k^2a^2}\right]\left[\frac{\Omega^2}{k^2a^2} - 1\right]\left[\frac{\Omega^2}{k^2a^2} - \frac{1-\nu}{2}\right] = 0 \tag{43}$$

This yields the following asymptotes for the dispersion curves:

$$\begin{aligned} &\Omega/ka \to kh/\sqrt{12} \\ &\Omega/ka \to 1 \qquad\qquad \text{as} \quad ka \to \infty \\ &\Omega/ka \to [(1-\nu)/2]^{\frac{1}{2}} \quad . \end{aligned} \tag{44}$$

As ka approaches zero, Eq. (42) degenerates to:

$$Z_1^0(k,\Omega)\Big|_{ka\to 0} \cong \left[\Omega^2 - \frac{1-\nu}{2}\right]\left\{\left[\Omega^2 - 1\right]^2 - 1\right\} = 0 \quad . \tag{45}$$

This implies that the three branches of dispersion curves should start

at:

$$\Omega = 0 \tag{46a}$$

$$\Omega = [(1 - \nu)/2]^{\frac{1}{2}} \quad \text{as } ka \to 0 \tag{46b}$$

$$\Omega = \sqrt{2} \quad . \tag{46c}$$

Again, the phase velocities and group velocities can be calculated from these three dispersion curves as shown in Fig. 4b and 4c.

In a case analogous to that for $n=0$, the phase and group velocities of the radial mode (top branch) in Fig. 4a approach the extensional wave speed of a thin plate. For the extensional mode (bottom branch) in Fig. 4a, the phase and group velocities approach zero when $ka > 4$ in Fig. 4b and 4c.

The middle branch of the dispersion curves in Fig. 4a is a torsional mode. The phase and group velocities approach the transverse wave speed $C_p[(1-\nu)/2]^{\frac{1}{2}}$. Due to axial symmetry, this torsional mode does not exist for the case of $n=0$.

The dispersion curves for the higher circumferential modes, $n=2,3,4,\ldots$, can be similarly obtained. Because of the cubic equation in Ω^2 in Eq. (35), there are three branches of dispersion curves for each value of n, each branch corresponding to a vibrational mode.

To assess the range of applicability of Donnell's equations of motion for a thin cylindrical shell, the aforementioned dispersion curves and those based on the exact theory of elasticity for thick-walled cylinders [11, 12] have been compared. Unlike those reported in Ref. 11 and 12, the dispersion relation is derived from three displacement potentials, and the calculation of the dispersion curves is

programmed for a hollow cylinder of arbitrary thickness. The results are shown as dashed lines in Figs. 3 and 4. It is seen that a small error exists at the cut-off frequencies for the higher branches, and this error propagates for ka > 0.

It should be noted that based on the exact theory, there are many more higher branches which are not included in Donnell's theory. Therefore, Donnell's equations should be applied only to analyze the vibrations of cylindrical thin shells at a frequency lower than the next highest cut-off frequency.

To include the effect of the reacting acoustic pressure for a submerged cylindrical shell, the impedance of Eq. (22) should be considered. The vanishing of the total impedance

$$Z_n(k,\Omega) = Z_{np}(k,\Omega) + Z_{nm}(k,\Omega) + Z_{na}(k,\Omega) = 0 \qquad (47)$$

gives rise to dispersion curves in a three dimensional space formed by, real k and imaginary k. Because the acoustic impedance of ρc of water is 30 times smaller than that of steel, the effect of added impedance $z_{na}(k, \Omega)$ is expected to be negligible.

The numerical calculation indicates that there is only a small difference between the real part of $k = k_R + ik_I$ in Eq. (47) and k in Eq. (35) for the extensional and radial vibrational mode. However, no real branches for the torsional mode were found for every circumferential mode $n > 0$. This implies that the torsional mode is a non-radiating mode for the vibrating submerged cylindrical shell surrounded by the inviscid fluid. Nevertheless, the bending motion of

the cylindrical shell caused by the extensional vibrational mode should still contribute to the radiating energy in the fluid medium.

7. NUMERICAL RESULTS OF ACOUSTIC RADIATION

The integrals in Eq. (31) yield the radiated pressure field due to the harmonic force $F\exp(-i\omega t)$, one for each circumferential mode n. The total radiated pressure is then obtained by summing all circumferential modes. These indefinite integrals are evaluated numerically for real wave number k, and the summation of the series is truncated when a desired accuracy is reached.

Of the three factors of the integrand in Eq. (31), $1/Z_n(k)$ is regular because of the zeros of $Z_n(k)$ (Eq. (67)) are complex valued. The factor $Z_{nr}(k)$ or $Z_{na}(k)$ at r=a, however, has a singularity at $k=k_0$. It is due to the factor $(k_0^2 - k^2)^{\frac{1}{2}}$ and the zero argument of the Hankel functions.

For circumferential mode n larger than zero, however, the singularity at $k=k_0$ can be removed. If the Hankel functions are approximated for small arguments [16] by

$$H_n(z) \sim -(i/\pi)\Gamma(n)(z/2)^{-n} \; ; \; H_0(z) \sim (2i/\pi)\,\ell n\, z$$

$$\text{as } z \to 0 \qquad (48)$$

$$K_n(z) \sim \tfrac{1}{2}\Gamma(n)(z/2)^{-n} \; ; \; K_0(z) \sim -\ell n\, z$$

the Z_{nr} is simplified to

$$Z_{nr}(k)\big|_{k\to k_0} \sim -i\rho c k_0 (a/n)(a/r)^n \qquad n > 0 \qquad (49)$$

The integrand of Eq. (31) is then a smooth function. For n=0, the singularity is not removeable because

$$Z_{or}(k)\Big|_{k\to k_o} \sim i\rho c k_o a \, \ell n[|k_o - k^2|^{\frac{1}{2}} r] \quad . \tag{50}$$

To minimize the effect of this singularity during the numerical integrations, variable step Simpson's rule is used.

The numerical integration in Eq. (31) is truncated until the value of the indefinite integral converges to an error less than 10^{-6}. The infinite summation over n is also truncated when the sum converges to error less than 10^{-6}.

For numerical calculations a submerged stainless steel cylindrical shell is selected. The mean radius of the shell is a = 12.70 mm. (0.5 in.) and the wall thickness h = 0.508 mm (0.02 in.). The compressional wave speed of stainless steel c_p is 5.72×10^6 mm/sec; shear wave speed c_s is 3.10×10^6 mm/sec, the Poisson ratio $\nu = 0.298$ and its mass density $\rho_s = 7.7$ g/cm^3. A receiver is placed at r = 10a = 127.0 mm (5 in.) away from the axis of the submerged cylindrical shell. Figs. 5a, 5b, 5c show the calculated radiation pressure pattern when the point force is driven at 10 KHz, 50 KHz and 100 KHz (Ω = 0.139, 0.689, 1.395) respectively.

The angular distributions of the pressure fields for either z=0 or z=r are plotted in decible scale relative to the pressure p_o at r = 10a, $\theta = 0^o$ and z = 0. The magnitudes of the pressure, P_o, are 1.25×10^{-2} dyne/cm^2, 6.14×10^{-2} dyne/cm^2 and 1.31×10^{-1} dyne/cm^2 at 10 KHz, 50 KHz and 100 KHz respectively with a harmonic driving

force of $F = 1$ dyne. For the two degenerate cases, however, the magnitude of the ring force is $F = 1/2\pi a$ dyne/cm and that of the line force at $\theta = 0$ is $F = 1$ dyne/cm.

8. DISCUSSION

To perform the numerical integration of Eq. (31) for the acoustic radiation over the real wave number k from 0 to infinity at a fixed frequency and a fixed circumferential mode n is equivalent to integrating along a horizontal line perpendicular to the Ω axis of the dispersion curves in Figs. 3a and 4a. These horizontal lines may intersect more than once on the real part of the complex branches of the dispersion curves. The integrand of Eq. (31) evaluated along this horizontal line may become very large at these intersections, which provide a dominant contribution to the total pressure intensity.

As shown in Figs. 3a and 4a, the cut-off frequencies of the cylindrical shell in vacco increase as the circumferential mode n increases. Therefore at higher frequencies the contribution from higher circumferential mode n is more important than that at lower frequencies. Also, at higher frequencies, the radial mode is more pronounced, especially at small wave numbers. Since the radiation pressure depends strongly on the radial motion of the shell, the pressure may be higher when the frequency is large. The dependence of the reference pressure P_o on the driving frequency is shown in Fig. 6.

In Fig. 5a, the radiation pattern for a submerged cylindrical shell driven by a point force peaks at $\theta = 0$ and $\theta = \pi$, and dips approximately at $\pi/2$. As can be seen from the Fourier series in Eq. (31), this pattern suggests that the first circumferential mode ($n=1$) dominates the vibration of the shell. In Figure 7 the contributions to the total radiation pressure for 10 KHz from each circumferential mode are shown for $n = 0$ to 15. The ordinate is the absolute value of

each term in the series of Eq. (31) for $r = 10a(127\ mm)$, $\theta = 0^{o}$, $z = 0$ or $10a$. The $n = 1$ mode (translational mode) is indeed dominant.

Fig. 5b exhibits two peak pressures at $\theta = 0$ and $\theta = 2\pi/3$ for a submerged cylindrical shell driven by a point force at 50 KHz. Because of the $\cos n\theta$ dependence of the radiated field, these two peaks seem to be the effect of a term with $n \tilde{=} 3/2$. In terms of the integral circumferential mode number, the combination of $n = 1$ and $n = 2$ mode could be the dominant source for the radiation field. This is substantiated by the contributions from each mode as shown in Fig. 7b.

At 100 KHz in Fig. 5c, there are no distinct peaks and dips. Therefore not a single or two circumferential modes are dominant. This is verified by the results shown in Fig. 7c.

As for the submerged cylindrical shell driven by a ring source at $z = 0$, because of the axisymmetrical source, the radiation pattern is independent of θ as shown in the lower half of Figs. 5a, 5b, and 5c. Similarly for the shell driven by a line source at $\theta = 0$, the radiation field is independent of the z-coordinate.

To summarize, the radiation patterns of the pressure field in a fluid surrounding a circular cylindrical shell are strongly influenced by the nature of the force that excites the shell (a point force, a ring force, and a line force), and are dependent on the frequencies of the driving force. At lower frequencies, the circumferential modes $n = 1$ and 2 are dominant and the angular distribution of the pressure peaks at $\theta = 0$ and π and dips near $\theta = \pi/2$ for $n = 1$. At higher frequencies, the lowest four or five circumferential modes are equally important in the contribution to the total wave field. Since the

highest branch of the dispersion curve of the shell based on Donnell's equation is predominantly radial motion (at lower wave numbers), and the radiation field is excited mainly by the radial motion of the shell, the pressure field is found to be stronger for a driving force with higher frequencies.

REFERENCES

1. Hanish, S., A Treatise on Acoustic Radiation, Naval Research Laboratory, Washington, D.C., 1981.

2. Brigham, G.A. and Borg, M.F., An Approximate Solution to the Acoustic Radiation of a Finite Cylinder, J. of Acoustic Soc. of Am., Aug. 1960, p. 971-981.

3. Farn, C.L.S. and Huang, H., Transient Acoustic Fields Generated by a Body of Arbitrary Shape, J. of Acou. Soc. of Am., Feb. 1968, p. 252-257.

4. Williams, W., Parke, N.G., Moran, D.A., and Sherman, C.H., Acoustic Radiation from a Finite Cylinder, J. of Acou. Soc. of Am., Dec. 1964, p. 2326-2322.

5. Butler, D.J., Vibrations of an Infinitely Long Cylindrical Shell in a Semi-infinite Acoustic Medium, J. of Ship Research, Dec. 1959, p. 41-49.

6. Heckl, M., Vibration of Point-Driven Cylindrical Shells, J. of Acou. Soc. of Am., Oct. 1962, p. 1553-1557.

7. Junger, M.C., Vibrations of Elastic Shells in a Fluid Medium and the Associated Radiation of Sound, J. of App. Mech., Dec. 1952, p. 439-445.

8. Junger, M.C., Dynamic Behavior of Reinforced Cylindrical Shells in a Vacuum and in Fluid, J. of App. Mech., March 1954, p. 35-41.

9. Warburton, G.B., Vibration of a Cylindrical Shell in an Acoustic Medium, J. of Mech. Eng. Sc., Vol. 3 No. 1, 1961, p. 69-79.

10. Junger, M.C. and Feit, D., Sound, Structure and Their Interaction, The MIT Press, Cambridge, Massachusetts, 1972.

11. Armenakas, A.E., Gazis, D.C. and Herman, G., Free Vibration of Circular Cylindrical Shells, Pergamon, Oxford, 1969.

12. Greenspon, J.E., Vibration of a Thick-Walled Cylindrical Shell - Comparison of the Exact Theory with Approximate Theories, J. of Acou. Soc. of Am., May 1960, p. 571-578.

13. Kraus, H., Thin Elastic Shells, Wiley, N.Y., 1967.

14. Timoshenko, S. and Woinowsky-Krieger, S., Theory of Plates and Shells, McGraw-Hill, NY, 1959.

15. Voger, W. and Feit, D., Response of Point-Excited Shell Immersed in

Acoustic Medium, NSRDC Report 80-061, November, 1980.

16. Abramowitz, M. and Stegun, I.A., Handbook of Mathematical Functions, National Bureau of Standards, June, 1964.

Figure Captions

Fig. 1. A harmonic point force acting on a submerged circular cylindrical shell.

Fig. 2. Relation between the wave number k_0 and k.

Fig. 3. Dispersion curves of extensional waves in a thin shell (n = 0)
(a) Frequency versus wave number
(b) Phase velocity versus wave number
(c) Group velocity versus wave number

Fig. 4. Dispersion of flexural waves in a thin shell (n = 1)
(a) Frequency versus wave number
(b) Phase velocity versus wave number
(c) Group velocity versus wave number

Fig. 5. Angular distribution of radiation pressure at r = 10 a for a submerged steel shell of mean radius a = 12.7 mm. The shell is driven by a point force of one dyne at r = a, θ = 0, z = 0 (the upper half circle). Solid lines are for pressure at z = 0 and dashed lines for pressure at z = 10 a. Pressure fields generated by a line force at r = a, θ = 0 are shown in the lower half circle by dotted lines. All pressures are measured in db relative to the peak reference pressure p_0 at r = 10 a, θ = 0, z = 0.
(a) Shell driven at 10 KHz, p_0 = 0.00125 dyne/cm^2.
(b) Shell driven at 50 KHz, p_0 = 0.00614 dyne/cm^2.
(c) Shell driven at 100 KHz, p_0 = 0.0131 dyne/cm^2.

Fig. 6. Variation of the reference pressure with the driving frequency.

Fig. 7. Absolute values of the pressure field at (10a, 0, 0) in solid line, or at (10a, 0, 10a) in dashed lines due to each component of the circumferential mode (n = 0 to 15).

(a) Shell driven at 10 KHz.

(b) Shell driven at 50 KHz.

(c) Shell driven at 100 KHz.

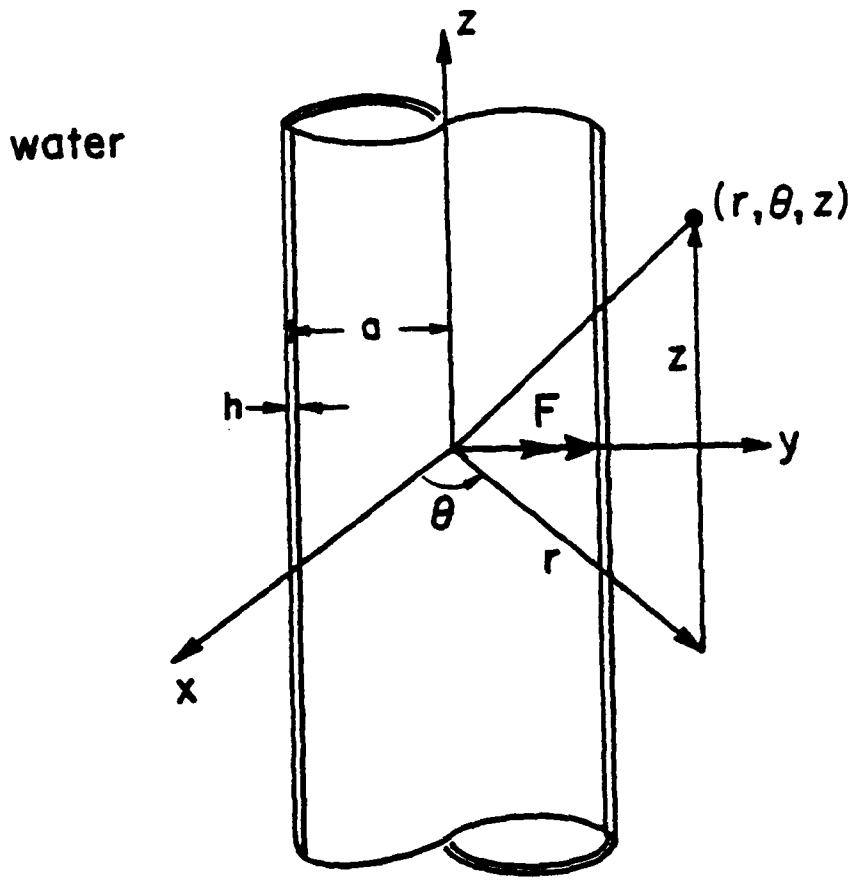

Fig. 1. A harmonic point force acting on a submerged circular cylindrical shell.

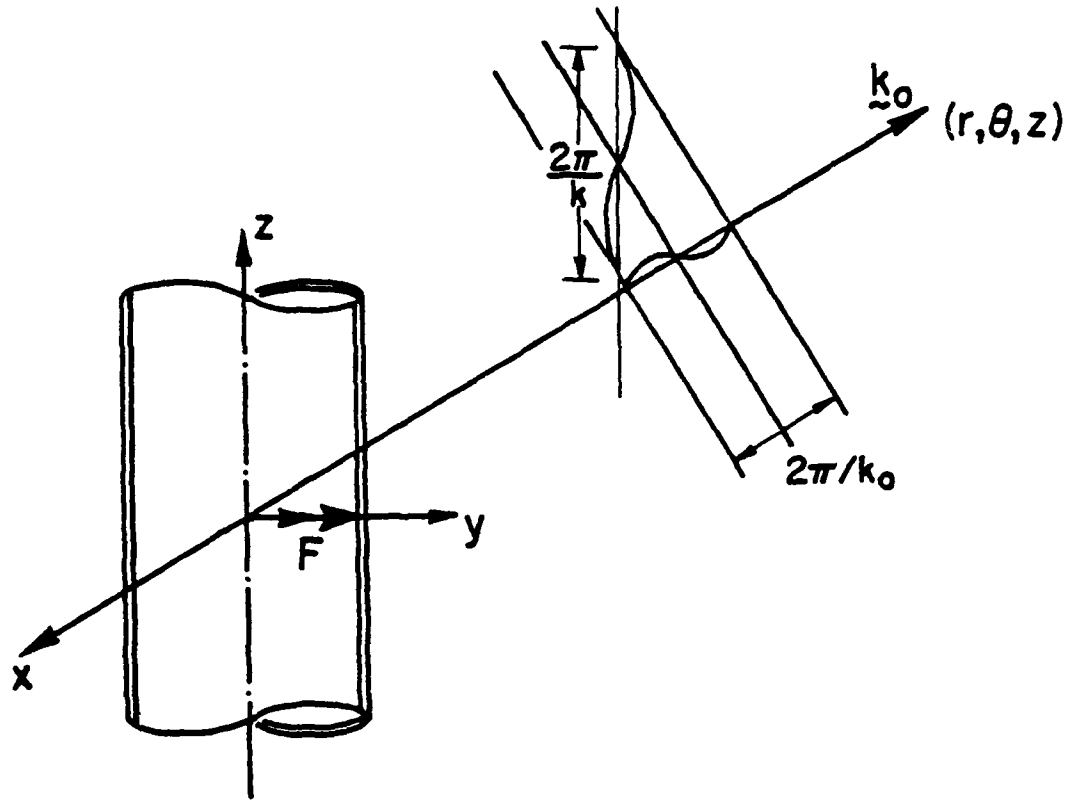

Fig. 2. Relation between the wave number k_o and k.

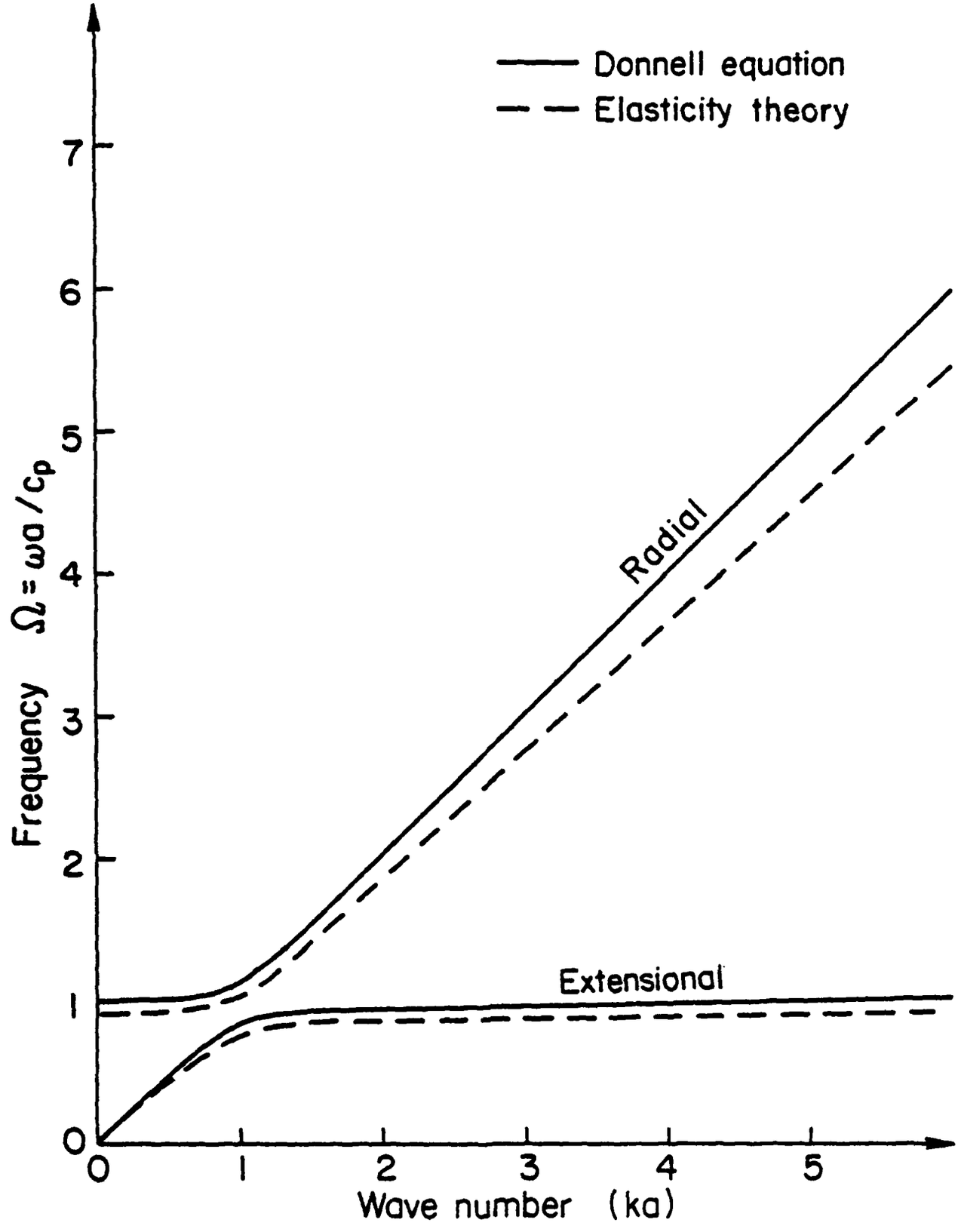

Fig. 3(a) Dispersion curves of extensional waves in a thin shell (n = 0) - frequency versus wave number

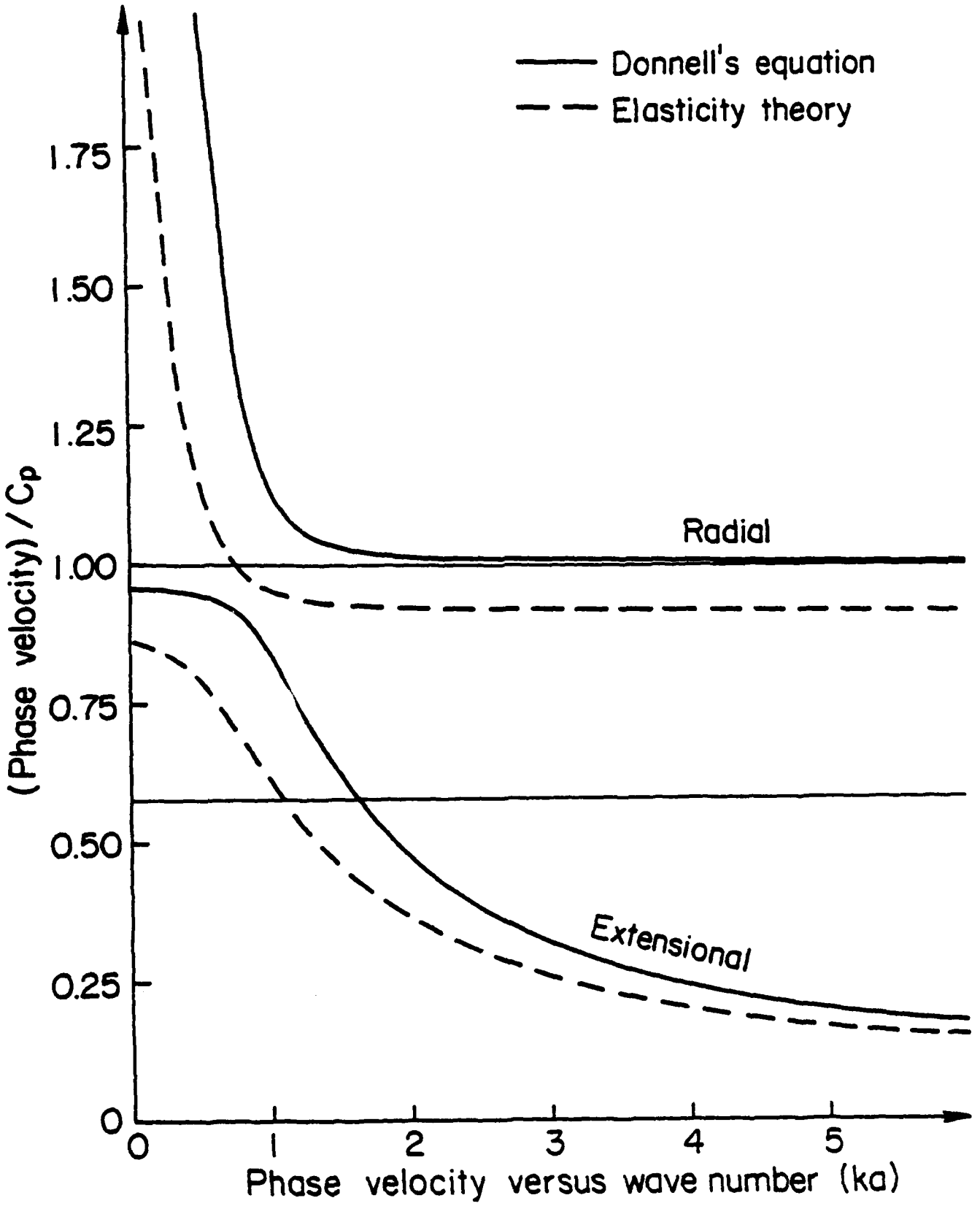

Fig. 3(b) Dispersion curves of extensional waves in a thin shell (n = 0) - phase velocity versus wave number

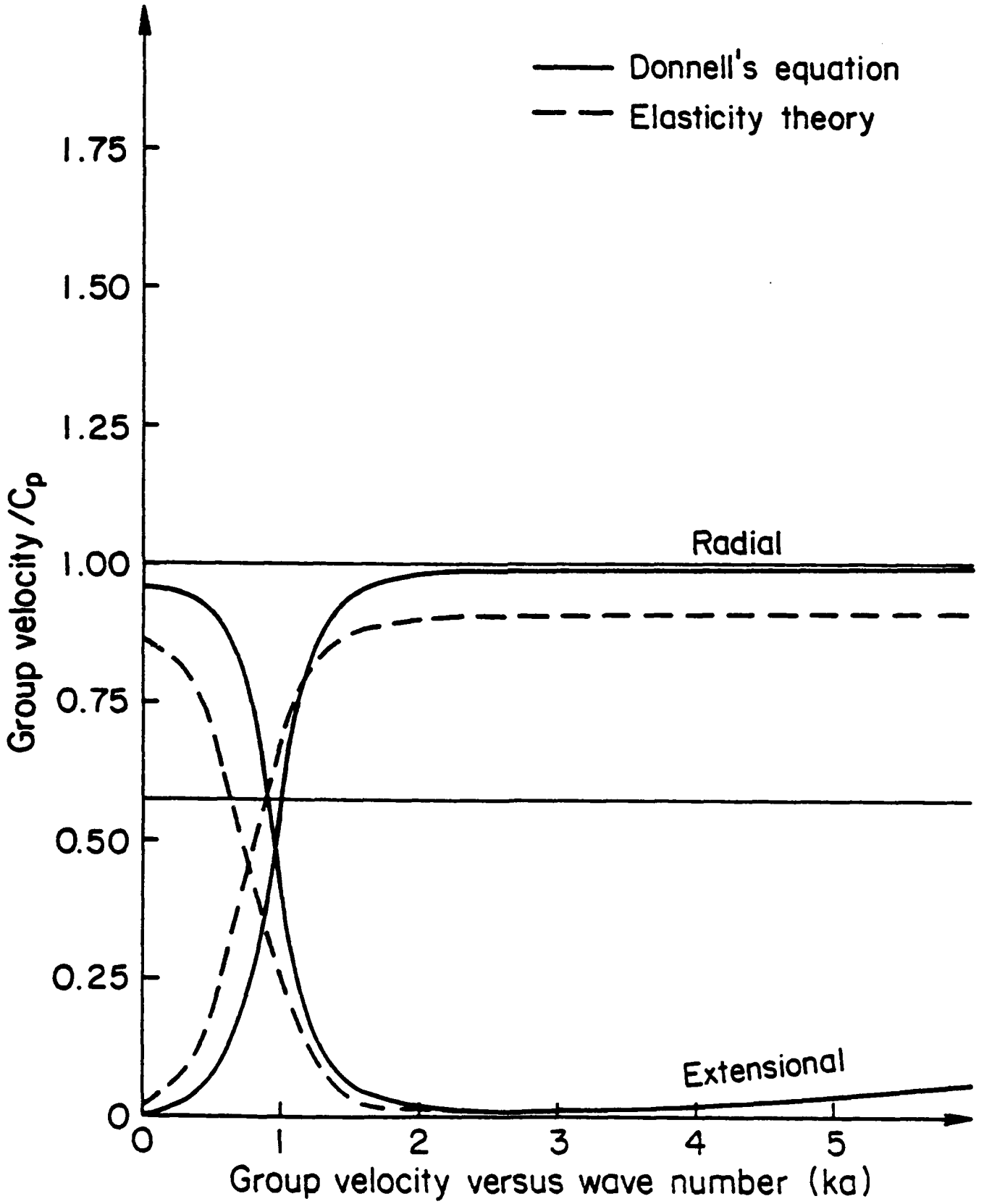

Fig. 3(c) Dispersion curves of extensional waves in a thin shell (n = 0) - group velocity versus wave number

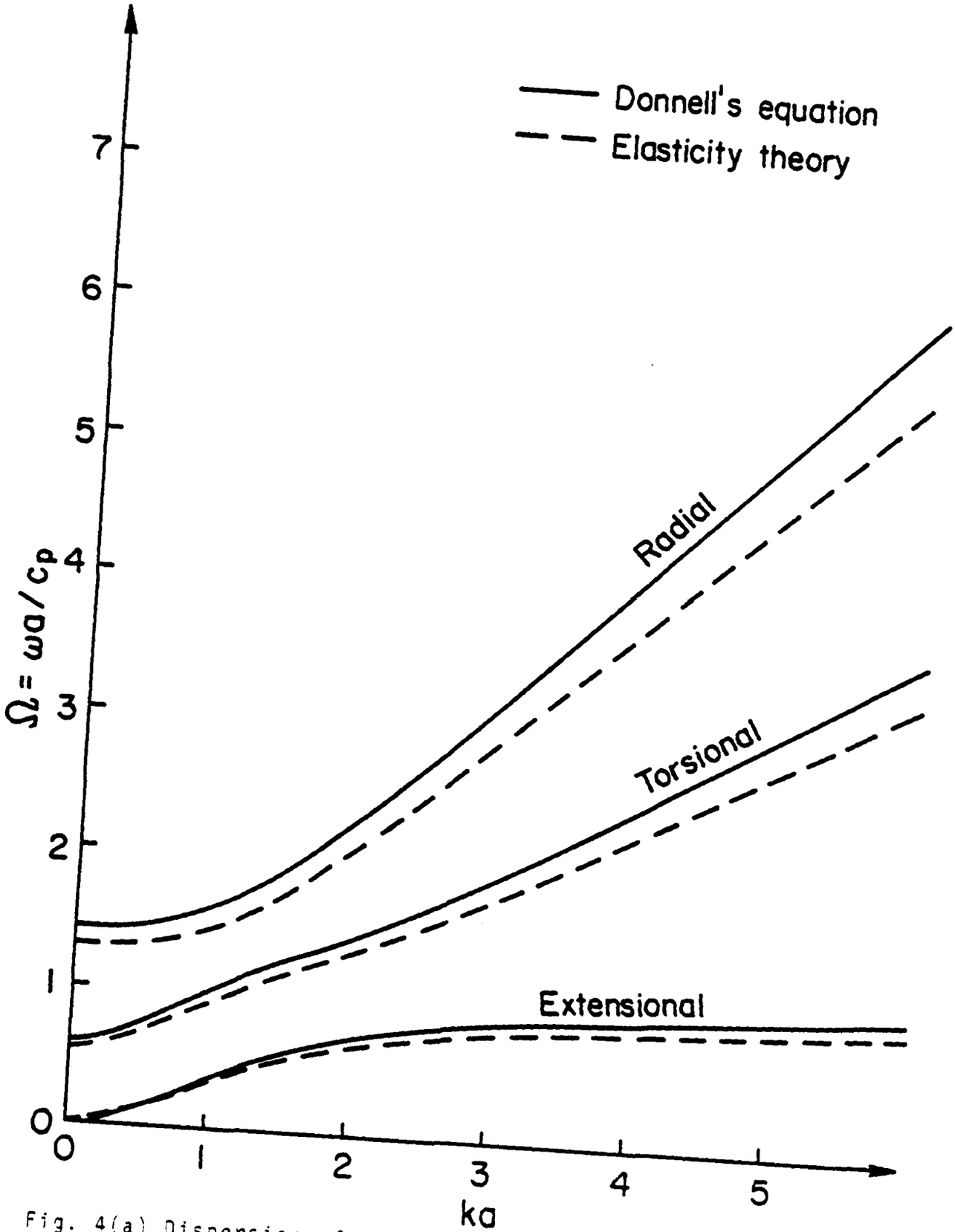

Fig. 4(a) Dispersion of flexural waves in a thin shell (n = 1)
Frequency versus wave number

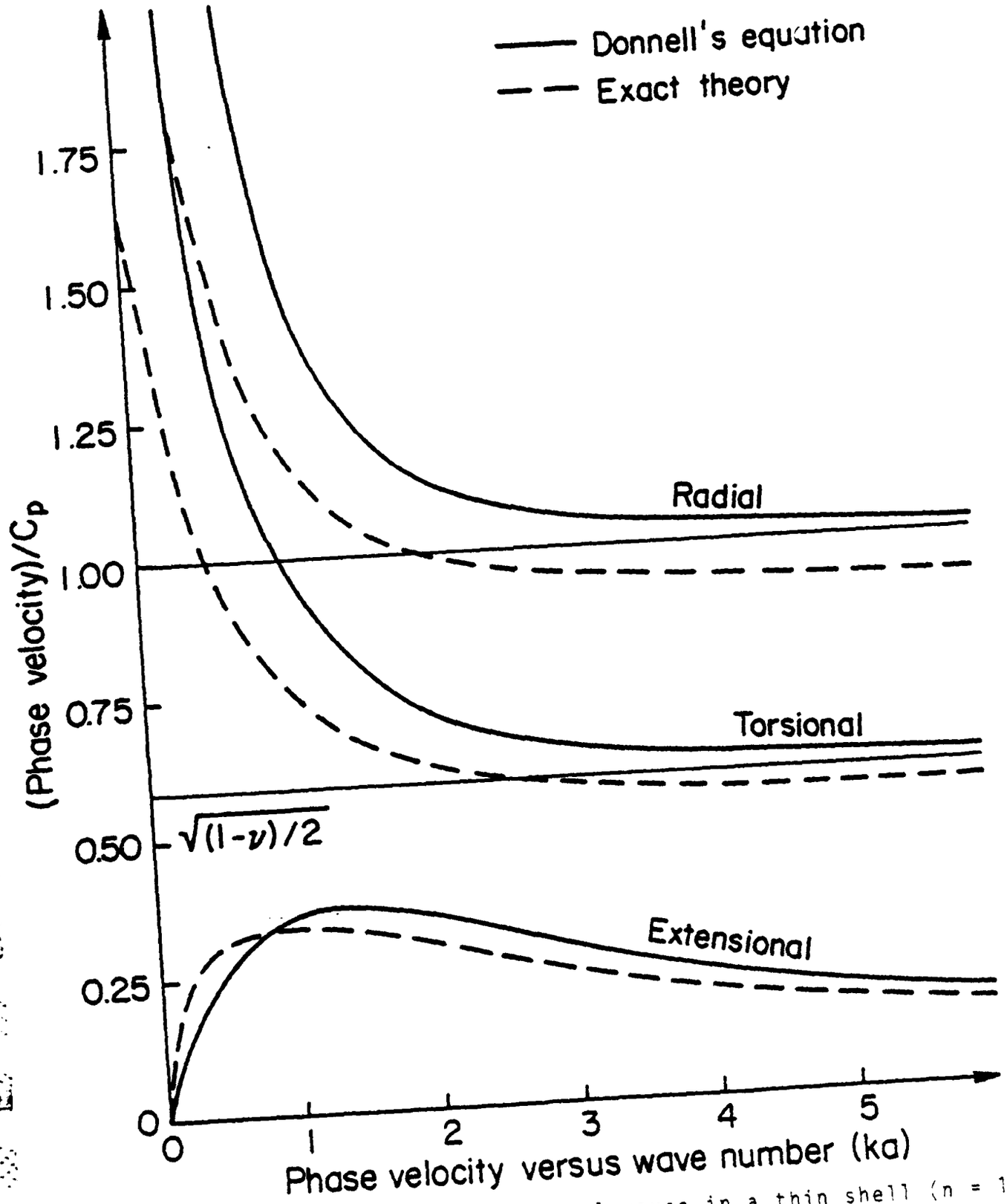

Fig. 4(b) Dispersion of flexural waves in a thin shell (n = 1)
Phase velocity versus wave number

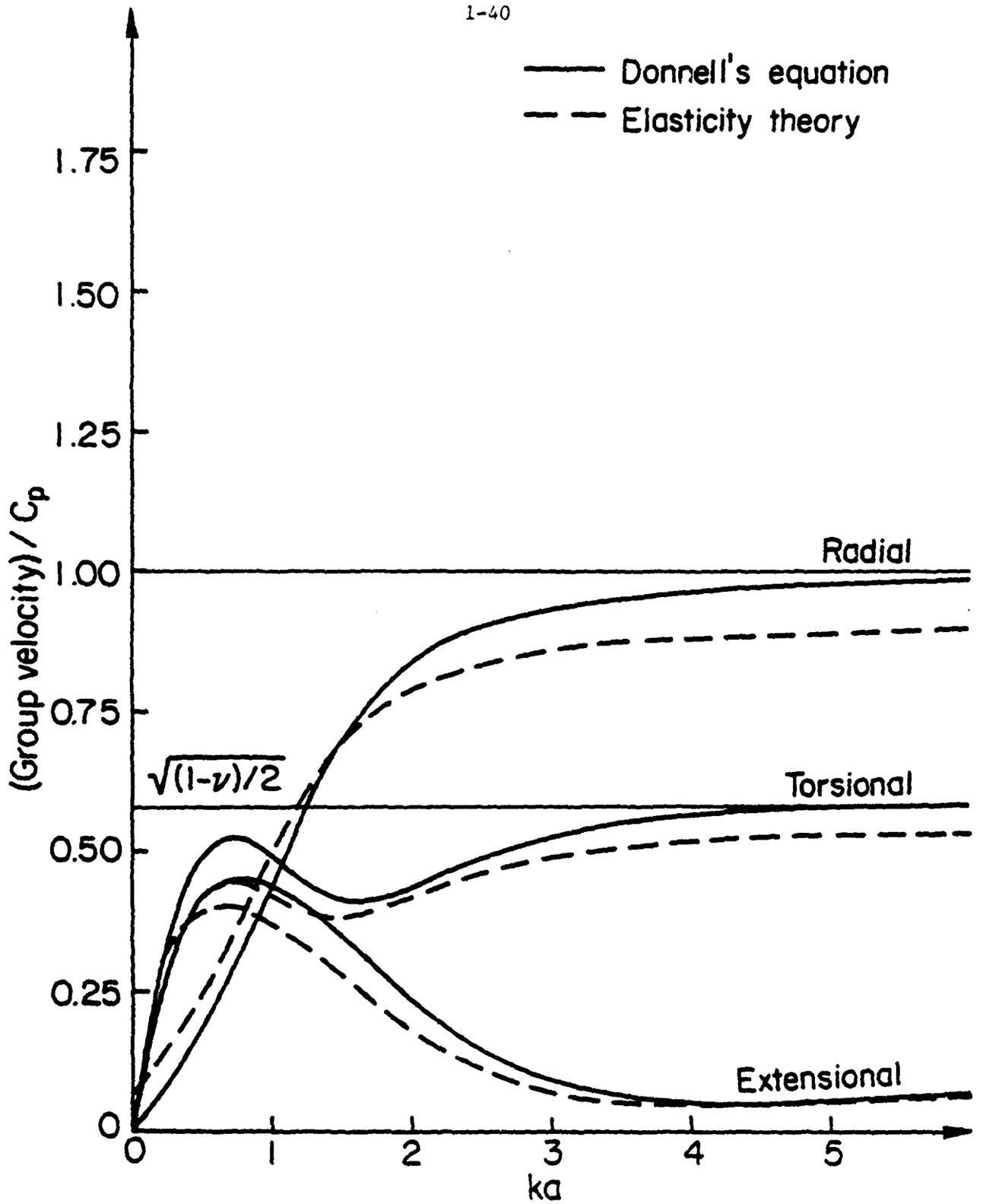

Fig. 4(c) Dispersion of flexural waves in a thin shell (n = 1)
Group velocity versus wave number

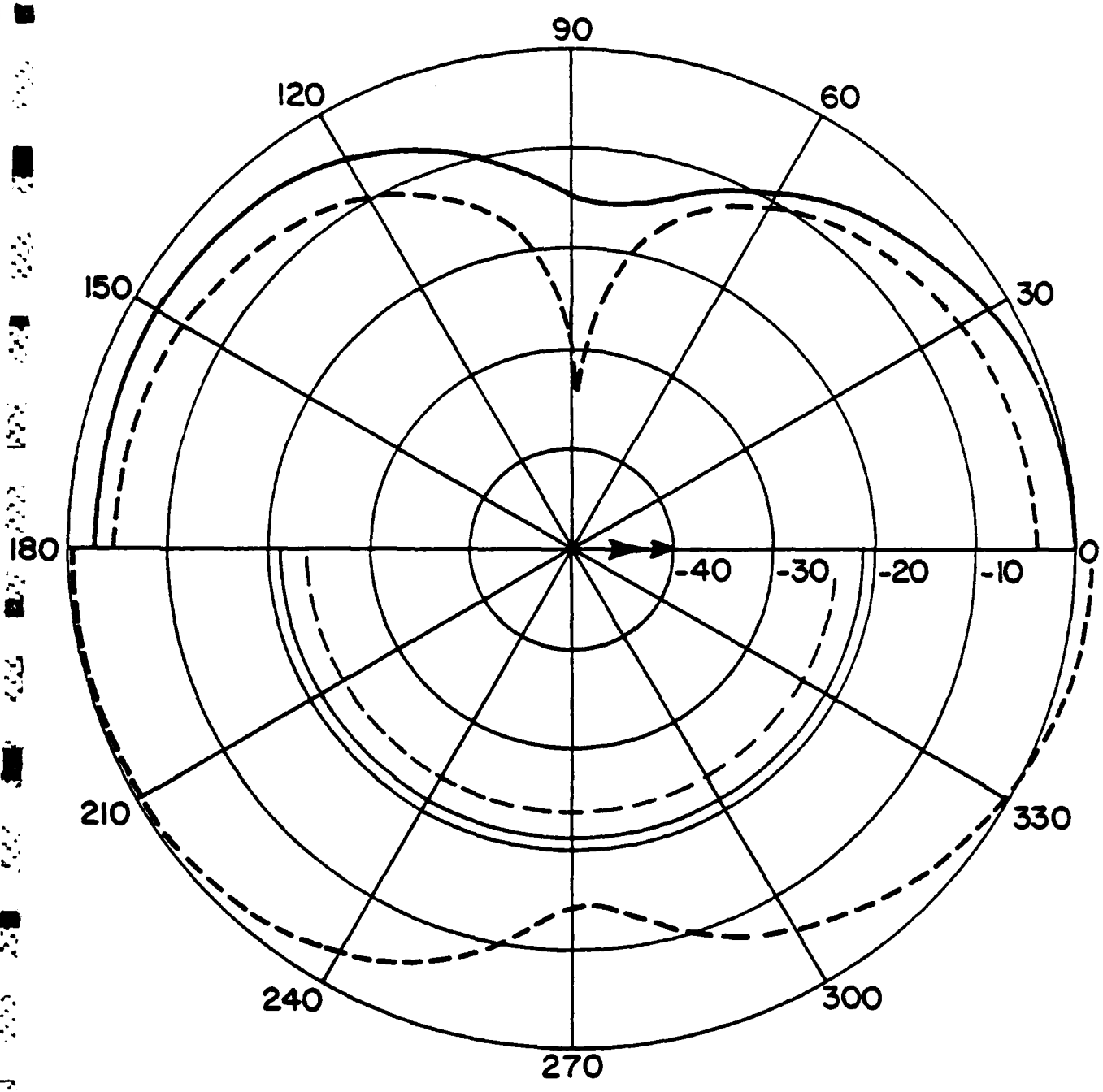

Fig. 5. Angular distribution of radiation pressure at r = 10 a for a submerged steel shell of mean radius a = 12.7 mm. The shell is driven by a point force of one dyne at r = a, θ = 0, z = 0 (the upper half circle). Solid lines are for pressure at z = 0 and dashed lines for pressure at z = 10 a. Pressure fields generated by a line force at r = a, θ = 0 are shown in the lower half circle by dotted lines. All pressures are measured in db relative to the peak reference pressure p_0 at r = 10 a, θ = 0, z = 0.

(a) Shell driven at 10 KHz, p_0 = 0.00125 dyne/cm^2.

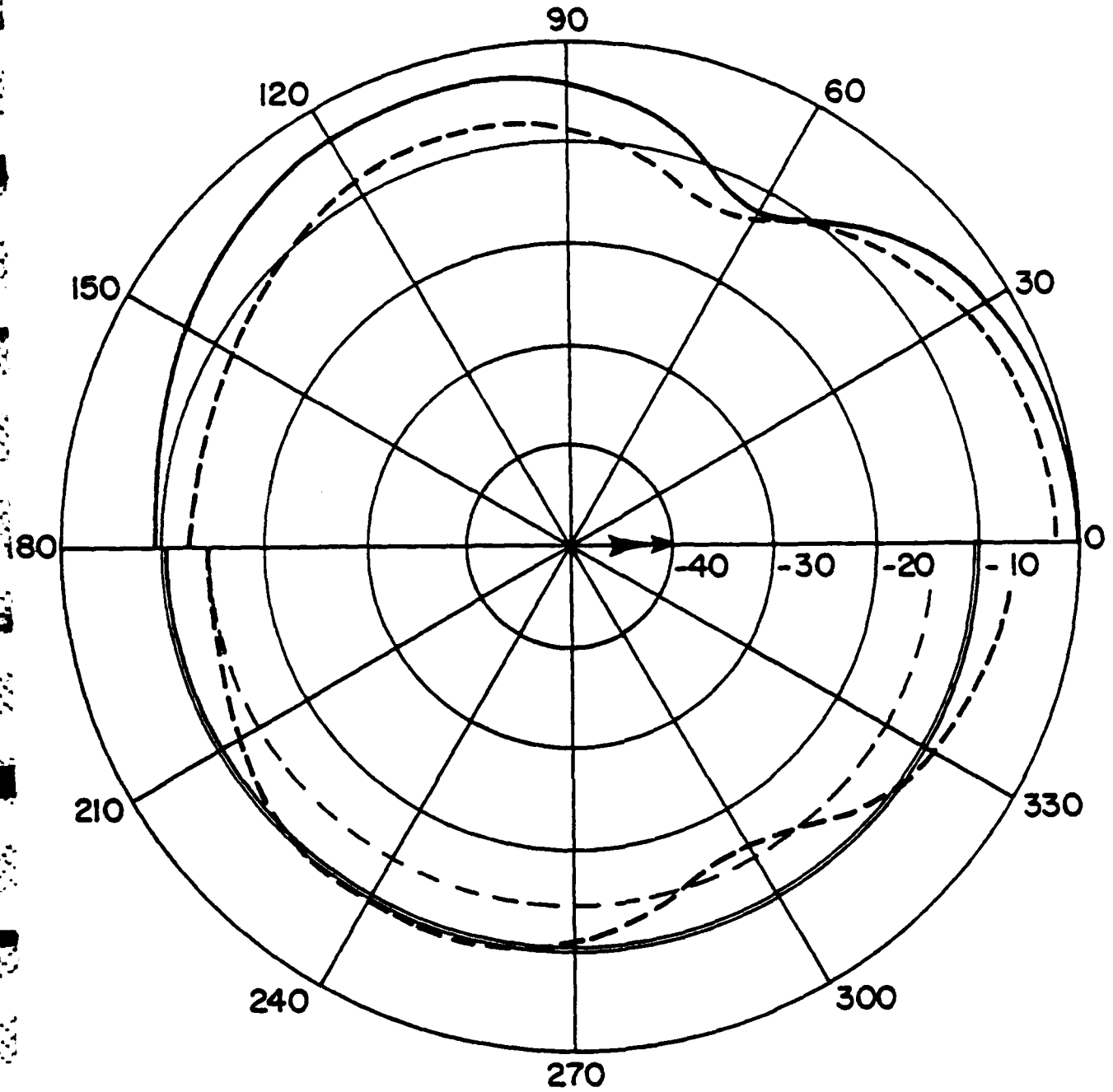

Fig. 5. Angular distribution of radiation pressure at r = 10 a for a submerged steel shell of mean radius a = 12.7 mm. The shell is driven by a point force of one dyne at r = a, θ = 0, z = 0 (the upper half circle). Solid lines are for pressure at z = 0 and dashed lines for pressure at z = 10 a. Pressure fields generated by a line force at r = a, θ = 0 are shown in the lower half circle by dotted lines. All pressures are measured in db relative to the peak reference pressure p_o at r = 10 a, θ = 0, z = 0.

(b) Shell driven at 50 KHz, p_o = 0.00614 dyne/cm^2.

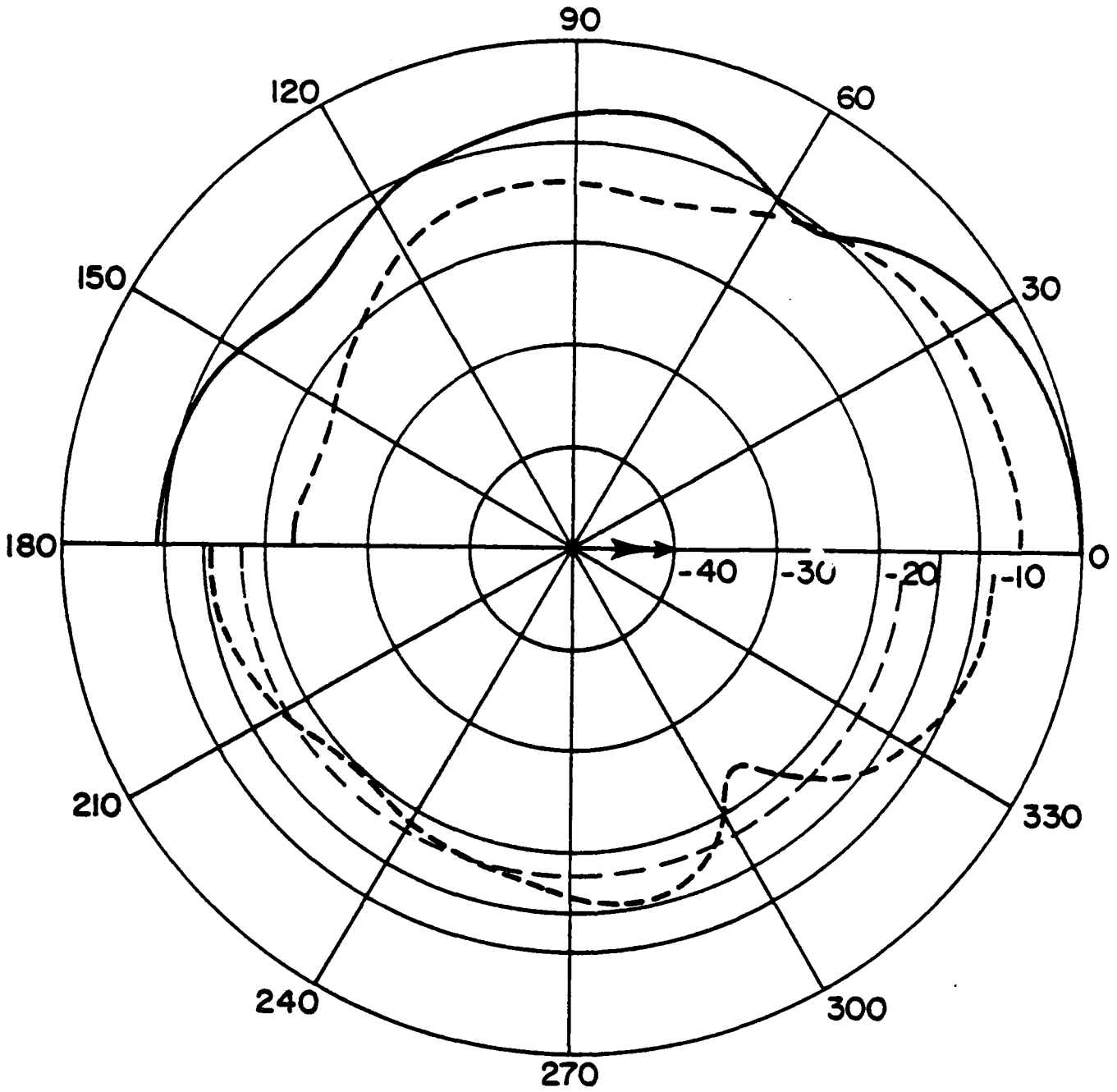

Fig. 5. Angular distribution of radiation pressure at r = 10 a for a submerged steel shell of mean radius a = 12.7 mm. The shell is driven by a point force of one dyne at r = a, θ = 0, z = 0 (the upper half circle). Solid lines are for pressure at z = 0 and dashed lines for pressure at z = 10 a. Pressure fields generated by a line force at r = a, θ = 0 are shown in the lower half circle by dotted lines. All pressures are measured in db relative to the peak reference pressure p_o at r = 10 a, θ = 0, z = 0.

(c) Shell driven at 100 KHz, p_o = 0.0131 dyne/cm^2

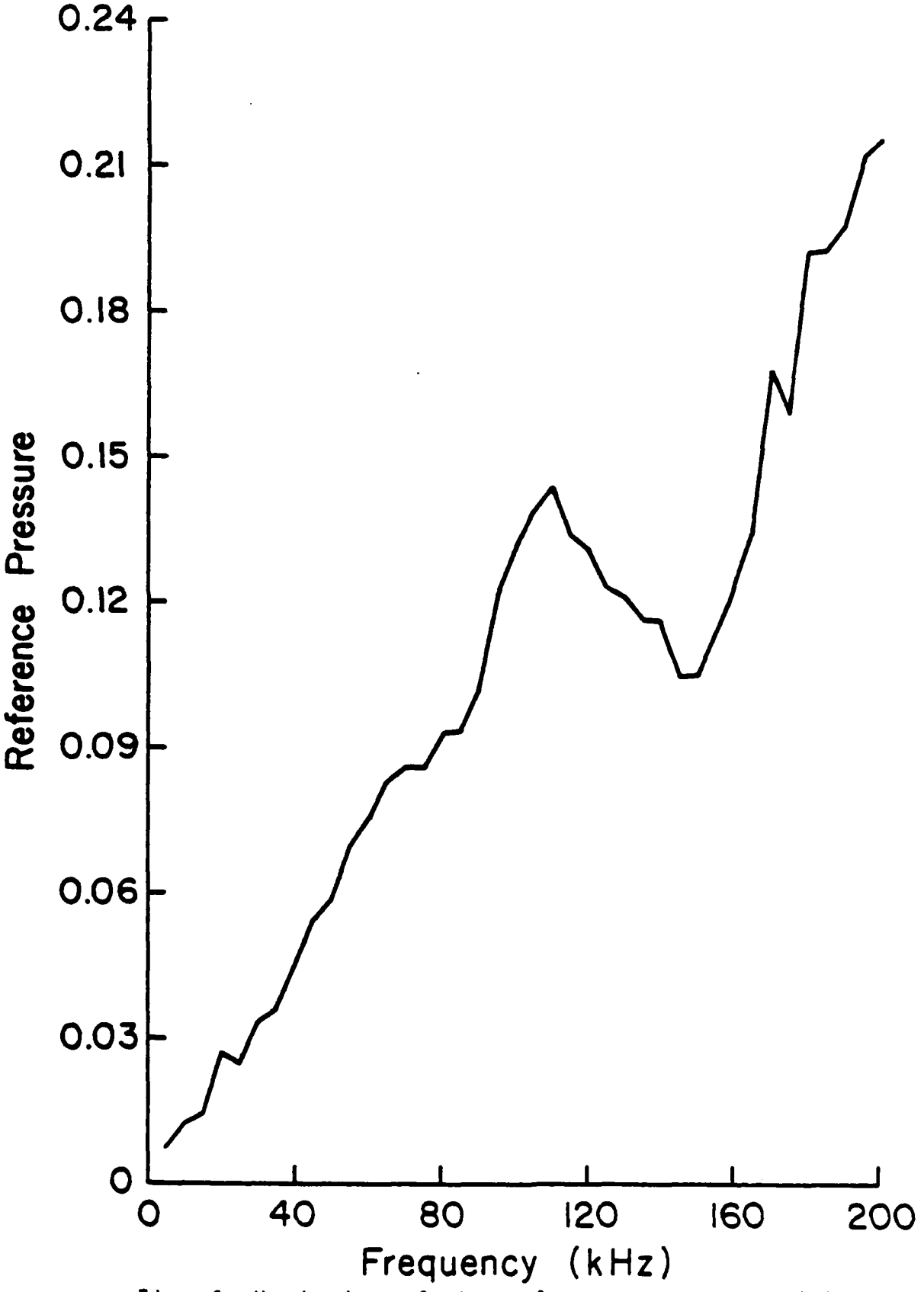

Fig. 6 Variation of the reference pressure with the driving frequency.

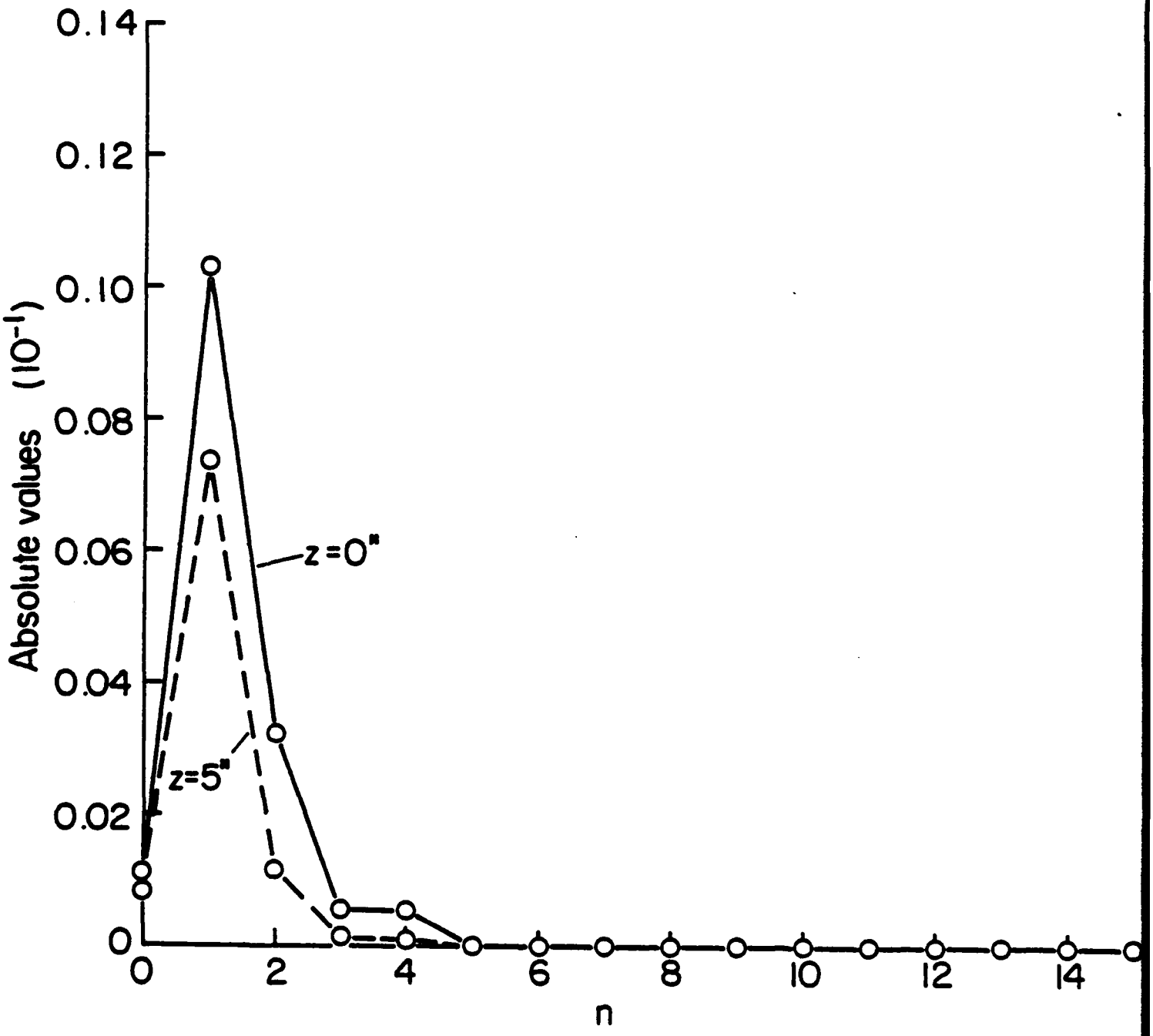

Fig. 7. Absolute values of the pressure field at (10a, 0, 0) in solid line, or at (10a, 0, 10a) in dashed lines due to each component of the circumferential mode (n = 0 to 15).
(a) Shell driven at 10 KHz.

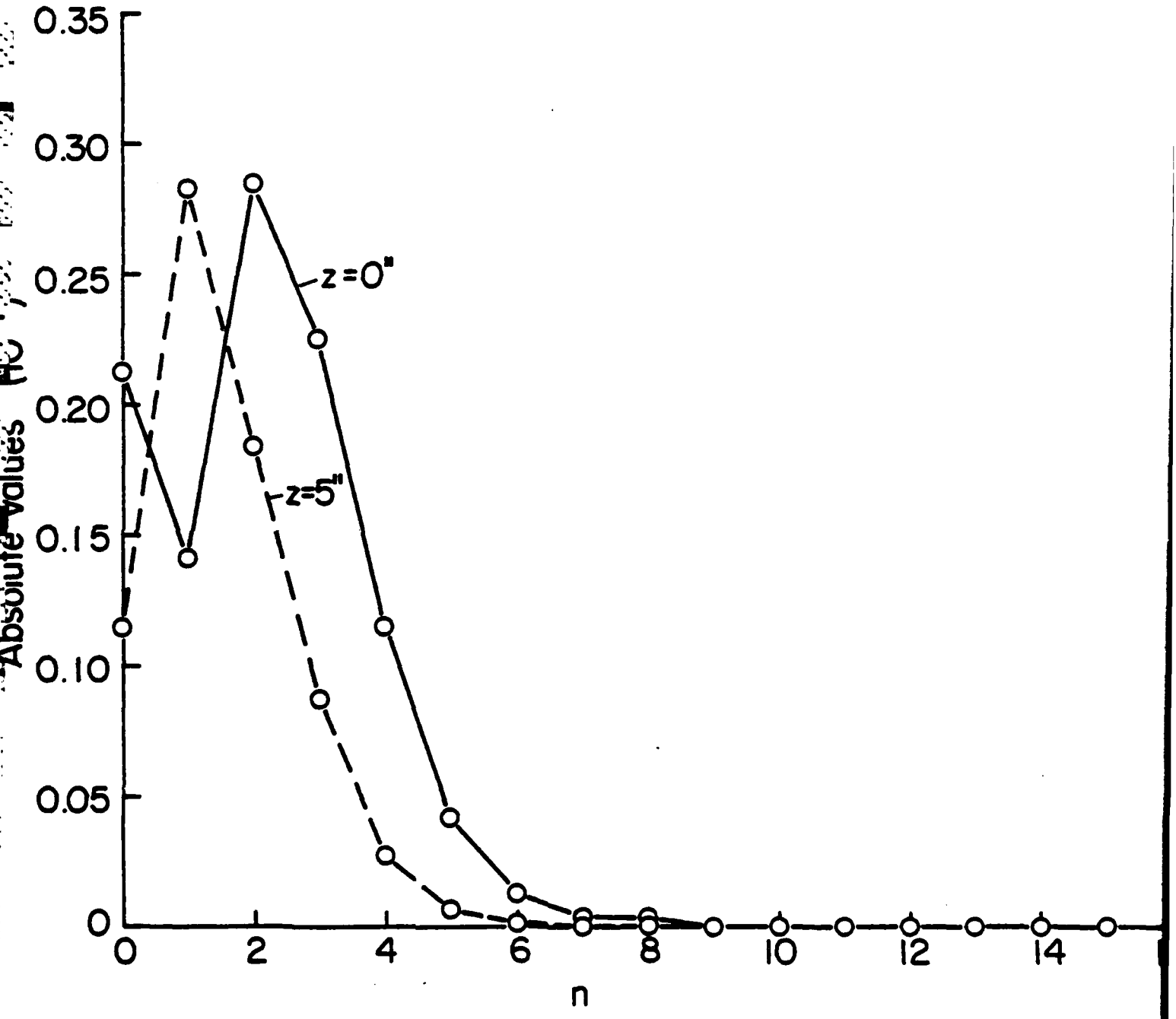

Fig. 7. Absolute values of the pressure field at (10a, 0, 0) in solid line, or at (10a, 0, 10a) in dashed lines due to each component of the circumferential mode (n = 0 to 15).

(b) Shell driven at 50 KHz.

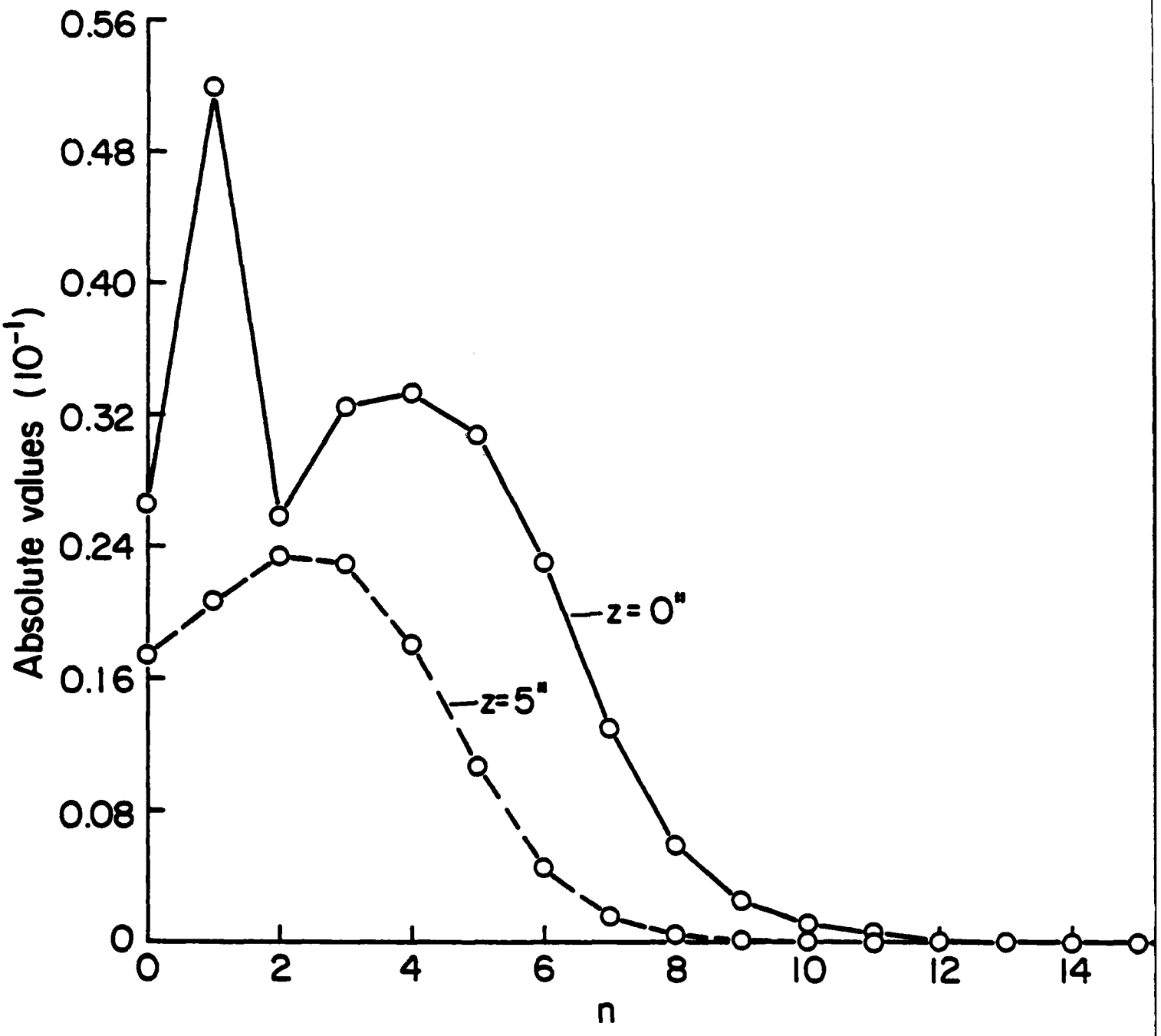

Fig. 7. Absolute values of the pressure field at (10a, 0, 0) in solid line, or at (10a, 0, 10a) in dashed lines due to each component of the circumferential mode (n = 0 to 15).

(c) Shell driven at 100 KHz.

Technical Report No. 2*

ACOUSTIC RADIATION FROM A SUBMERGED FINITE CIRCULAR CYLINDRICAL THIN SHELL DRIVEN BY A HARMONIC POINT FORCE

George C.C. Ku
Department of Theoretical and Applied Mechanics
Cornell University, Ithaca, New York 14853

Abstract

A submerged shell of finite length is driven by a concentrated force in steady state, and radiates acoustic waves into the surrounding fluid. The coupled motions of the shell and the fluid particles are expressed in terms of Fourier series, and the unknown coefficients are shown to satisfy a system of integral equations. These equations can be reduced to a system of algebraic equations and solved numerically.

---

*NRL Contract No. N00014-81-C-2122

ACOUSTIC RADIATION FROM A SUBMERGED FINITE CIRCULAR CYLINDRICAL THIN SHELL DRIVEN BY A HARMONIC POINT FORCE

George C. C. Ku

1. INTRODUCTION

The acoustic radiation of a submerged vibrator is a subject of many studied [4,9,12,15]. The importance of this topic lies in its application to the noise reduction of a vibrator and to the understanding of the dynamic response of submerged vehicles. The common approach of analyses can be divided into two categories; one is the application of Green's function integrated over the entire surface of the submerged object for a prescribed excitation at the fluid-vibrator interface [4], the other is to solve the coupled equations for the vibrator and the surrounding fluid medium [12]. The first approach eliminates the complexity of the interaction between the reactive pressure and the vibrating object. The second is usually very complicated except for those vibrators with simple geometries such as a cylindrical or spherical shell.

In this paper, a theoretical study of the acoustic radiation from a submerged finite cylindrical thin shell driven by a point harmonic force is presented. Donnell's equations of motion for the circular cylindrical thin shell are adopted to analyze the deformation of the thin shell, and the scalar wave equation for the surrounding fluid medium is used to investigate the acoustic radiation field induced by the vibration of the shell.

The cylindrical shell of finite length is sealed by two flat end caps. For simplicity, the deformation of the flat end caps are neglected in the analysis. Thus the end caps move like a rigid body synchronous to the longitudinal motion of the thin shell. The piston-like motion generates additional acoustic waves into the surrounding medium. The induced acoustic pressure field at the fluid-shell interface resulted in a reacting force for the vibration of the cylindrical thin shell. This interaction between the motion of the thin shell and the acoustic pressure renders the analysis very complex.

In the first part of this paper, Donnell's equations of motion for the cylindrical thin shell are introduced. Because of the symmetric condition of the point excitation in the circumferential direction, the displacement of the shell can be expressed in the form of Fourier series in the angular coordinate. The pressure wave field is expanded in terms of the spherical harmonic as it forms a spherical wave front in the far field. In the next section, the scalar wave equation for the pressure field is solved by using the method of Green's function for the Helmholtz equation. Through the continuity condition of the fluid particle velocity and the normal velocities of the thin shell, the pressure field is expressed in terms of the deformation of the shell. In the third section, the appropriated boundary conditions for the finite cylindrical thin shell are applied. In the fourth section, the coupled equations between the motion of the shell and the fluid medium

are reduced to an inhomogeneous integral equation for the displacements with a separable kernel. This integral equation is solved by reduction to a system of algebraic equations. Then the radiated pressure is readily obtained from the displacement of the cylindrical thin shell. In the last section, the difference between the continuous and discrete wave number is discussed. In addition, some possible modifications for the analysis of a submerged finite cylindrical thin shell with different end caps are also discussed.

2. MOTION OF A SUBMERGED FINITE CYLINDRICAL THIN SHELL

Consider a cylindrical thin shell of finite length 2L sealed with two flat, rigid caps immersed in an infinitely extended fluid medium. The cylindrical thin shell is excited by a harmonic point force F $\exp(-i\omega t)$, where F is the amplitude of the driving force, and ω is the circular frequency of the force acting in the radial direction against the inner surface of the shell. The two sealed end caps are assumed to be weightless thin plate with negligible rigidity. For simplicity, the deformation of the end caps are neglected in the following analysis. Thus the boundary conditions for the vibrating cylindrical thin shell are assumed free at both ends. It is assumed that the cylindrical shell is in steady state vibration and a time dependence of the form $\exp(-i\omega t)$ for all dependent variables is assumed throughout the derivation.

Because of the circular cylindrical geometry, Donnell's equation for cylindrical thin shell is applied to analyze the dynamic behavior of the shell. This equation of motion had been studied extensively [6,7,9,14]. The omission of higher overtones of the radial, torsional and longitudinal vibrational modes of cylindrical shell in Donnell's theory limits its applicability below the cut-off frequency of its lowest simple thickness-shear vibrational mode [3]. Thus, the present derivation is valid only at lower frequencies.

The vibration of the cylindrical shell radiates acoustic waves into the surrounding fluid medium. Because of the

finite dimension of the vibrator, the radiation is in the form of spherical waves in the far field. The radiated pressure wave is thus expressed in the spherical coordinate system. The addition theorem is used to transform the spherical wave functions into those in the cylindrical coordinates in order to match the wave field with the vibration of the cylindrical shell.

For a thin cylindrical shell, as shown in Fig. 1, the equations of motion are [8]

$$\frac{\partial^2 u}{\partial z^2} + \frac{1-\nu}{a^2}\frac{\partial^2 u}{\partial \theta^2} + \frac{1+\nu}{2a}\frac{\partial^2 v}{\partial z \partial \theta} + \frac{\nu}{a}\frac{\partial w}{\partial z} - \frac{\ddot{u}}{C_p^2}$$

$$= \frac{1-\nu^2}{Eh}\bar{p}(r,\theta,L,t)\Big|_{r=a} - \frac{1-\nu^2}{Eh}\bar{p}(r,\theta,-L,t)\Big|_{r=a} \qquad (1a)$$

$$\frac{1+\nu}{2a}\frac{\partial^2 u}{\partial z \partial \theta} + \frac{1-\nu}{2}\frac{\partial^2 v}{\partial z^2} + \frac{1}{a^2}\frac{\partial^2 v}{\partial \theta^2} + \frac{1}{a^2}\frac{\partial w}{\partial \theta} - \frac{\ddot{v}}{C_p^2} = 0 \qquad (1b)$$

$$\frac{\nu}{a}\frac{\partial u}{\partial z} + \frac{1}{a^2}\frac{\partial v}{\partial \theta} + \frac{w}{a^2} + \frac{h^2}{12}\left(\frac{\partial^2}{\partial z^2} + \frac{1}{a^2}\frac{\partial^2}{\partial \theta^2}\right)^2 w + \frac{\ddot{w}}{C_p^2}$$

$$= \frac{1-\nu^2}{Eh}\left[\frac{F\delta(z-z')\delta(\theta)}{a} - p_o(r,\theta,z)\Big|_{r=a}\right]e^{-i\omega t} \qquad (1c)$$

where r,θ,z are the cylindrical coordinates, u,v,w are the displacements in the longitudinal, tangential and radial directions, respective, ν is the Poisson ratio, E is the Young's modulus, $C_p = [E/\rho_s(1-\nu^2)]^{\frac{1}{2}}$ is the compressional wave speed of the plate, ρ_s is the mass density, h is the thickness, and a is the mean radius of the shell.

On the right-hand side of Eq. (1a), the acoustic pressure $\bar{p}(a,\theta,+L,t)$ and $\bar{p}(a,\theta,-L,t)$ at two end caps form two reacting longitudinal forces. On the right-hand side of the third equation, the first term is due to the radially driven point force and the second is the reacting acoustic pressure on the cylindrical fluid-shell interface.

Due to the symmetry of the driving point force $F\delta(\theta)/a$, the displacements u, v, w and the Kronecker delta function $\delta(\theta)$ can be expressed as

$$u(a,\theta,z,t) = \sum_{m=0}^{\infty} \bar{U}_m(z)\cos m\theta e^{-i\omega t} \tag{2a}$$

$$v(a,\theta,z,t) = \sum_{m=0}^{\infty} \bar{V}_m(z)\sin m\theta e^{-i\omega t} \tag{2b}$$

$$w(a,\theta,z,t) = \sum_{m=0}^{\infty} \bar{W}_m(z)\cos m\theta e^{-i\omega t} \tag{2c}$$

and

$$F\delta(\theta) = \frac{F}{2\pi} \sum_{m=0}^{\infty} \varepsilon_m \cos m\theta, \quad \varepsilon_m = \begin{cases} 1, & m=0 \\ 2, & \text{otherwise} \end{cases} \tag{3}$$

where the index m for the circumferential vibrational mode indicates the number in pairs of the nodal points along the circumference of the circular cylindrical shell (see Fig. 2).

Because of the spherical wave front of the radiation at far field, the pressure wave $P(r,\theta,z)$ is conveniently expressed in terms of spherical harmonics

$$p(r,\theta,z) = p(\rho,\theta,\phi) = \sum_{n=0}^{\infty} \sum_{m=0}^{n} A_{nm} P_n^m(\cos\phi) h_n^{(1)}(k\rho) \cos m\theta \tag{4}$$

where ρ,θ,ϕ are the spherical coordinates, $P_n^m(\cos\phi)$ is the Legendre function, $h_n^{(1)}(k\rho)$ is the spherical Hankel function of the first kind [1], A_{nm} are the unknown coefficients and

$$\rho = \sqrt{r^2+z^2} \quad , \quad \cos\phi = \frac{z}{\sqrt{r^2+z^2}} \quad , \quad k = \frac{\omega}{C_w} \quad . \tag{5}$$

Substituting Eqs. (2), (3) and (4) into Eq. (1) and utilizing the orthogonality properties of the sinusoidal functions, we have

$$\frac{d^2\bar{U}_m}{dz^2} - \frac{1-\nu}{2a^2}m^2\bar{U}_m + \frac{1+\nu}{2a} m \frac{d\bar{V}_m}{dz} + \frac{\nu}{a}\frac{d\bar{W}_m}{dz} + \frac{\omega^2}{C_p^2}\bar{U}_m$$

$$= \frac{1-\nu^2}{Eh^2a}\delta(z-L)\sum_{n=0}^{\infty} A_{nm}\int_0^a \left[P_n^m\left(\frac{z}{\sqrt{r^2+z^2}}\right) h_n^{(1)}(k\sqrt{r^2+z^2})\right]_{z=L} r\,dr$$

$$- \frac{1-\nu^2}{Eh^2a}\delta(z+L)\sum_{n=0}^{\infty} A_{nm}\int_0^a \left[P_n^m\left(\frac{z}{\sqrt{r^2+z^2}}\right) h_n^{(1)}(k\sqrt{r^2+z^2})\right]_{z=-L} r\,dr \tag{6a}$$

$$\frac{1+\nu}{2a}m\frac{d\bar{U}_m}{dz} - \frac{1-\nu}{2}\frac{d^2\bar{V}_m}{dz^2} + \frac{m^2}{a^2}\bar{V}_m + \frac{m}{a^2}\bar{W}_m - \frac{\omega^2}{C_p^2}\bar{V}_m = 0 \tag{6b}$$

$$\frac{\nu}{a}\frac{d\bar{U}_m}{dz} + \frac{m}{a^2}\bar{V}_m + \frac{\bar{W}_m}{a^2} + \frac{h^2}{12}\left(\frac{d^2}{dz^2} - \frac{m^2}{a^2}\right)^2\bar{W}_m - \frac{\omega^2}{C_p^2}\bar{W}_m$$

$$= \frac{1-\nu^2}{Eh}\frac{\varepsilon_m}{2\pi}\frac{F\delta(z-z')}{a} - \frac{1-\nu^2}{Eh}[H(z+L)-H(z-L)]\sum_{n=0}^{\infty} \cdot$$

$$\cdot A_{nm} P_n^m\left(\frac{z}{\sqrt{a^2+z^2}}\right) h_n^{(1)}(k\sqrt{a^2+z^2}) \tag{6c}$$

where H(z+L), H(z-L) in Eq. (6c) are the Heaviside step functions and the equivalent reacting pressures in Eq. (6a) are obtained by integration over a surface area substended by a small angle $\Delta\theta$ on both end caps.

To solve the simultaneous equations of motion (6), the axial dependence of the displacements in Eqs. (2) are assumed to be

$$\bar{U}_m(z) = \int_{-\infty}^{\infty} U_m(\lambda) e^{i\lambda z} d\lambda$$

$$\bar{V}_m(z) = \int_{-\infty}^{\infty} V_m(\lambda) e^{i\lambda z} d\lambda \qquad (7)$$

$$\bar{W}_m(z) = \int_{-\infty}^{\infty} W_m(\lambda) e^{i\lambda z} d\lambda$$

where λ is the wave number in the axial direction. The coefficients $U_m(\lambda)$, $V_M(\lambda)$ and $W_m(\lambda)$ in Eq. (7) can be obtained by using the generalized Fourier transform

$$U_m(\lambda) = \frac{1}{2\pi}\int_{-L}^{L} \bar{U}_m(z) e^{-i\lambda z} ez$$

$$V_m(\lambda) = \frac{1}{2\pi}\int_{-L}^{L} \bar{V}_m(z) e^{-i\lambda z} dz \qquad (8)$$

$$W_m(\lambda) = \frac{1}{2\pi}\int_{-L}^{L} \bar{W}_m(z) e^{-i\lambda z} dz \quad .$$

Substituting Eq. (7) into Eq. (6) and utilizing the generalized Fourier transform (8), we have the Donnell's equations (1) expressed in the wave number domain (m,λ)

$$-\lambda^2 U_m - \frac{1-\nu}{2a^2}m^2 U_m + im\lambda\frac{1+\nu}{2a}V_m + i\lambda\frac{\nu}{a}W_m + \frac{\omega^2}{C_p{}^2}U_m$$

$$= \frac{1-\nu^2}{ah^2E}e^{-i\lambda L}\sum_{n=0}^{\infty}A_{nm}\int_o^a P_n{}^m\left(\frac{L}{\sqrt{\xi^2+L^2}}\right)h_n{}^{(1)}(k\sqrt{\xi^2+L^2})\xi d\xi$$

$$- \frac{1-\nu^2}{ah^2E}e^{i\lambda L}\sum_{n=0}^{\infty}A_{nm}\int_o^a P_n{}^m\left(\frac{-L}{\sqrt{\xi^2+L^2}}\right)h_n{}^{(1)}(k\sqrt{\xi^2+L^2})\xi d\xi$$

$$+ \frac{1}{2\pi}\left[\left(-\frac{d\bar{U}_m}{dz} - i\lambda\bar{U}_m - \frac{1+\nu}{2a}m\bar{V}_m - \frac{\nu}{a}\bar{W}_m\right)e^{-i\lambda z}\right]_{z=-L}^{z=L} \qquad (9a)$$

$$im\lambda\frac{1+\nu}{2a}U_m + \frac{1-\nu}{2}\lambda^2 V_m + \frac{m^2}{a^2}V_m + \frac{m}{a^2}W_m - \frac{\omega^2}{C_p{}^2}V_m$$

$$= \frac{1}{2\pi}\left[\left(-m\frac{1+\nu}{2a}\bar{U}_m + \frac{1-\nu}{2}\frac{d\bar{V}_m}{dz} + i\lambda\frac{1-\nu}{2}\bar{V}_m\right)e^{-i\lambda z}\right]_{z=-L}^{z=L} \qquad (9b)$$

$$i\lambda\frac{\nu}{a}U_m + \frac{m}{a^2}V_m + \frac{W_m}{a^2} + \frac{h^2}{12}\left(\lambda^2 + \frac{m^2}{a^2}\right)^2 W_m - \frac{\omega^2}{C_p{}^2}W_m$$

$$= \frac{1-\nu^2}{hE}\frac{\epsilon_m F}{2\pi a}e^{-i\lambda z'} - \frac{1-\nu^2}{hE}\sum_{n=0}^{\infty}A_{nm}\int_{-L}^{L}P_n^m\left(\frac{\xi}{\sqrt{a^2+\xi^2}}\right)$$

$$+ \frac{1}{2\pi}\left[\left(-\frac{\nu}{a}\bar{U}_m - \frac{h^2}{12}\frac{d^3\bar{W}_m}{dz^3} - i\lambda\frac{h^2}{12}\frac{d^2\bar{W}_m}{dz^2} + \lambda^2\frac{h^2}{12}\frac{d\bar{W}_m}{dz}\right.\right.$$

$$\left.\left. + i\lambda^3\frac{h^2\bar{W}_m}{12} + \frac{m^2h^2}{6a^2}\frac{d\bar{W}_m}{dz} + i\lambda\frac{m^2h^2\bar{W}_m}{6a^2}\right)e^{-i\lambda z}\right]_{z=-L}^{z=L} \qquad (9c)$$

Replacing the expression $[....]_{z=-L}^{z=L}$ in the right hand side of Eq. (9) by the integral defined in Eq. (7)

$$\bar{U}_m(\pm L) = \int_{-\infty}^{\infty}U_m(\lambda)e^{\pm i\lambda L}d\lambda \qquad (10a)$$

and

$$\left[\frac{d^{\ell}\bar{U}_m}{dz^{\ell}}e^{-i\lambda z}\right]_{z=L} - \left[\frac{d^{\ell}\bar{U}_m}{dz^{\ell}}e^{-i\lambda z}\right]_{z=-L} = 2i\int_{-\infty}^{\infty}(i\xi)^{\ell}U_m(\xi)\sin[(\lambda-\xi)L]d\xi \tag{10b}$$

we have Eq. (9) rewritten in the matrix form as

$$[S]\{U\} = [Q]\{A\} + \{B\} + \frac{1}{2\pi}\int_{-\infty}^{\infty}[S'(\lambda,\xi)]\{U(\xi)\}\sin[(\lambda-\xi)L]d\xi \tag{10c}$$

where

$$[S] = \begin{bmatrix} -\lambda^2 - \frac{1-\nu}{2a^2}m^2 + \frac{\omega^2}{C_p^{\,2}} & im\lambda\frac{1+\nu}{2a} & i\lambda\frac{\nu}{a} \\ im\lambda\frac{1+\nu}{2a} & \frac{1-\nu}{2}\lambda^2 + \frac{m^2}{a^2} - \frac{\omega^2}{C_p^{\,2}} & \frac{m}{a^2} \\ i\lambda\frac{\nu}{a} & \frac{m}{a^2} & \frac{1}{a^2} + \frac{h^2}{12}(\lambda^2+\frac{m^2}{a^2})^2 - \frac{\omega^2}{C_p^{\,2}} \end{bmatrix} \tag{11a}$$

$$[Q] = \begin{bmatrix} P_o^{\,m} & P_1^{\,m} & P_2^{\,m} & P_3^{\,m} & \cdots\cdots \\ 0 & 0 & 0 & 0 & \cdots\cdots \\ q_o^{\,m} & q_1^{\,m} & q_2^{\,m} & q_3^{\,m} & \cdots\cdots \end{bmatrix} \tag{11b}$$

$$[S'(\lambda,\xi)] = \begin{bmatrix} -2(\lambda+\xi) & im\frac{1+\nu}{a} & 2i\,\frac{\nu}{a} \\ im\frac{1+\nu}{a} & (1-\nu)(\lambda+\xi) & 0 \\ 2i\frac{\nu}{a} & 0 & \frac{h^2}{6}\left[(\lambda+\xi)(\lambda^2+\xi^2)+\frac{2m^2}{a^2}(\lambda+\xi)\right] \end{bmatrix} \quad (11c)$$

$$\{U\} = \begin{Bmatrix} U_m \\ V_m \\ W_m \end{Bmatrix}, \qquad \{A\} = \begin{Bmatrix} A_{om} \\ A_{1m} \\ A_{2m} \\ \vdots \end{Bmatrix}, \qquad \{B\} = \begin{Bmatrix} 0 \\ 0 \\ \frac{1}{2\pi}\frac{-\nu^2}{ahE}F\varepsilon_m e^{-i\lambda z'} \end{Bmatrix} \quad (11d,e,f)$$

$$P_n^m = \frac{1-\nu^2}{ah^2E}\left[e^{-i\lambda L}\int_o^a P_n^m\left(\frac{L}{\sqrt{\xi^2+L^2}}\right)h_n^{(1)}(k\sqrt{\xi^2+L^2})\xi d\xi \right.$$

$$\left. - e^{i\lambda L}\int_o^a P_n^m\left(\frac{-L}{\sqrt{\xi^2+L^2}}\right)h_n^{(1)}(k\sqrt{\xi^2+L^2})\xi d\xi\right] \quad (11g)$$

$$q_n^m = -\frac{1-\nu^2}{hE}\int_{-L}^{L} P_n^m\left(\frac{\xi}{\sqrt{a^2+\xi^2}}\right)h_n^{(1)}(k\sqrt{a^2+\xi^2})e^{-i\lambda\xi}d\xi \quad (11h)$$

3. ACOUSTIC WAVES IN THE FLUID MEDIUM

The radial motion of the vibrating cylindrical shell associated with the longitudinal motion of the end caps generate a radiating pressure field in the surrounding fluid medium. If this disturbance in the inviscid fluid medium is infestimal, the pressure field $P(\rho,\theta,\phi,t)$ satisfies the linear wave equation [2]

$$\nabla^2 P(\rho,\theta,\phi,t) = \frac{1}{C_w^2}\ddot{P}(\rho,\theta,\phi,t) \quad , \quad C_w = \sqrt{\lambda_w/\rho_w} \tag{12}$$

where ρ,θ,ϕ are the spherical coordinates, ∇^2 is the Laplacian operator and C_w, ρ_w, λ_w are the wave speed, mass density and Lame's constant of the fluid medium, respectively. In steady state

$$P(\rho,\theta,\phi,t) = p(\rho,\theta,\phi)e^{-i\omega t} \quad , \tag{13}$$

Eq. (12) is transformed into Helmhortz equation

$$\nabla^2 p(\rho,\theta,\phi) + k^2 p(\rho,\theta,\phi) = 0 \quad , \; k = \omega/C_w \tag{14}$$

subjected to the boundary conditions at the fluid-shell interfaces where continuity requires the shell and fluid particle velocities to be equal.

Equation (14) is solved by the method of Green's function so as to include the yet undetermined boundary conditions at the

shell surface. Green's function satisfies an inhomogeneous three dimensional equation,

$$\nabla^2 G(\underset{\sim}{r}|\underset{\sim}{r}_o) + k^2 G(\underset{\sim}{r}|\underset{\sim}{r}_o) = \delta(\underset{\sim}{r} - \underset{\sim}{r}_o) \quad . \tag{15}$$

In an unbounded medium [10], the solution is

$$G(\underset{\sim}{r}|\underset{\sim}{r}_o) = \frac{-1}{4\pi} \frac{e^{ikR}}{R}$$

where

$$R^2 = r^2 + r_o^2 - 2rr_o \cos(\theta-\theta_o) + (z - z_o)^2$$

$$= \rho^2 \sin^2\phi + \rho_o^2 \sin^2\phi_o - 2\rho\rho_o \sin\phi \sin\phi_o \cos(\theta-\theta_o)$$

$$+(\rho \cos\phi - \rho_o \cos\phi_o)^2 \tag{17}$$

is the distance between the source point $(\rho_o,\theta_o,\phi_o)[(r_o,\theta_o,z_o)$ in the cylindrical coordinate] and the observation point $(\rho,\theta,\phi)[(r,\theta,z)$ in the cylindrical coordinate]. The Green's function $G(\underset{\sim}{r}|\underset{\sim}{r}_o)$ of Eq. (16) can be expanded in terms of the spherical harmonics [11]

$$G(\underset{\sim}{r}|\underset{\sim}{r}_o) = \frac{-1}{4\pi} \frac{e^{ikR}}{R} = -\frac{ik}{4\pi} h_o^{(1)}(kR) = -\frac{ik}{4\pi} \sum_{n=0}^{\infty} (2n+1) \sum_{m=0}^{n} \varepsilon_m \frac{(n-m)!}{(n+m)!} \cdot$$

$$\cdot P_n^m(\cos\phi_o) P_n^m(\cos\phi) \begin{cases} (j_n(kr_o) h_n^{(1)}(kr), & r \geq r_o \\ (j_n(kr) h_n^{(1)}(kr_o), & r < r_o \end{cases} \tag{18}$$

To obtain the solution of Eq. (14), we multiply Eq. (14) by $G(\underset{\sim}{r}|\underset{\sim}{r}_o)$ and Eq. (15) by $p(\underset{\sim}{r})$ and subtract, exchanging $\underset{\sim}{r}$ for $\underset{\sim}{r}_o$ at the same time

$$G(\underset{\sim}{r}|\underset{\sim}{r}_o)\nabla_o^2 p(\underset{\sim}{r}_o) - p(\underset{\sim}{r}_o)\nabla_o^2 G(\underset{\sim}{r}|\underset{\sim}{r}_o) = p(\underset{\sim}{r}_o)\delta(\underset{\sim}{r}_o-\underset{\sim}{r}) \quad . \qquad (19)$$

Integrating this equation over all the source coordinate $\underset{\sim}{r}_o$, we obtain

$$\iiint_{V_o} [G(\underset{\sim}{r}|\underset{\sim}{r}_o)\nabla_o^2 p(\underset{\sim}{r}_o) - p(\underset{\sim}{r}_o)\nabla_o^2 G(\underset{\sim}{r}|\underset{\sim}{r}_o)]dV = \begin{cases} p(\underset{\sim}{r}) & \underset{\sim}{r} \text{ outside the shell} \\ 0 & \underset{\sim}{r} \text{ inside the shell} \end{cases} \qquad (20)$$

Then tne Green's Theorem is used to simplify the volume integral of Eq. (20) into a surface integral

$$\oint_{S_o} [-G(\underset{\sim}{r}|\underset{\sim}{r}_o)\nabla_o p(\underset{\sim}{r}_o) + p(\underset{\sim}{r}_o)\nabla_o G(\underset{\sim}{r}|\underset{\sim}{r}_o)]\cdot d\underset{\sim}{A}_o = \begin{cases} p(\underset{\sim}{r}) & \underset{\sim}{r} \text{ outside the shell} \\ 0 & \underset{\sim}{r} \text{ inside the shell} \end{cases} \qquad (21)$$

The gradient of the surface element $d\underset{\sim}{A}_o$ is pointing outward from the cylindrical shell into the infinitely extended fluid medium.

Since the fluid-shell interface are made of three distinct surfaces of the vibrating body, one cylindrical shell and two flat end caps, the total surface area s_o of Eq. (21) is then subdivided as

$$p(\underset{\sim}{r}) = [\int_{-L}^{L}\int_{0}^{2\pi} \underset{\sim}{e}_r a d\theta_o dz_o + \int_{0}^{a}\int_{0}^{2\pi} \underset{\sim}{e}_z r_o d\theta_o dr_o + \int_{0}^{a}\int_{0}^{2\pi} (-\underset{\sim}{e}_z) r_o d\theta_o dr_o] \cdot$$

$$\cdot [-G(\underset{\sim}{r}|\underset{\sim}{r}_o)\nabla_o p(\underset{\sim}{r}_o) + p(\underset{\sim}{r}_o)\nabla_o G(\underset{\sim}{r}|\underset{\sim}{r}_o)]$$

$$= \frac{1}{4\pi}\{ \int_{-L}^{L}\int_{0}^{2\pi} \left[\frac{e^{ikR}}{R} \frac{\partial p(\underset{\sim}{r}_o)}{\partial r_o} - p(\underset{\sim}{r}_o) \frac{\partial}{\partial r_o}\left(\frac{e^{ikR}}{R}\right)\right]_{r_o=a} a d\theta_o dz_o$$

$$+ \int_{0}^{a}\int_{0}^{2\pi} \left[\frac{e^{ikR}}{R} \frac{\partial p(\underset{\sim}{r}_o)}{\partial z_o} - p(\underset{\sim}{r}_o)\frac{\partial}{\partial z_o}\left(\frac{e^{ikR}}{R}\right)\right]_{z_o=L} r_o d\theta_o dr_o$$

$$+ \int_{0}^{a}\int_{0}^{2\pi} \left[\frac{e^{ikR}}{R} \frac{\partial p(\underset{\sim}{r}_o)}{\partial z_o} - p(\underset{\sim}{r}_o)\frac{\partial}{\partial z_o}\left(\frac{e^{ikR}}{R}\right)\right]_{z_o=-L} r_o d\theta_o dr_o \qquad (22)$$

The pressure p is related to the fluid particle velocities $\underset{\sim}{v}_f$ by the balance of momentum [2]

$$-\nabla p = \rho_w \dot{\underset{\sim}{v}}_f \qquad (23)$$

and the fluid particle velocities are equal to the normal components of the velocities of the shell at the fluid-shell interface s_o

$$[v_f]_{r_o=a,\,\underset{\sim}{n}=\underset{\sim}{e}_r} = \dot{w}(a,\theta_o,z_o)$$

$$[v_f]_{z=L,\,\underset{\sim}{n}=\underset{\sim}{e}_z} = \dot{u}(a,\theta_o,z_o) \qquad (24)$$

$$[v_f]_{z=-L,\,\underset{\sim}{n}=-\underset{\sim}{e}_z} = -\dot{u}(a,\theta_o,z_o) \quad .$$

The gradient of pressure $\nabla_o p(\underset{\sim}{r}_o)$ in Eq. (22) is then written as

$$\left[\frac{\partial p(\underset{\sim}{r}_o)}{\partial r_o}\right]_{r_o=a} = \rho_w \omega^2 [w(a,\theta_o,z_o)]_{-L\le z_o\le L,\, 0\le\theta_o<2\pi}$$

$$\left[\frac{\partial p(\underset{\sim}{r}_o)}{\partial z_o}\right]_{z_o=L} = \rho_w \omega^2 [u(a,\theta_o,L)]_{0\le\theta_o<2\pi} \qquad (25)$$

$$\left[\frac{\partial p(\underset{\sim}{r}_o)}{\partial z_o}\right]_{z_o=-L} = -\rho_w \omega^2 [u(a,\theta_o,-L)]_{0\le\theta_o<2\pi} \quad .$$

Thus, Eq. (22) is

$$\begin{aligned} p(\underset{\sim}{r}) = \frac{1}{4\pi}\Big\{ & \int_{-L}^{L}\int_{0}^{2\pi}\left[\frac{e^{ikR}}{R}\rho_w\omega^2 W - p\frac{\partial}{\partial r_o}\left(\frac{e^{ikR}}{R}\right)\right]_{r_o=a} a\,d\theta_o\,dz_o \\ & + \int_{0}^{a}\int_{0}^{2\pi}\left[\frac{e^{ikR}}{R}\rho_w\omega^2 u - p\frac{\partial}{\partial z_o}\left(\frac{e^{ikR}}{R}\right)\right]_{z_o=L} r_o\,d\theta_o\,dr_o \qquad (26) \\ & + \int_{0}^{a}\int_{0}^{2\pi}\left[-\frac{e^{ikR}}{R}\rho_w\omega^2 u - p\frac{\partial}{\partial z_o}\left(\frac{e^{ikR}}{R}\right)\right]_{z_o=-L} r_o\,d\theta_o\,dr_o \quad . \end{aligned}$$

Substituting the expressions in Eqs. (2), (4), (7) and (18) into Eq. (26), we have

$$\begin{aligned} p(\underset{\sim}{r}) &= \sum_{n=0}^{\infty}\sum_{m=0}^{n} A_{nm} P_n^m(\cos\phi) h_n^{(1)}(k\rho)\cos m\theta \\ &= \sum_{n=0}^{\infty}\sum_{m=0}^{n}\left[\sum_{\ell=0}^{\infty} A_{\ell m}(Z_{1n\ell}^m + Z_{2n\ell}^m + Z_{3n\ell}^m)\right] P_n^m(\cos\phi) h_n^{(1)}(k\rho)\cos m\theta \\ &\quad - \sum_{n=0}^{\infty}\sum_{m=0}^{n}\left[\int_{-\infty}^{\infty}(W_m Z_{4nm} + U_m Z_{5nm} + U_m Z_{6nm})\,d\lambda\right] P_n^m(\cos\phi) h_n^{(1)}(k\rho)\cos m\theta \end{aligned} \qquad (27)$$

where

$$Z^m_{1n\ell} = \frac{(2n+1)}{2} ika \frac{(n-m)!}{(n+m)!} \int_{-L}^{L} \{P^m_\ell\left(\frac{\xi}{\sqrt{\zeta^2+\xi^2}}\right) h^{(1)}_\ell (k\sqrt{\zeta^2+\xi^2}) \cdot$$

$$\cdot \frac{\partial}{\partial \zeta}\left[P^m_n\left(\frac{\xi}{\sqrt{\zeta^2+\xi^2}}\right) j_n(k\sqrt{\zeta^2+\xi^2}\right]\}_{\zeta=a} d\xi \qquad (28a)$$

$$Z^m_{2n\ell} = ika \frac{(2n+1)}{2} \frac{(n-m)!}{(n+m)!} \int_0^a \{P^m_\ell\left(\frac{\zeta}{\sqrt{\zeta^2+\xi^2}}\right) h^{(1)}_\ell (k\sqrt{\zeta^2+\xi^2}) \cdot$$

$$\cdot \frac{\partial}{\partial \zeta}\left[P^m_n\left(\frac{\zeta}{\sqrt{\zeta^2+\xi^2}}\right) j_n(k\sqrt{\zeta^2+\xi^2})\right]\}_{\zeta=L} \xi d\xi \qquad (28b)$$

$$Z^m_{3n\ell} = ika \frac{(2n+1)}{2} \frac{(n-m)!}{(n+m)!} \int_0^a \{P^m_\ell\left(\frac{\zeta}{\sqrt{\zeta^2+\xi^2}}\right) h^{(1)}_\ell (k\sqrt{\zeta^2+\xi^2})$$

$$\cdot \frac{\partial}{\partial \zeta}\left[P^m_n\left(\frac{\zeta}{\sqrt{\zeta^2+\xi^2}}\right) j_n(k\sqrt{\zeta^2+\xi^2})\right]\}_{\zeta=-L} \xi d\xi \qquad (28c)$$

$$Z_{4nm} = ika \frac{(2n+1)}{2} \frac{(n-m)!}{(n+m)!} \rho_w \omega^2 \int_{-L}^{L} P^m_n\left(\frac{\xi}{\sqrt{a^2+\xi^2}}\right) j_n(k\sqrt{a^2+\xi^2}) e^{i\lambda\xi} d\xi \qquad (28d)$$

$$Z_{5nm} = ika \frac{(2n+1)}{2} \frac{(n-m)!}{(n+m)!} \rho_w \omega^2 e^{i\lambda L} \int_0^a P^m_n\left(\frac{L}{\sqrt{\xi^2+L^2}}\right) j_n(k\sqrt{\xi^2+L^2}) \xi d\xi \qquad (28e)$$

$$Z_{6nm} = -ika \frac{(2n+1)}{2} \frac{(n-m)!}{(n+m)!} \rho_w \omega^2 e^{-i\lambda L} \int_0^a P^m_n\left(\frac{-L}{\sqrt{\xi^2+L^2}}\right) j_n(k\sqrt{\xi^2+L^2}) \xi d\xi . \qquad (28f)$$

Note that Eq. (27) can be rewritten as

$$\sum_{n=0}^{\infty} \sum_{m=0}^{n} \left[\sum_{\ell=0}^{\infty} A_{\ell m}(Z^m_{1n\ell} + Z^m_{2n\ell} + Z^m_{3n\ell} - \delta_{n\ell}) - \int_{-\infty}^{\infty} [W_m Z_{4nm} + U_m(Z_{5nm} + Z_{6nm})] d\lambda\right] . \qquad (29)$$

or

$$\sum_{\ell=0}^{\infty} A_{\ell m} D^m_{n\ell} = \int_{-\infty}^{\infty} [W_m Z_{4nm} + U_m (Z_{5nm} + Z_{6nm})] d\lambda \tag{30}$$

$$D^m_{n\ell} = E^m_{n\ell} - \delta_{n\ell} = Z^m_{1n\ell} + Z^m_{2n\ell} + Z^m_{3n\ell} - \delta_{n\ell}$$

by using the orthogonality properties of the spherical harmonics. Then in the matrix form, Eq. (30) is

$$[D]\{A\} = \int_{-\infty}^{\infty} [C(\lambda)]\{U\} d\lambda \quad \text{for fixed } m \tag{31}$$

where

$$[C]_{(m=0)} = \begin{bmatrix} E^m_{00}-1 & E^m_{01} & E^m_{02} & \cdots \\ E^m_{10} & E^m_{11}-1 & E^m_{12} & \cdots \\ E^m_{20} & E^m_{21} & E^m_{22}-1 & \cdots \\ \vdots & & \ddots & \\ \vdots & & & E^m_{n\ell}-\delta_{n\ell} \end{bmatrix} \tag{32a}$$

$$[C]_{(m=0)} = \begin{bmatrix} (Z_{50m}+Z_{60m}) & 0 & Z_{40m} \\ (Z_{51m}+Z_{61m}) & 0 & Z_{41m} \\ (Z_{52m}+Z_{62m}) & 0 & Z_{42m} \\ \vdots & \vdots & \vdots \end{bmatrix} \tag{32b}$$

and {A}, {U} are defined in Eq. (11).

Due to the fact that $Z^m_{1n\ell} = Z^m_{2n\ell} = Z^m_{3n\ell} = Z_{4nm} = Z_{5nm} = Z_{6nm} = 0$ when $m > n$ or $m > \ell$, the matrices A, C and D in Eq.

(31) will degenerate to their submatrices, for example,

$$[D]_{(m=1)} = \begin{bmatrix} E^1_{11}-1 & E^1_{12} & E^1_{13} & \cdots \\ E^1_{21} & E^1_{22}-1 & E^1_{23} & \cdots \\ E^1_{31} & E^1_{32} & E^1_{33}-1 & \cdots \\ \vdots & & \ddots & \end{bmatrix} \tag{33a}$$

$$[C]_{(m=1)} = \begin{bmatrix} (Z_{511}+Z_{611}) & 0 & Z_{411} \\ (Z_{521}+Z_{621}) & 0 & Z_{421} \\ (Z_{531}+Z_{631}) & 0 & Z_{431} \\ \vdots & \vdots & \vdots \end{bmatrix} \tag{33b}$$

$$\{A\}_{(m=1)} = \begin{Bmatrix} A_{11} \\ A_{21} \\ A_{31} \\ A_{41} \\ \vdots \end{Bmatrix} \tag{33c}$$

4. BOUNDARY CONDITIONS

The boundary conditions for the present finite cylindrical thin shell are assumed to be two free ends provided this shell is sealed by two end caps with negligible mass. For cylindrical shell, the free ends implies [13]

$$\text{longitudinal force: } N_z = \frac{Eh}{1-\nu^2}\left[\frac{\partial u}{\partial z} + \nu\left(\frac{\partial v}{a\partial\theta} - \frac{W}{a}\right)\right] = 0 \qquad (34a)$$

$$\text{shear force: } S_z = \frac{Eh}{2(1+\nu)}\left[\frac{\partial^2 u}{a\partial\theta} + \frac{\partial v}{\partial z}\right] + \frac{D(1-\nu)}{a^2}\left[\frac{\partial v}{\partial z} + \frac{\partial^2 w}{\partial z\partial\theta}\right] = 0 \quad \text{at } z = \pm L \qquad (34b)$$

$$\text{bending moment: } M_z = -D\left[\frac{\partial^2 w}{\partial z^2} + \frac{\nu}{a^2}\left(\frac{\partial v}{\partial\theta} + \frac{\partial^2 w}{\partial\theta^2}\right)\right] = 0 \qquad (34c)$$

$$\text{torque: } T_z = -D\frac{\partial^3 w}{\partial z^3} - \frac{D}{a^3}(2-\nu)\left(\frac{\partial^2 v}{\partial z\partial\theta} + \frac{\partial^3 w}{\partial z\partial\theta^2}\right) = 0 \qquad (34d)$$

where $D = Eh^3/[12(1-\nu^2)]$ is the flexural rigidity of the cylindrical shell. After replacing the displacements by their Fourier expansion defined in Eq. (2) and utilizing the orthogonality property of the sinusoidal function, the above boundary conditions can be simplified as

$$\frac{d\bar{U}_m}{dz} + \frac{\nu}{a}(m\bar{V}_m - \bar{W}_m) = 0 \qquad (35a)$$

$$-\frac{m}{a}\bar{U}_m + \frac{d\bar{V}_m}{dz} + \frac{h^2}{6a^2}\left(\frac{d\bar{V}_m}{dz} - m\frac{d\bar{W}_m}{dz}\right) = 0 \quad \text{at } z = \pm L \qquad (35b)$$

$$\frac{d^2\bar{W}_m}{dz^2} + \frac{\nu m}{a^2}(\bar{V}_m - m\bar{W}_m) = 0 \qquad (35c)$$

$$\frac{d^3\bar{W}_m}{dz^3} - \frac{2-\nu}{a^2}m\left(\frac{d\bar{V}_m}{dz} - m\frac{d\bar{W}_m}{dz}\right) = 0 \quad . \tag{35d}$$

Substituting the above boundary conditions (35) into the corresponding expression $[....]_{z=-L}^{z=L}$ on the right-hand side of Eq. (9); e.g. $d\bar{U}_m/dz$ in Eq. (35a) into Eq. (9a), $d\bar{V}_m/dz$ in Eq. (35b) into Eq. (9b), $d^2\bar{W}_m/dz^2$ and $d^3\bar{W}_m/dz^3$ in Eq. (35c) and (35d), respectively, into Eq. (9c); the integral equation of Eq. (10c) should be rewritten as

$$[S]\{U\} = [Q]\{A\} + \{B\} + \frac{1}{2\pi}\int_{-\infty}^{\infty}[K'(\lambda,\xi)]\{U(\xi)\}\sin[(\lambda-\xi)L]d\xi \tag{36}$$

where the kernel $[K'(\lambda,\xi)]$ is

$$[K'(\lambda,\xi)] = \begin{bmatrix} K_{11} & K_{12} & K_{13} \\ K_{21} & K_{22} & K_{23} \\ K_{31} & K_{32} & K_{33} \end{bmatrix} \tag{37a}$$

$$K_{11} = -2\lambda \tag{37b}$$

$$K_{12} = im\frac{1-\nu}{a} \tag{37c}$$

$$K_{13} = 4i\frac{\nu}{a} \tag{37d}$$

$$K_{21} = i\frac{m}{a}\left[\frac{12\nu a^2 + (1-\nu)h^2}{6a^2 + h^2}\right] \tag{37e}$$

$$K_{22} = (1-\nu)\lambda \tag{37f}$$

$$K_{23} = \frac{mh^2}{6a^2 + h^2}(1-\nu) \tag{37g}$$

$$K_{31} = 2i\frac{\nu}{a} \tag{37h}$$

$$K_{32} = \frac{mh^2}{6a^2}[\nu\lambda - (2-\nu)\xi] \tag{37i}$$

$$K_{33} = \frac{h^2}{6}\{\frac{m^2}{a^2}[(2-\nu)\lambda + (4-\nu)\xi] + \lambda^3 + \lambda^2\xi\} \tag{37j}$$

5. DISPLACEMENTS OF THE CYLINDRICAL THIN SHELL

Substituting Eq. (31) into Eq. (36), we have the integral equation for the displacements {U}

$$[S(\lambda)]\{U(\lambda)\} = [Q(\lambda)][D]^{-1}\int_{-\infty}^{\infty}[C(\lambda)]\{U(\xi)\}d\xi + \{B(\lambda)\}$$

$$+ \frac{1}{2\pi}\int_{-\infty}^{\infty}[K'(\lambda,\xi)]\{U(\xi)\}\sin[(\lambda-\xi)L]d\xi \qquad (38a)$$

or

$$[S(\lambda)]\{U(\lambda)\} = \{B(\lambda)\} + \int_{-\infty}^{\infty}[K(\lambda,\xi)]\{U(\xi)\}d\xi \qquad (38b)$$

where

$$[K(\lambda,\xi)] = \frac{1}{2\pi}\sin[(\lambda-\xi)L][K'(\lambda,\xi)] + [Q(\lambda)][D]^{-1}[C(\xi)] \; . \qquad (38c)$$

To solve for the displacements {U}, we notice that this integral equation (38b) has a degenerate kernel

$$[K(\lambda,\xi)] = \frac{1}{2\pi}\sin[(\lambda-\xi)L]\{[K_1''(\lambda)] + [K_2''(\xi)] + \lambda^2[K_3''(\xi)]$$

$$+ [Q(\lambda)][D]^{-1}[C(\xi)] \qquad (39a)$$

where

$$[K_1''(\lambda)] = \begin{bmatrix} -2\lambda & im\frac{1-\nu}{a} & 4i\frac{\nu}{a} \\ i\frac{m}{a}\left[\frac{12\nu a^2+(1-\nu)h^2}{6a^2+h^2}\right] & (1-\nu)\lambda & 0 \\ 2i\frac{\nu}{a} & \frac{m\nu h^2}{6a^2}\lambda & \frac{h^2}{6}\left[\frac{m^2}{a^2}(2-\nu)\lambda + \lambda^3\right] \end{bmatrix} \qquad (39b)$$

$$[K_2''(\xi)] = \begin{bmatrix} 0 & 0 & 0 \\ 0 & 0 & \frac{mh^2}{6a^2+h^2}(1-\nu)\xi \\ 0 & \frac{-mh^2}{6a^2}(2-\nu)\xi & \frac{m^2h^2}{6a^2}(4-\nu)\xi \end{bmatrix} \tag{39c}$$

$$[K_3''(\xi)] = \begin{bmatrix} 0 & 0 & 0 \\ 0 & 0 & 0 \\ 0 & 0 & \frac{h^2}{6}\xi \end{bmatrix} \tag{39d}$$

Thus, this integral equation can be solved by reduction to a system of algebraic equations [10].

Substituting (39a) into Eq. (38b), we have the following system of integral equation for this displacement {U}

$$\{U(\lambda)\} - \sum_{i=1}^{7} [G_i(\lambda)] \int_{-\infty}^{\infty} [K_i(\xi)]\{U(\xi)\}d\xi = \{B'(\lambda)\} \tag{40}$$

where

$$[G_1(\lambda)] = \frac{1}{2\pi}[S(\lambda)]^{-1}[K_1''(\lambda)]\sin(\lambda L) \tag{41a}$$

$$[G_2(\lambda)] = \frac{-1}{2\pi}[S(\lambda)]^{-1}[K_1''(\lambda)]\cos(\lambda L) \tag{41b}$$

$$[G_3(\lambda)] = \frac{1}{2\pi}[S(\lambda)]^{-1}\sin(\lambda L) \tag{41c}$$

$$[G_4(\lambda)] = \frac{-1}{2\pi}[S(\lambda)]^{-1}\cos(\lambda L) \tag{41d}$$

$$[G_5(\lambda)] = \frac{\lambda^2}{2\pi}[S(\lambda)]^{-1}\sin(\lambda L) \tag{41e}$$

$$[G_6(\lambda)] = \frac{-\lambda^2}{2\pi}[S(\lambda)]^{-1}\cos(\lambda L) \tag{41f}$$

$$[G_7(\lambda)] = [S(\lambda)]^{-1}[Q(\lambda)][D]^{-1} \tag{41g}$$

$$[K_1(\xi)] = [I]\cos(\xi L) \tag{41h}$$

$$[K_2(\xi)] = [I]\sin(\xi L) \tag{41i}$$

$$[K_3(\xi)] = [K_2''(\xi)]\cos(\xi L) \tag{41j}$$

$$[K_4(\xi)] = [K_2''(\xi)]\sin(\xi L) \tag{41k}$$

$$[K_5(\xi)] = [K_3''(\xi)]\cos(\xi L) \tag{41ℓ}$$

$$[K_6(\xi)] = [K_3''(\xi)]\sin(\xi L) \tag{41m}$$

$$[K_7(\xi)] = [C(\xi)] \tag{41n}$$

$$\{B'(\lambda)\} = [S(\lambda)]^{-1}\{B(\lambda)\} \quad . \tag{41o}$$

If we define

$$\{e_i\} = \int_{-\infty}^{\infty}[K_i(\xi)]\{U(\xi)\}d\xi \ , \quad i = 1,2,\ldots 7 \tag{42}$$

the integral equation (40) is then rewritten as

$$\{U(\lambda)\} = \sum_{i=1}^{7} [G_i(\lambda)]\{e_i\} + \{B'(\lambda)\} \quad . \tag{43}$$

The column matrix $\{e_i\}$ in Eq. (42) are unknown constants, since the function $\{U(\lambda)\}$ is unknown. To solve for the unknown constants $\{e_i\}$, we substitute Eq. (43) into the integral equation (40) and obtain a linear combination of the functions $[G_i(\lambda)]$

$$\sum_{i=7}^{7} [G_i(\lambda)]\{\{e_i\} - \int_{-\infty}^{\infty} [K_i(\xi)]\ \{B'(\xi)\} + \sum_{k=1}^{7} [G_k(\xi)]\{e_k\}]d\xi\} = 0 \ . \tag{44}$$

Because of the linear independence of the functions $[G_i(\lambda)]$ within the interval $\{\lambda;\ -\infty < \lambda < \infty\}$, the above Eq. (44) implies

$$\{e_i\} - \int_{-\infty}^{\infty} [K_i(\xi)][\{B'(\xi)\} + \sum_{k=1}^{7} [G_k(\xi)]\{e_k\}]d\xi \ = 0 \quad ,$$

$$i = 1,2,\ldots,7. \tag{45}$$

This introduces two calculable integrals which may be denoted as follows

$$[\alpha_{ij}] = \int_{-\infty}^{\infty} [K_i(\xi)][G_j(\xi)]d\xi \tag{46}$$

$$[\beta_i\ ] = \int_{-\infty}^{\infty} [K_i(\xi)]\{B'(\xi)\}d\xi \quad . \tag{47}$$

Then, Eq. (45) can be rewritten as

$$\{e_i\} - \sum_{k=1}^{7}[\alpha_{ik}]\{e_k\} - \{\beta_i\} = 0 \tag{48}$$

or

$$\sum_{k=1}^{7}[I - \alpha_{ik}]\{e_k\} = \{\beta_i\} \quad , \quad i = 1,2,\ldots,7 \tag{49}$$

where [I] is a unit matrix of order 3 and $[\alpha_{ik}]$ is also a matrix defined in Eq. (46). Note that we have obtained a system of linear algebraic equations for the determination of the unknown constants $\{e_k\}$. Solving these simultaneous Eqs. (49) with a 21 x 21 coefficient matrix $[I - \alpha_{ik}]$, the solution of the displacements {U} are then given by Eq. (43).

We note that the determinant of the coefficient matrix

$$E(\omega) = [I - \alpha_{ik}(\omega)] = \begin{bmatrix} I-\alpha_{11}(\omega) & -\alpha_{12}(\omega) & \cdots & -\alpha_{17}(\omega) \\ -\alpha_{21}(\omega) & 1-\alpha_{22}(\omega) & \cdots & -\alpha_{27}(\omega) \\ \vdots & \ddots & & \vdots \\ -\alpha_{71}(\omega) & & \ddots & 1-\alpha_{77}(\omega) \end{bmatrix} \tag{50}$$

is a transcendental function of the frequency ω. Therefore, it is possible to determine numerically the resonant frequencies of the submerged finite cylindrical thin shell such that $\det[E(\omega)] = 0$. In such case, the system of Eq. (49) does not have a unique solution. In another words, at least one of the $\{e_k\}$'s should be assigned arbitrary, and the remaining $\{e_k\}$'s can be determined accordingly.

For those frequencies $\det[E(\omega)] \neq 0$, we may determine uniquely the unknown constants $\{e_k\}$ according to the frequency and the position of the excitation specified in Eq. (10). Substituting these constants $\{e_k\}$ into Eq. (43), we obtain the displacements of the submerged finite cylindrical thin shell $\{U(\lambda)\}$ in the wave number domain λ. Then, the inverse Fourier transform (7) and the summation of Fourier series (2) are performed to obtain the displacements $\{u(a, \theta, z)\}$ in the spatial domain.

6. ACOUSTIC RADIATION FIELD OF A SUBMERGED FINITE CYLINDRICAL SHELL

Once the displacements $\{U(\lambda)\}$ in the wave number domain λ are determined by Eq. (43), the expansion coefficients A_{nm} for the acoustic radiation field can be obtained from Eq. (31)

$$\{A\} = [D]^{-1}\int_{-\infty}^{\infty}[C(\lambda)]\{U(\lambda)\}d\lambda \quad \text{for fixed } m \ . \tag{51}$$

Substituting these coefficients A_{nm} into Eq. (14), the acoustic radiation field outside the vibrating cylindrical shell is obtained

$$P(r,\theta,z,t) = P(\rho,\theta,\phi,t) = \sum_{n=0}^{\infty}\sum_{m=0}^{n} A_{nm}P_n^m\left(\frac{z}{\sqrt{r^2+z^2}}\right)h_n^{(1)}(k\sqrt{r^2+z^2}) \cdot \cos m\theta e^{-i\omega t} \ . \tag{52}$$

7. DISCUSSION

It is known that the vibration of an infinitely long cylindrical shell may be described by a continuous wave number in the axial direction. These broadband spatial spectra degenerate to a discrete set of wave numbers when the dimension of the vibrator is finite. In the previous derivation, the displacement $\{U(\lambda)\}$ in Eq. (7) and the acoustic field $P(\underset{\sim}{r})$ in Eqs. (51) and (52) indicate a continuous wave number λ should be included. These facts are mainly attributed to the reacting pressure field on the two flat end caps. These vibrating end caps generate the acoustic pressure wave propagating in the infinitely extended fluid medium. These acoustic waves will form a spherical wave front in the far field and have wave number with infinite kinds of projection in the axial direction. Thus the wave number λ should indeed have a continuous set. However, the previous study on the acoustic radiation from an infinitely long submerged cylindrical shell [9] indicates the fluid medium acts like a resistive impedance when the waves in the cylindrical shell have the wave number in the axial direction larger than the wave number in the fluid medium ω/c_w ($\lambda > \omega/c_w$). Thus, the dominant contribution of the infinitely extended integration of λ for the displacements $\{U\}$ in Eq. (7) and the radiated acoustic field in Eq. (51) should emerge from the integration when $|\lambda| < \omega/c_w$. Then, the infinitely extended integration can be truncated in according to the desired accuracy. Similarly, the infinite series of the circumferential

mode in Eqs. (2) and (52) may also be truncated because the increasing stiffness of the cylindrical thin shell at the higher circumferential vibrational modes.

In the present analysis, two flat end caps for the finite cylindrical shell have been assumed. By neglecting the deformation of the flat end caps, it is reasonable to assume the boundary conditions for this finite cylindrical shell to be two free ends. Should the end caps be replaced by two elastic flat plates or two spherical caps, the boundary conditions should be modified to the continuity of the displacements and the stresses at the junctions between the finite cylindrical shell and the sealed caps.

REFERENCES

1. Abramowitz, M. and Stegun, I. A., ed., Handbook of Mathematical Functions, National Bureau of Standards, Washington, D.C., 1964.
2. Achenbach, J. D., Wave Propagation in Elastic Solids, North-Holland, Amsterdam, 1975.
3. Armenakas, A. E., Gazis, D. C., and Herkmann, G., Free Vibrations of Circular Cylindrical Shells, Pergamon Press, N.Y., 1969.
4. Briham, G. A. and Borg, M. F., An Approximate Solution to the Acoustic Radiation of a Finite Cylinder, J. of Acou. Soc. of Am., Vol. 32, No. 8, August 1960, pp. 971-981.
5. Frazer, R. A., Duncan, W. J. and Collar, A. R., Elementary Matrixes, Cambridge University Press, 1965, pp. 43.
6. Greenspon, J. E., Vibrations of a Thick-Walled Cylindrical Shell - Comparison of the Exact Theory with Approximate Theories, J. of Acou. Soc. of Am., Vol. 32, No. 5, May 1960, pp. 571-578.
7. Hoff, N. J., The Accuracy of Donnell's Equations, J. of App. Mech., Trans. ASME, Vol. 77, 1955, pp. 329-334.
8. Kraus, H., Thin Elastic Shells, Wiley, N.Y., 1967.
9. Ku, C. C. and Pao, Y. H., Acoustic Radiation of a Submerged Cylindrical Shell, first part of this report.
10. Mikhlin, S. G., Integral Equations, Pergamon, 1964, pp. 19-22.
11. Morse, P. M. and Feshbach, H., Methods of Theoretical Physics, McGraw-Hill , N.Y., 1953.

12. Pillai, T. A., Varadan, V. K., Varadan, V. V., and Radlinski, R. P., Acoustic Wave Scattering by Elastic Cylindrical Shells in Water, J. of Acous. Soc. of Am., Vol. 74, No. 2, 1983, pp. 619-624.

13. Timoshenko, S. and Woinowsky-Krieger, S., Theory of Plates and Shells, McGraw-Hill, N.Y., 1959, p. 519.

14. Yu, Y. Y., Free Vibrations of Thin Cylindrical Shells Having Finite Length with Freely Supported and Clamped Edges. J. of Appl. Mech., Trans. ASME, Vol. 77, 1955, pp. 547-552.

15. Vogel, W. and Feit, D., Response of Point Excited Infinite Long Cylindrical Shell Immerged in Acoustic Medium, NSRDC Report 80-061, November 1980.

Figure Captions

Fig. 1 Finite circular cylindrical shell.

Fig. 2 Circumferential modes of a circular cylindrical shell.

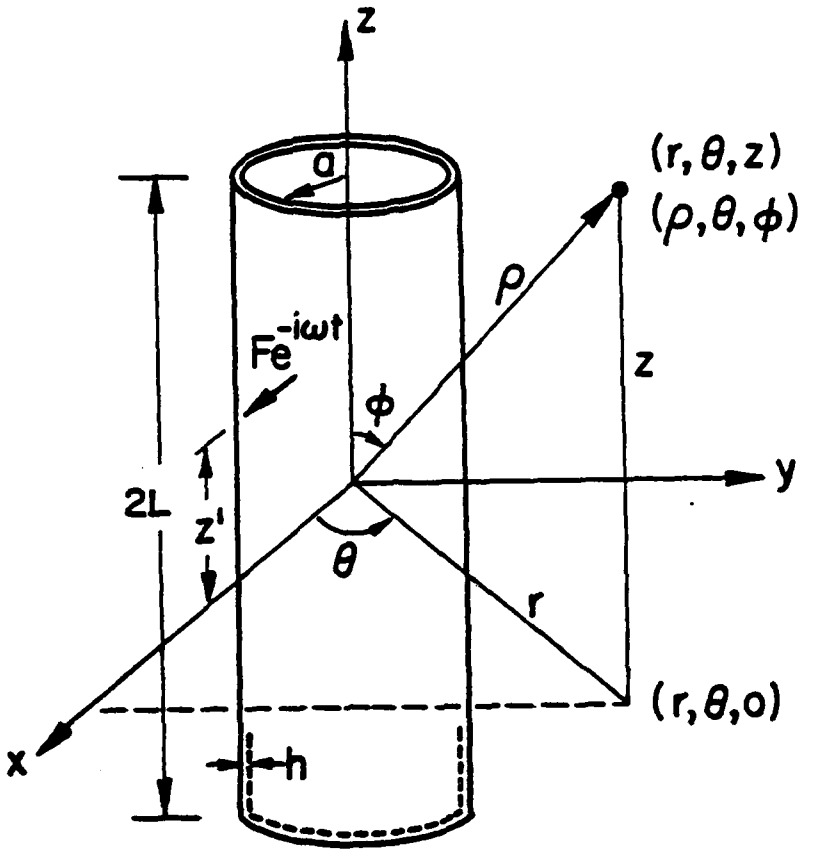

Fig. 1 Finite circular cylindrical shell.

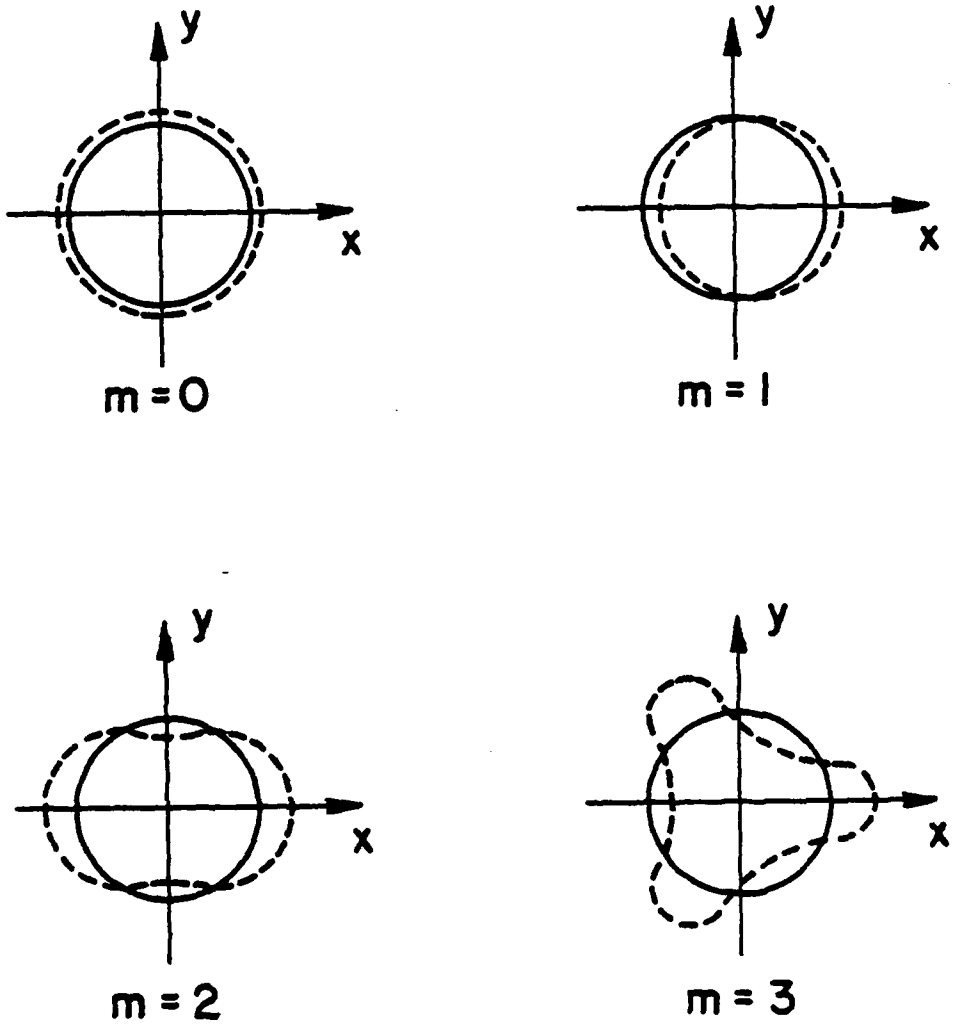

Fig. 2 Circumferential modes of a circular cylindrical shell.

Technical Report No. 3*

ATTENUATION CONSTANTS AND PHASE VELOCITIES OF EIGHTEEN POLYMERIC MATERIALS

C.P. Chen
Department of Theoretical and Applied Mechanics
Cornell University, Ithaca, New York 14853

Abstract

The phase velocities and attenuation constants of eighteen polymeric materials are measured by ultrasonic methods. Both longitudinal (pressure) waves and transverse (shear) waves are investigated. The attenuation constants are found to be approximated by a quadratic polynomial of the frequency variable within the range of 1 to 10 MHz.

---

*NRL Contract No. N00014-81-C-2122

ATTENUATION CONSTANTS AND PHASE VELOCITIES OF EIGHTEEN POLYMERIC MATERIALS

C.P. Chen

Experiments were conducted to measure the frequency dependent attenuation constants and phase velocities for both longitudinal and shear elastic waves in eighteen polymeric materials. The broadband pulse-echo method was used for all measurements. Frequency range was from 1 to 10 MHz.

Ultrasonic piezoelectric transducers are used as transmitter and receiver. The schematic diagram of the instruments is shown in Figure 1, and a typical record of the received signals is shown in Figure 2. Attenuation measurements, the first two echos of ultrasonic signal propagating back and forth in the specimen are digitized and windowed by the digital sampler. The sampled data are then analyzed by applying a FFT routine to obtain the Fourier amplitude spectra of two echos. The attenuation is calculated by the following formula:

$$\alpha(f)\ \frac{NP}{cm} = \frac{1}{2d}\ \log_e \frac{A_1(f)}{A_2(f)}$$

where $A_1(f)$ is the Fourier amplitude spectrum of the first echo and $A_2(f)$ is the Fourier amplitude spectrum of the second echo, both at the same frequency f, and d is the thickness of the specimen.

For phase velocity measurement, phase spectrum analysis technique is used to calculate the frequency dependence of phase velocity. The procedures of measurement is described in the paper by W. Sachse and Y. H. Pao, "On the determination of phase and group velocities of dispersive waves in solids," J. Appl. Phys., 48, pp. 4320-4327, 1978.

The 18 specimens and their thicknesses are listed in Table 1. The phase velocities as calculated from the phase spectrum of pulse propagation for each

specimen are shown in Figure 3, and their values listed in Table 2 for 5 frequencies.

The data for attenuations of 18 specimens are shown in Figure 4 for both P-waves and S-waves. The data for P-waves are smoother than those for S-waves. Even so, the data of the low end and high end of the spectrum should be discarded.

The signal of specimen #4 is not accurate enough for phase velocity measurement of the shear wave. For shear attenuation measurement, due to high attenuation or the mismatching of impedances of a few specimens to the transducer, we were unable to obtain the second echos, and thus the attenuation, for specimens #2, 4, 11, 13 and 17.

For the frequency range considered, the attenuation constants can be represented by the polynomial approximation

$$\alpha = a_0 + a_1 f + a_2 f^2$$

The coefficients a_0, a_1 and a_2 are listed in Table 3 for all materials.

Table 1. Dimension of 18 Polymeric Materials

No.	Specimen	Thickness (cm)
1	POLYSULFONE	1.28
2	UV curable, Acrylate based, polymer	0.694
3	White Delryn	1.28
4	Polyurethane (Conap)	0.715
5	High density Polyethylene	0.947
6	Noryl	1.51
7	FEP 100	0.803
8	TEFZEL	1.303
9	REXOLITE	1.269
10	POLYSTYRENE	1.273
11	POLYPROPYLENE 7823	0.65
12	POLYYINYL - CHLORIDE	1.26
13	HYTREL	0.644
14	NYLON 101	0.68
15	ACRYLIC	1.286
16	TEE ($\beta.\beta$)	0.949
17	DELRYN 157	1.257
18	POLYCARBONATE	1.26

Table 2. Phase Velocities of 18 Polymeric Materials

(A) P-waves (cm/μsec)

Specimen	Frequency 2 MHz	4 MHz	6 MHz	8 MHz	10 MHz
#1	0.2271	0.2278	0.2283	0.2286	0.2286
2	0.2233	0.2265	0.2284	0.2296	0.2300
3	0.2442	0.2460	0.2474	0.2488	0.2497
4	0.1675	0.1696	0.1708	0.1715	0.1658
5	0.2391	0.2400	0.2406	0.2409	0.2409
6	0.2694	0.2701	0.2707	0.2709	0.2709
7	0.1271	0.1297	0.1291	0.1261	0.1259
8	0.1647	0.1671	0.1660	0.1658	0.1647
9	0.2348	0.2351	0.2353	0.2354	0.2352
10	0.2314	0.2316	0.2319	0.2319	0.2318
11	0.2498	0.2544	0.2569	0.2583	0.2591
12	0.2343	0.2353	0.2360	0.2363	0.2364
13	0.2148	0.2180	0.2199	0.2208	0.2214
14	0.2633	0.2654	0.2668	0.2675	0.2676
15	0.2749	0.2754	0.2759	0.2761	0.2760
16	0.1378	0.1393	0.1394	0.1377	0.1378
17	0.2440	0.2436	0.2447	0.2457	0.2461
18	0.2303	0.2306	0.2309	0.2310	0.2310

Table 2. Phase Velocities for 18 Polymeric Materials

(B) S-waves (cm/μsec)

Specimen	Frequency 2 MHz	4 MHz	6 MHz	8 MHz
1	0.09303	0.09340	0.09366	0.09461
2	0.08879	0.08529	0.08351	0.08542
3	0.1036	0.1053	0.1033	0.1034
4				
5	0.09240	0.09406	0.09322	0.09494
6	0.1212	0.1216	0.1219	0.1220
7	0.03676	0.03459	0.03541	0.03541
8	0.05819	0.05568	0.05506	0.05411
9	0.1167	0.1166	0.1166	0.1184
10	0.1092	0.1118	0.1126	0.1142
11	0.2056	0.2199	0.2071	0.2055
12	0.1095	0.1101	0.1104	0.1085
13	0.07787	0.07550	0.07673	0.07485
14	0.1025	0.1072	0.1093	0.1101
15	0.1402	0.1404	0.1407	0.1428
16	0.05007	0.04817	0.04832	0.04752
17	0.1083	0.1092	0.1070	0.1053
18	0.1091	0.1117	0.1127	0.1143

Table 3. Quadratic Functions for Attenuation Coefficients

$$\alpha = a_0 + a_1 f_2 + a_2 f^2 \text{ (np/cm)}$$

(A) P-waves

Specimen	f (MHz)	a_0	a_1	a_2
1	2.5-10	0.21	0.13	0.0030
2	1-4	0.69	0.20	0.12
3	1-3	-0.029	0.47	-0.015
4	1-3	0.011	0.66	0.04
5	2.5-7.5	0.098	0.15	0.019
6	2.5-8.5	0.073	0.092	0.0056
7	0.5-2	-0.62	3.36	-1.0
8	0.5-1	-0.00017	0.50	0.44
9	5-20	-0.061	0.062	-0.0012
10	5-20	-0.076	0.062	-0.0011
11	1-3	0.39	0.78	-0.024
12	2-10	0.035	0.33	-0.015
13	1.5-4	-0.25	1.20	-0.089
14	1.5-8	0.22	0.28	0.012
15	3-15	0.25	0.084	-0.00074
16	0.3∿2.0	0.43	0.31	0.18
17	0.5∿3(straight line)	0.065	0.5	
18	4∿18	-0.134	0.071	-0.0021

Table 3. Quadratic Functions for Attenuation Coefficients

$$\alpha = a_0 + a_1 f + a_2 f^2 \text{ (np/cm)}$$

(B) S-waves

Specimen	f (MHz)	a_0	a_1	a_2
1	0.5-2.	0.27	0.68	0.019
2				
3	0.15-0.6	0.55	-2.36	6.49
4				
5	0.5-1.5	0.061	1.79	-0.27
6	0.5-3.0	0.21	0.41	0.050
7	0.05-0.3	0.29	9.00	1.84
8	0.05-0.4	1.04	-0.39	5.72
9	0.5~6.5 (SL)	0.38	0.10	
10	1 - 7 (SL)	0.37	0.082	
11				
12	0.5-2	0.51	0.90	-0.064
13				
14	0.75-2	1.19	-0.099	0.59
15	0.5-4	0.62	0.10	0.047
16	0.2-0.7	0.50	2.71	0.67
17				
18	1 - 7 (SL)	0.36	0.095	

Fig. 1 Schematic Diagram of Experimental Set Up

Fig. 2 Typical Transient Pulses and Their Spectra.

(A) First Echo

(B) Second Echo

(C) Spectra for Two Echos

Fig. 3 Phase Velocities

Specimen No. 1

Specimen No. 2

Specimen No. 3

Specimen No. 4

Specimen No. 5

Specimen No. 6

Specimen No. 7

Specimen No. 8

Specimen No. 9

Specimen No. 10

Specimen No. 11

Specimen No. 12

Specimen No. 13

Specimen No. 14

Specimen No. 15

Specimen No. 16

Specimen No. 17

Specimen No. 18

AD-A136 827 RADIATION AND DIFFRACTION OF UNDERWATER ACOUSTIC WAVES (U) CORNELL UNIV ITHACA NY DEPT OF THEORETICAL AND APPLIED MECHANICS Y PAO ET AL. 31 JUL 83 2/2

UNCLASSIFIED SBI-AD-E001 629 N00014-81-C-2122 F/G 17/1 NL

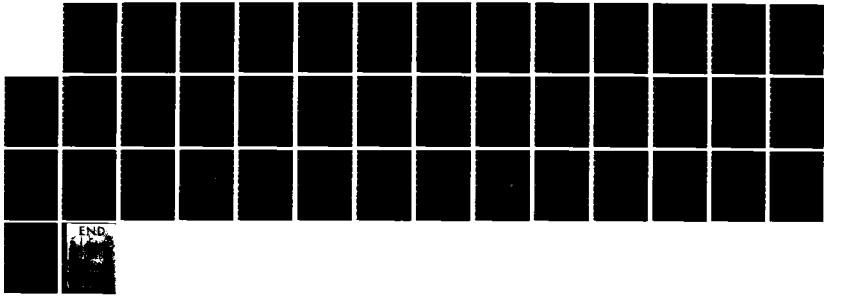

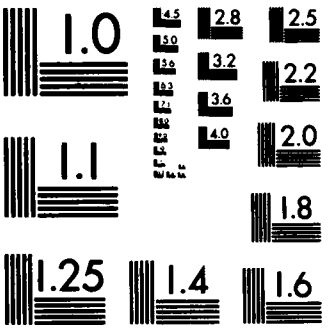

Fig. 4 Attenuation Coefficients

Specimen No. 1

Specimen No. 2

Specimen No. 3

Specimen No. 4

Specimen No. 5

Specimen No. 6

Specimen No. 7

Specimen No. 8

Specimen No. 9

Specimen No. 10

Specimen No. 11

Specimen No. 12

Specimen No. 13

Specimen No. 14

Specimen No. 15

Specimen No. 16

Specimen No. 17

Specimen No. 18

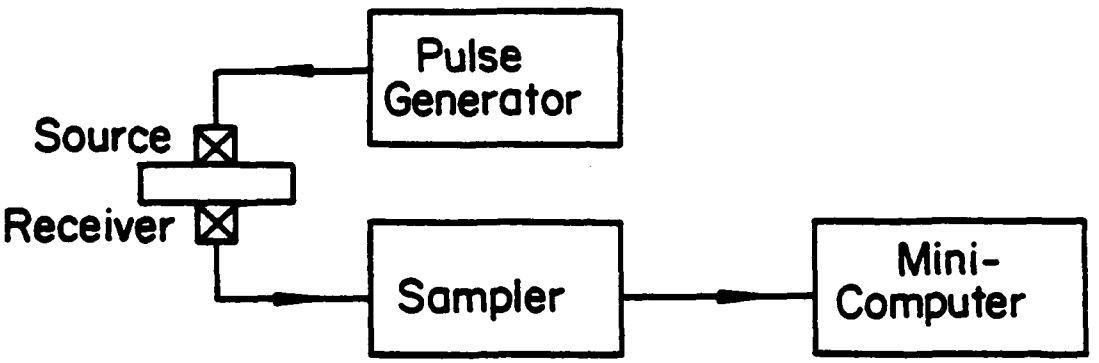

Figure 1. Schematic Diagram of Experimental Set Up

Figure 2. Typical Transient Pulses and Their Spectra. (A) First Echo

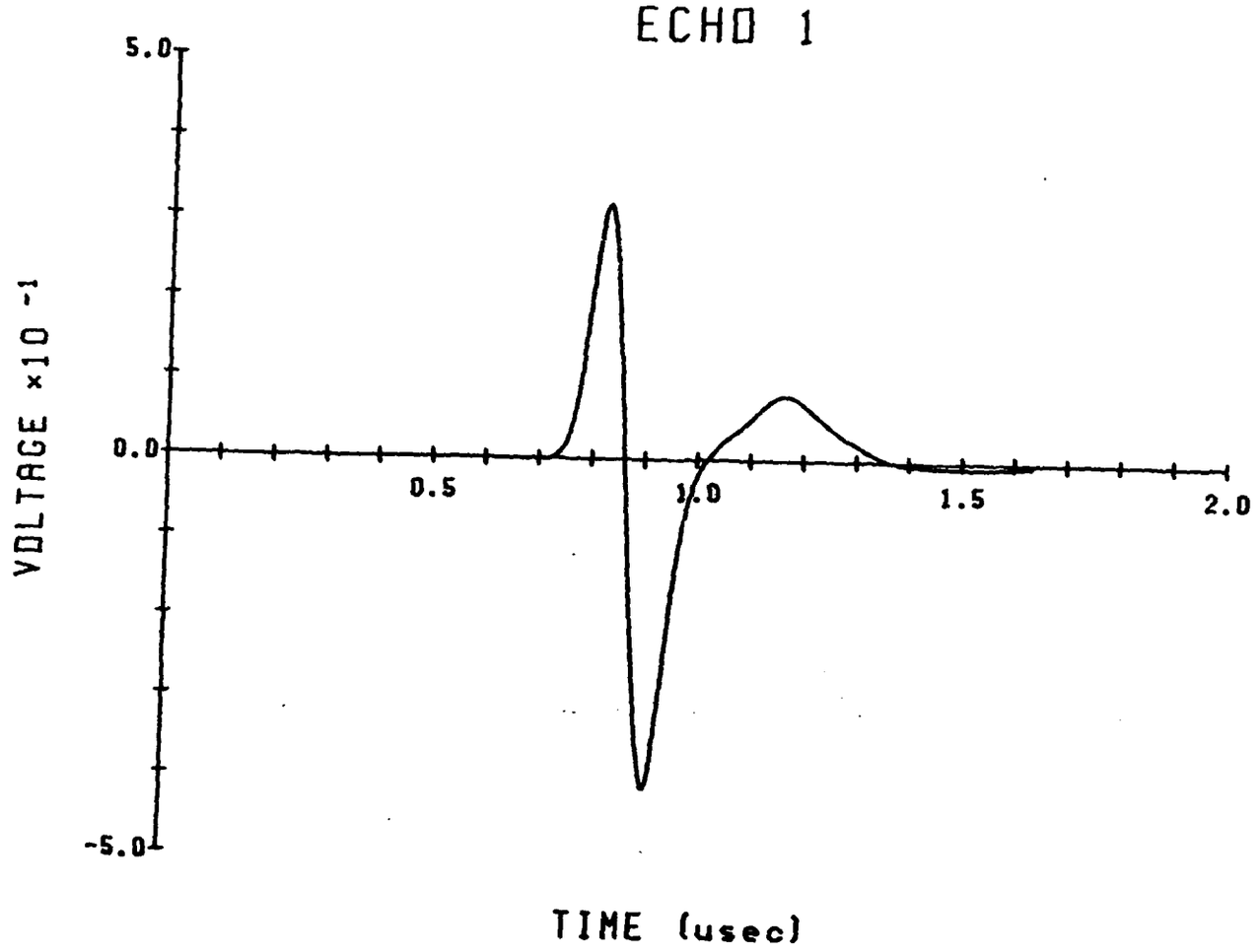

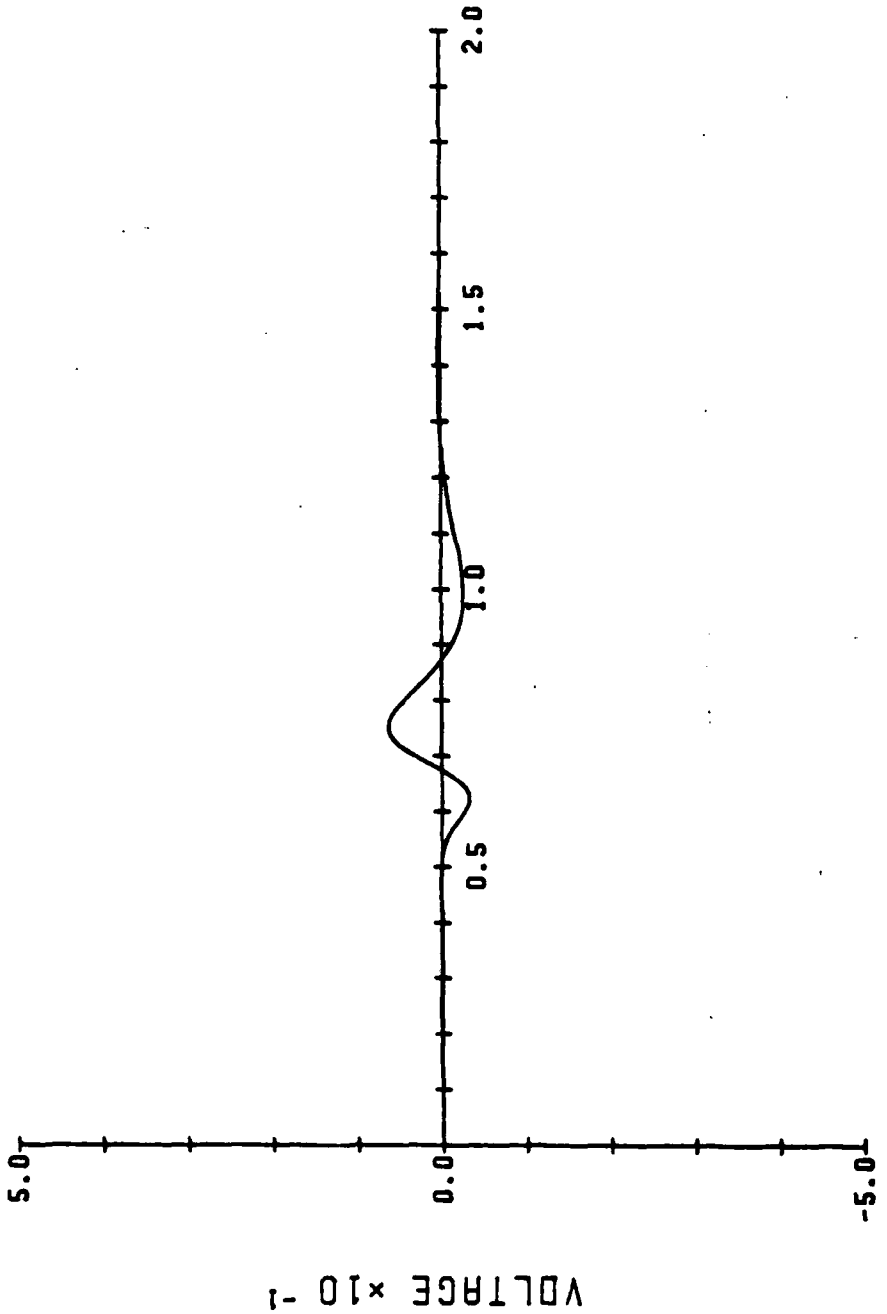

Figure 2. Typical Transient Pulses and Their Spectra. (B) Second Echo

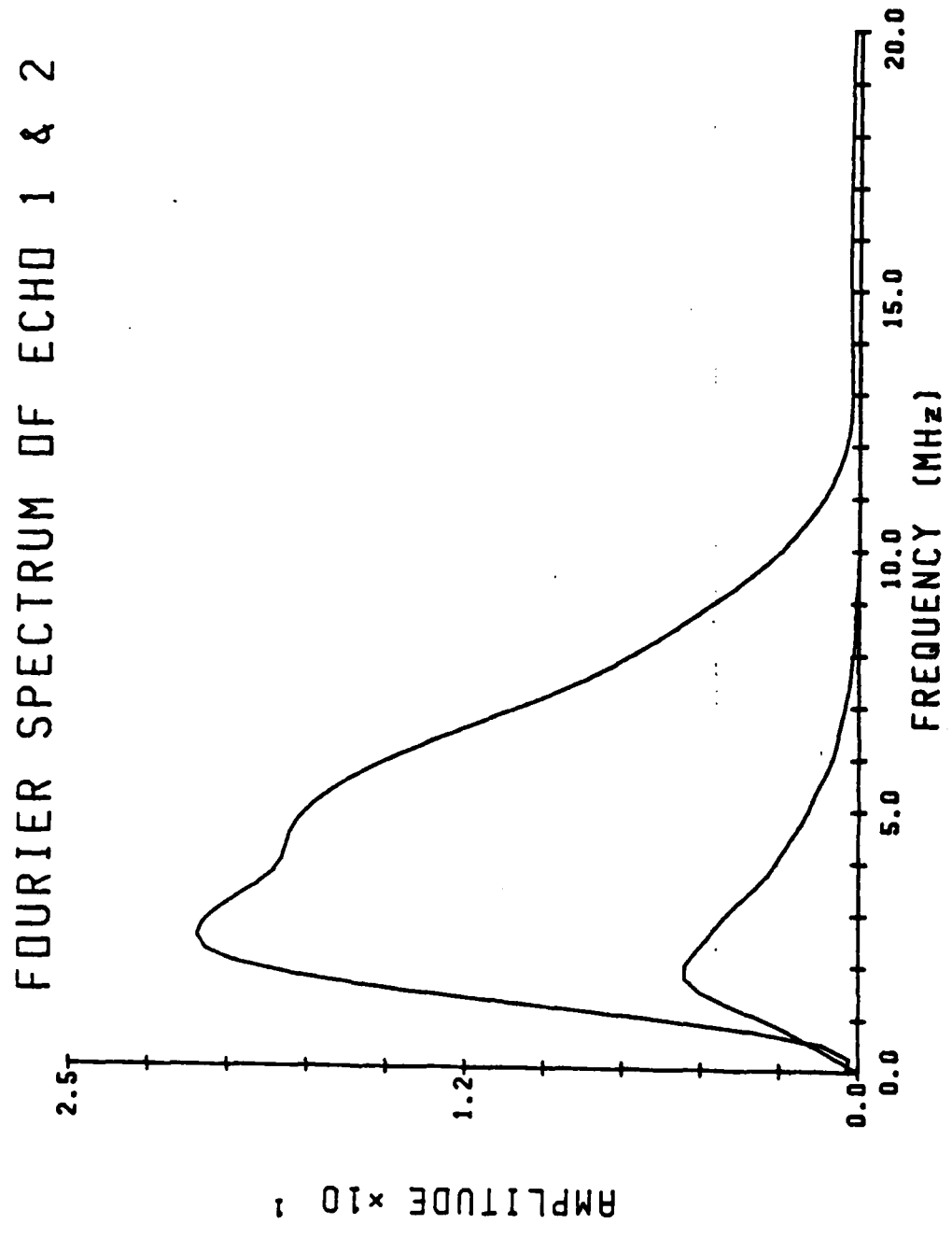

Figure 2. Typical Transient Pulses and Their Spectra. (C) Spectra for Two Echos

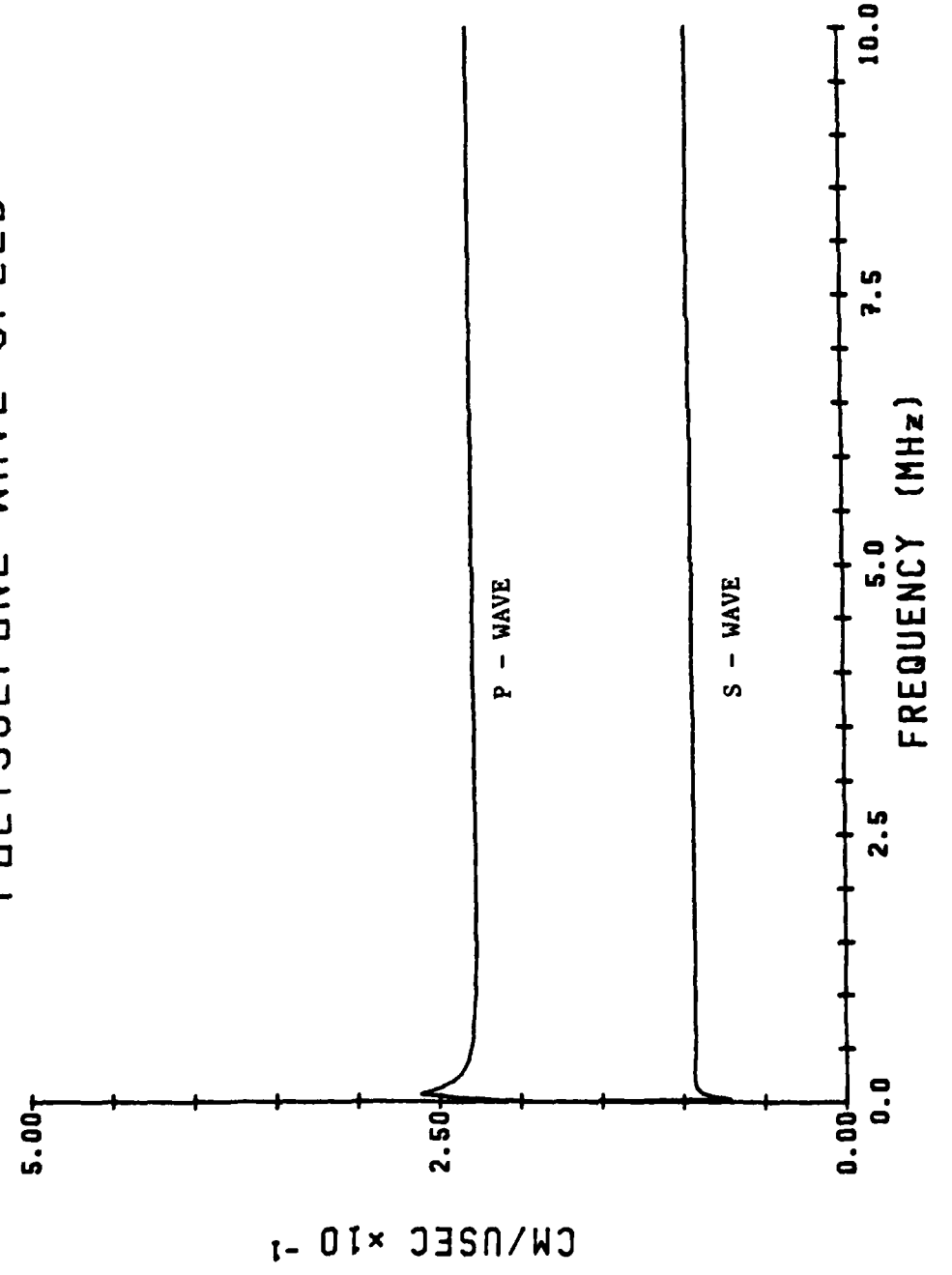

Figure 3. Phase Velocities - Specimen No. 1

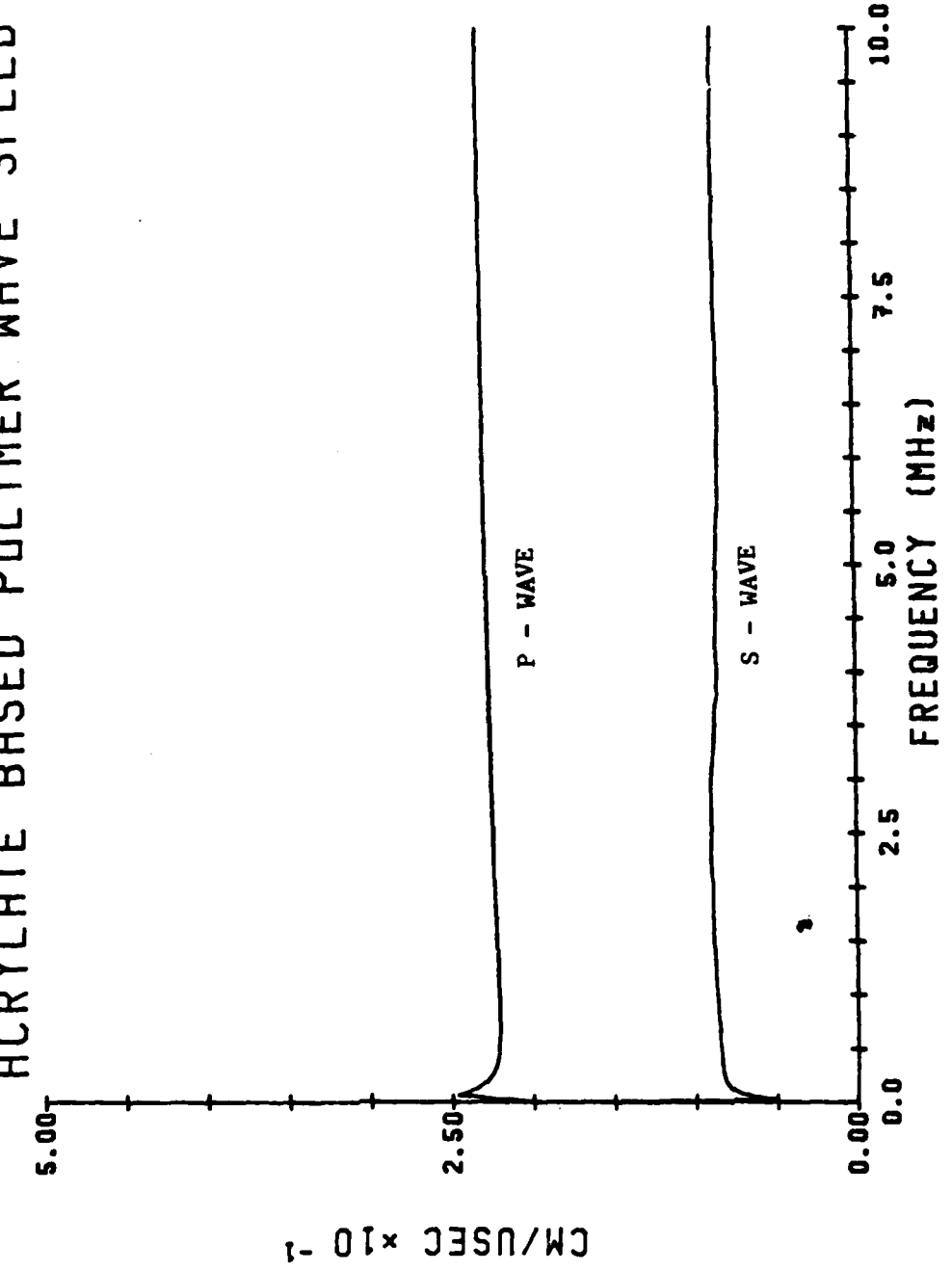

Figure 3. Phase Velocities - Specimen No. 2

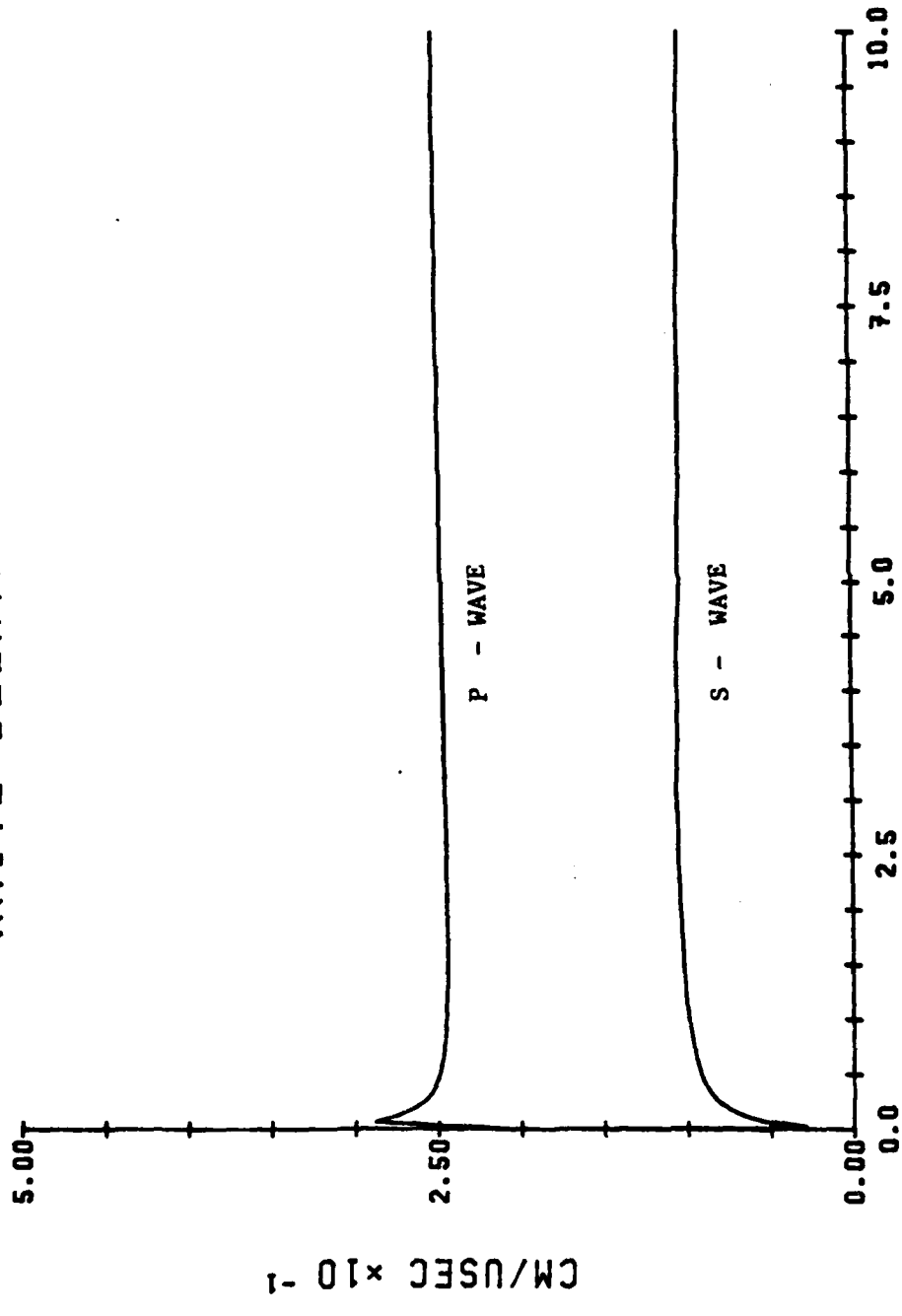

Figure 3. Phase Velocities - Specimen No. 3

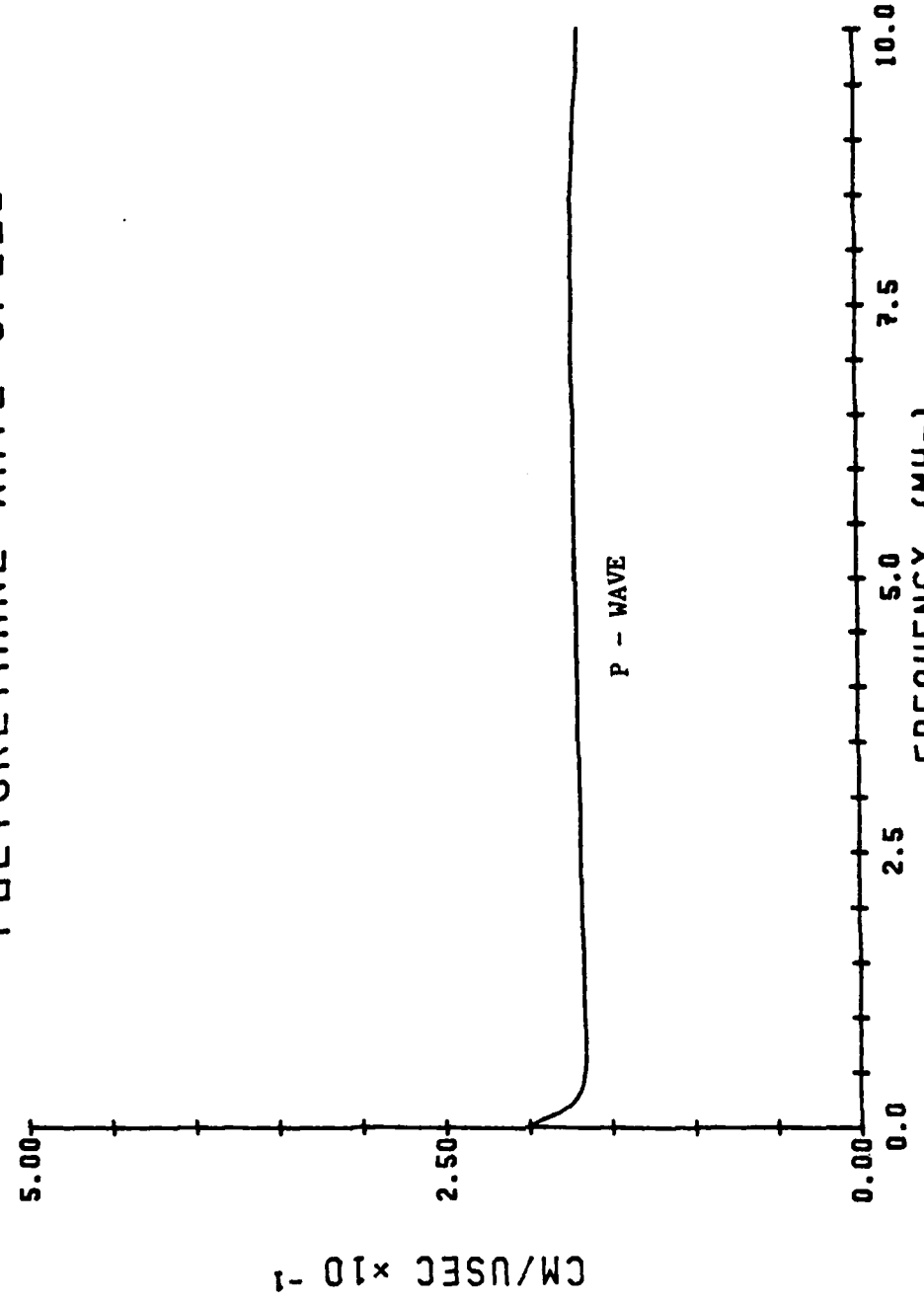

Figure 3. Phase Velocities - Specimen No. 4

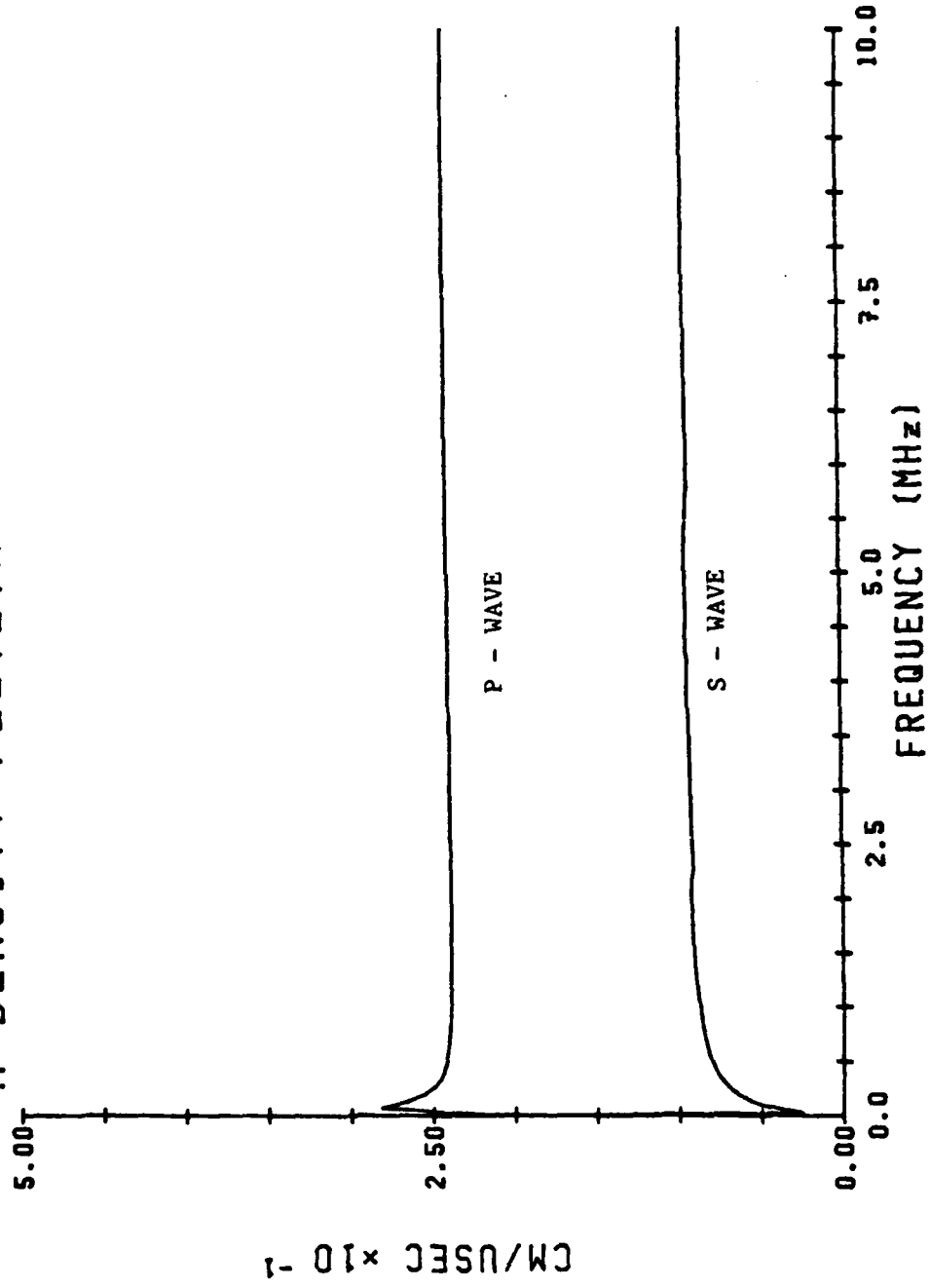

Figure 3. Phase Velocities - Specimen No. 5

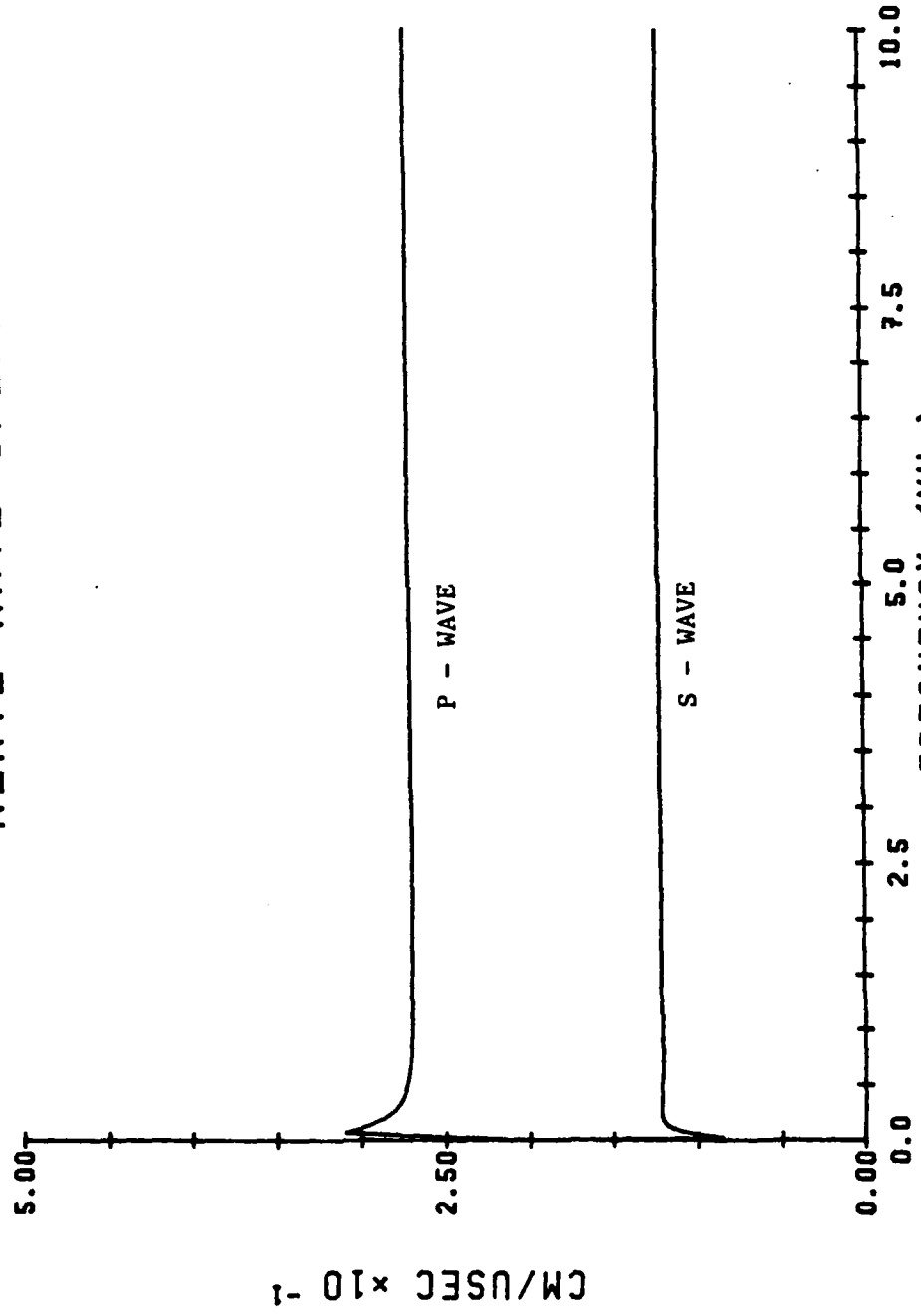

Figure 3. Phase Velocities - Specimen No. 6

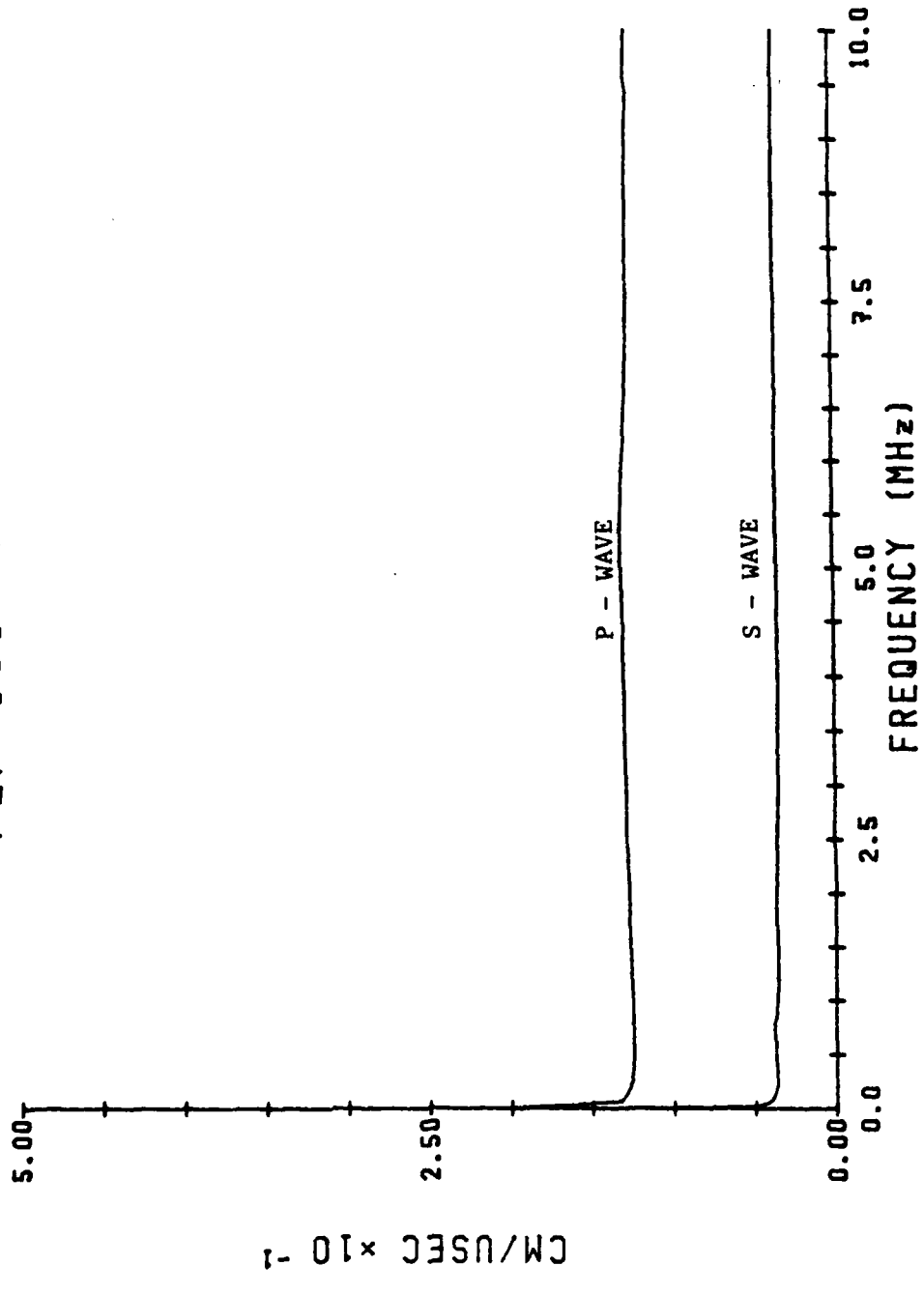

Figure 3. Phase Velocities - Specimen No. 7

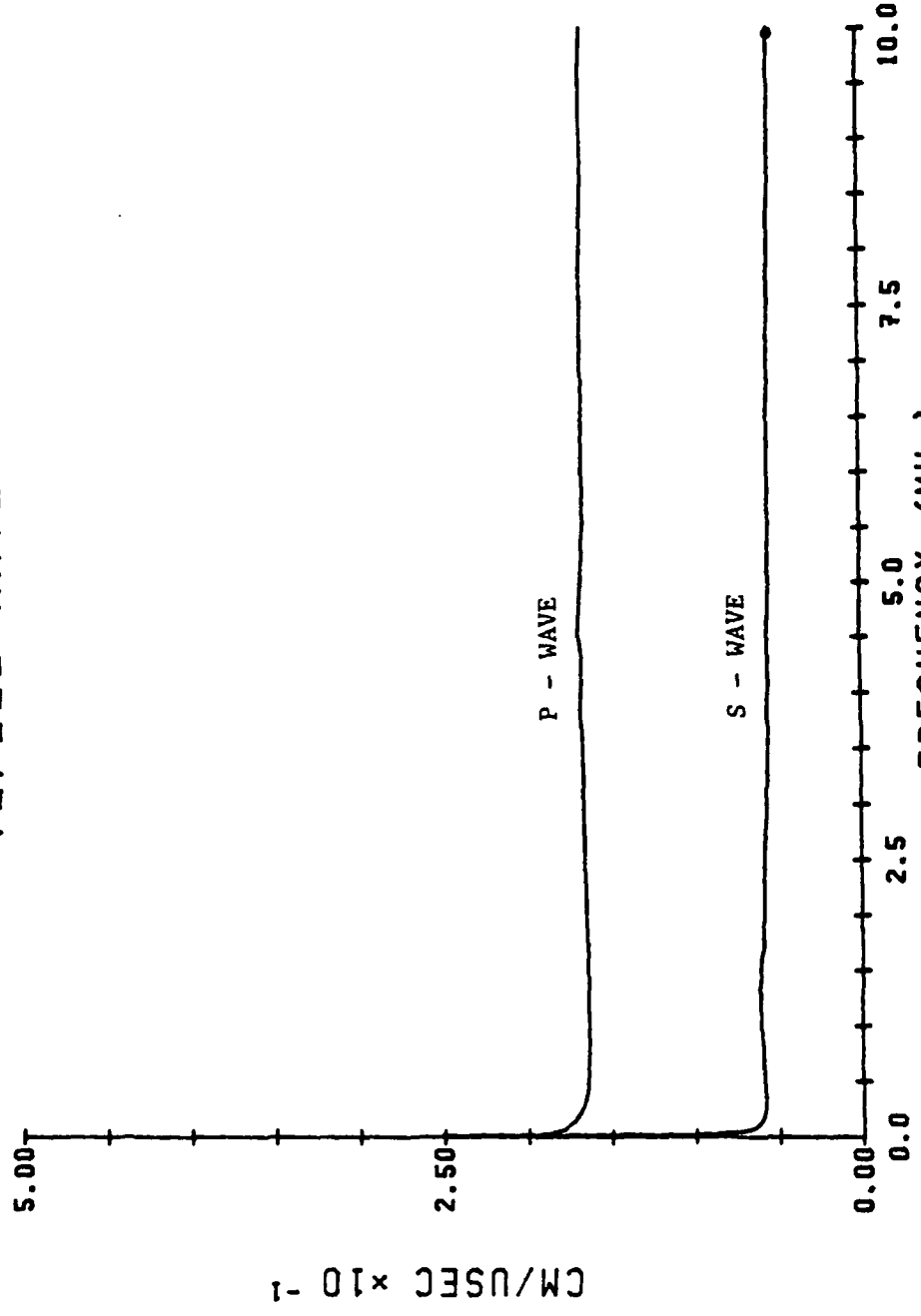

Figure 3. Phase Velocities - Specimen No. 8

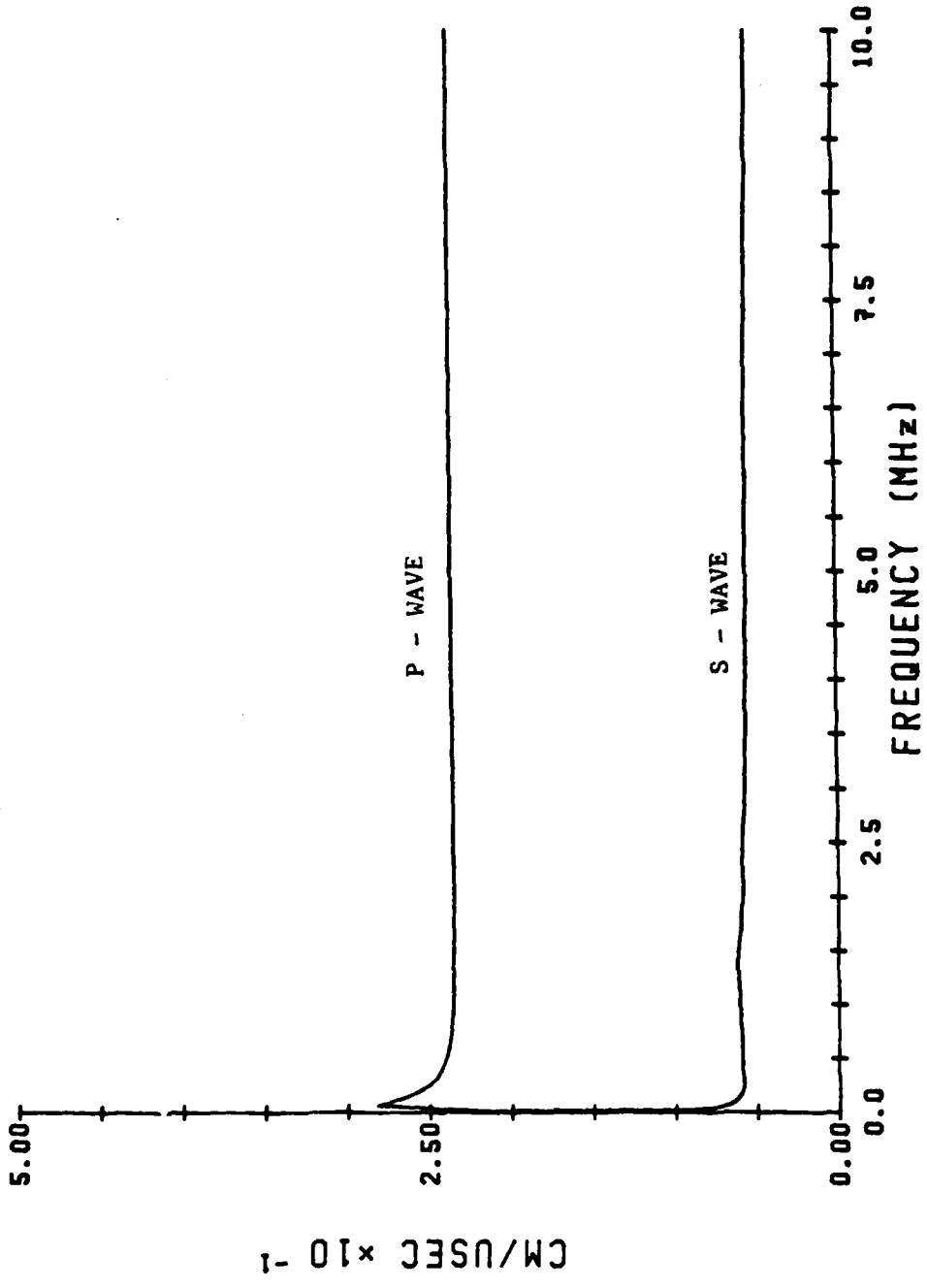

Figure 3. Phase Velocities - Specimen No. 9

Figure 3. Phase Velocities - Specimen No. 10

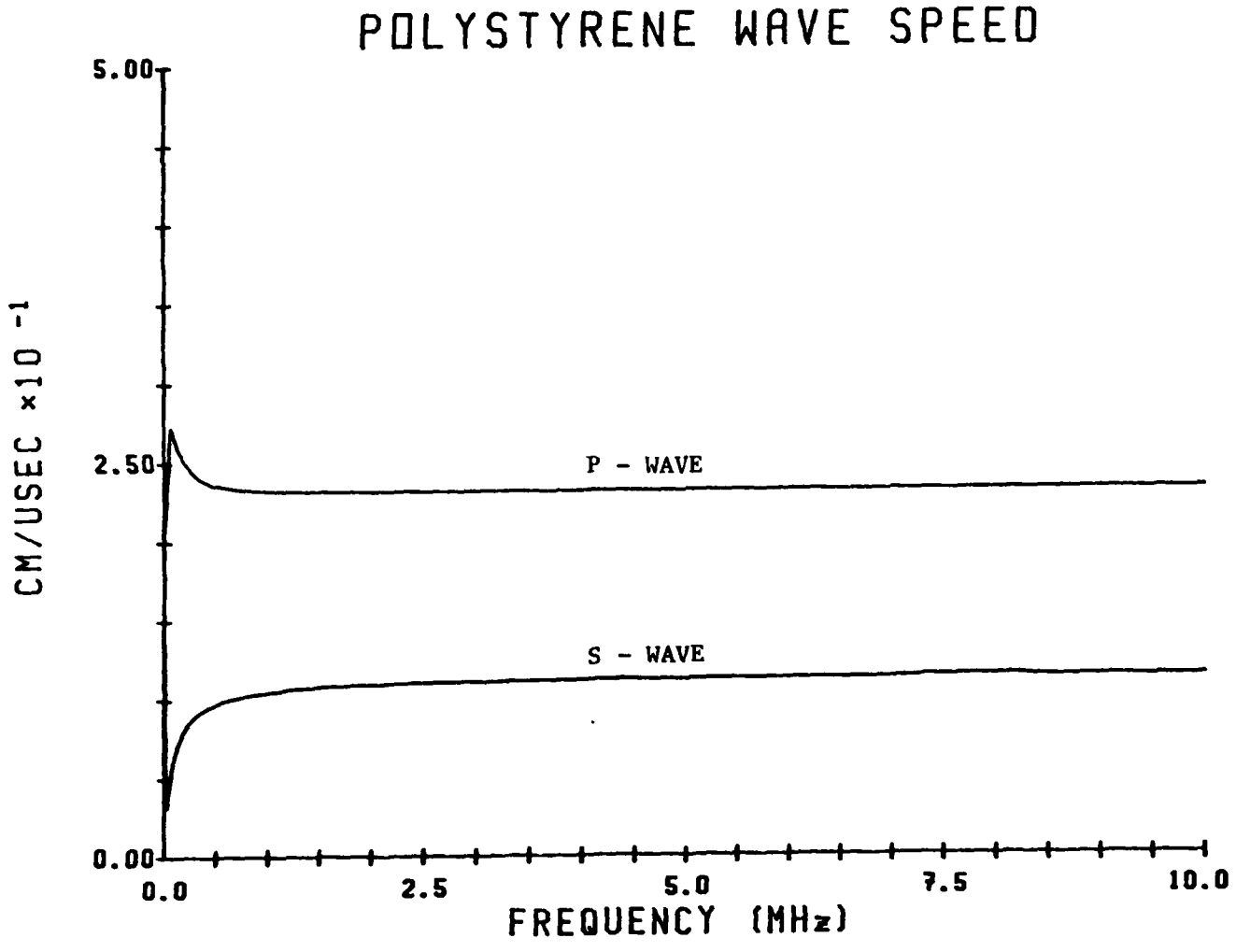

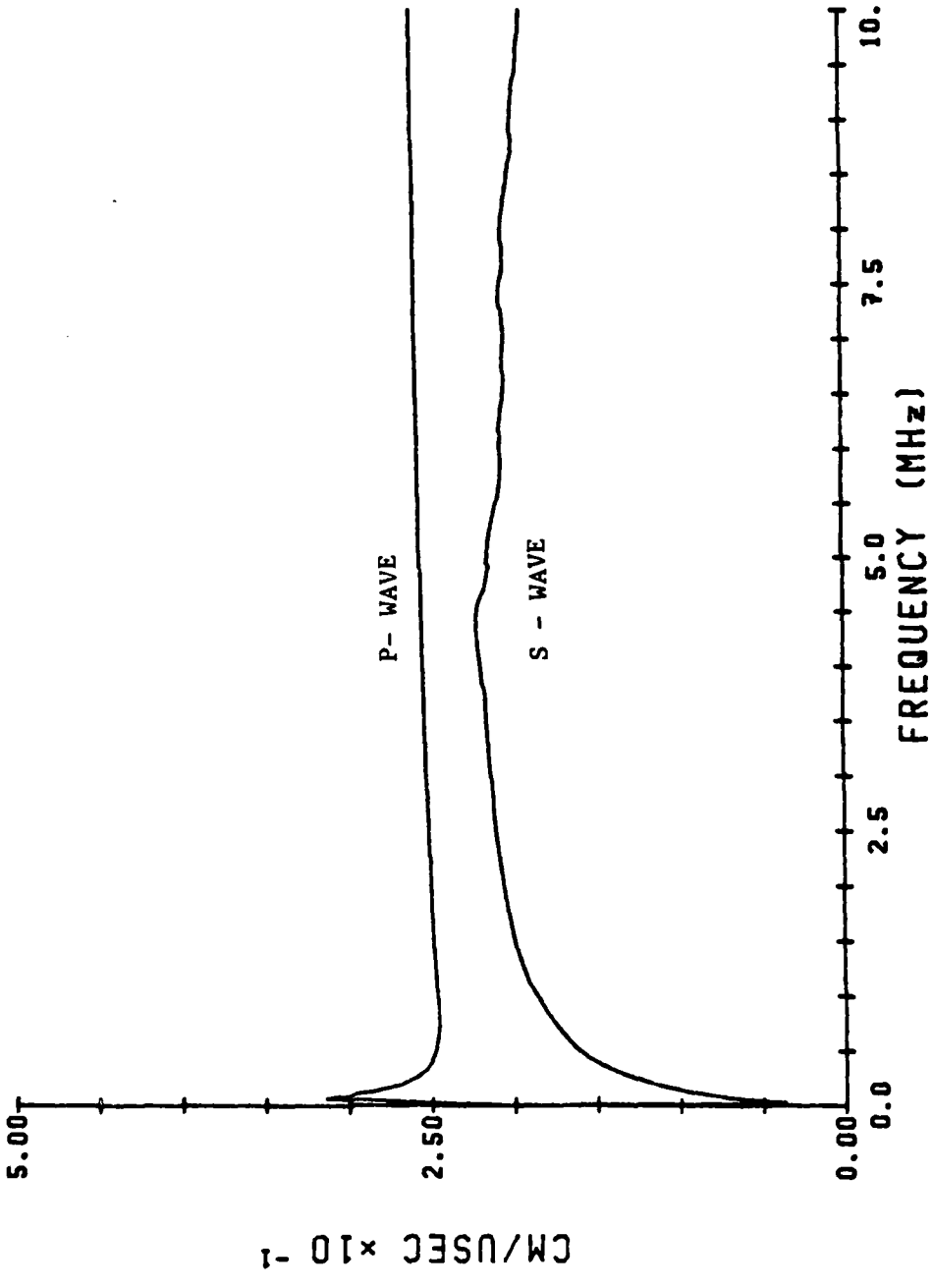

Figure 3. Phase Velocities - Specimen No. 11

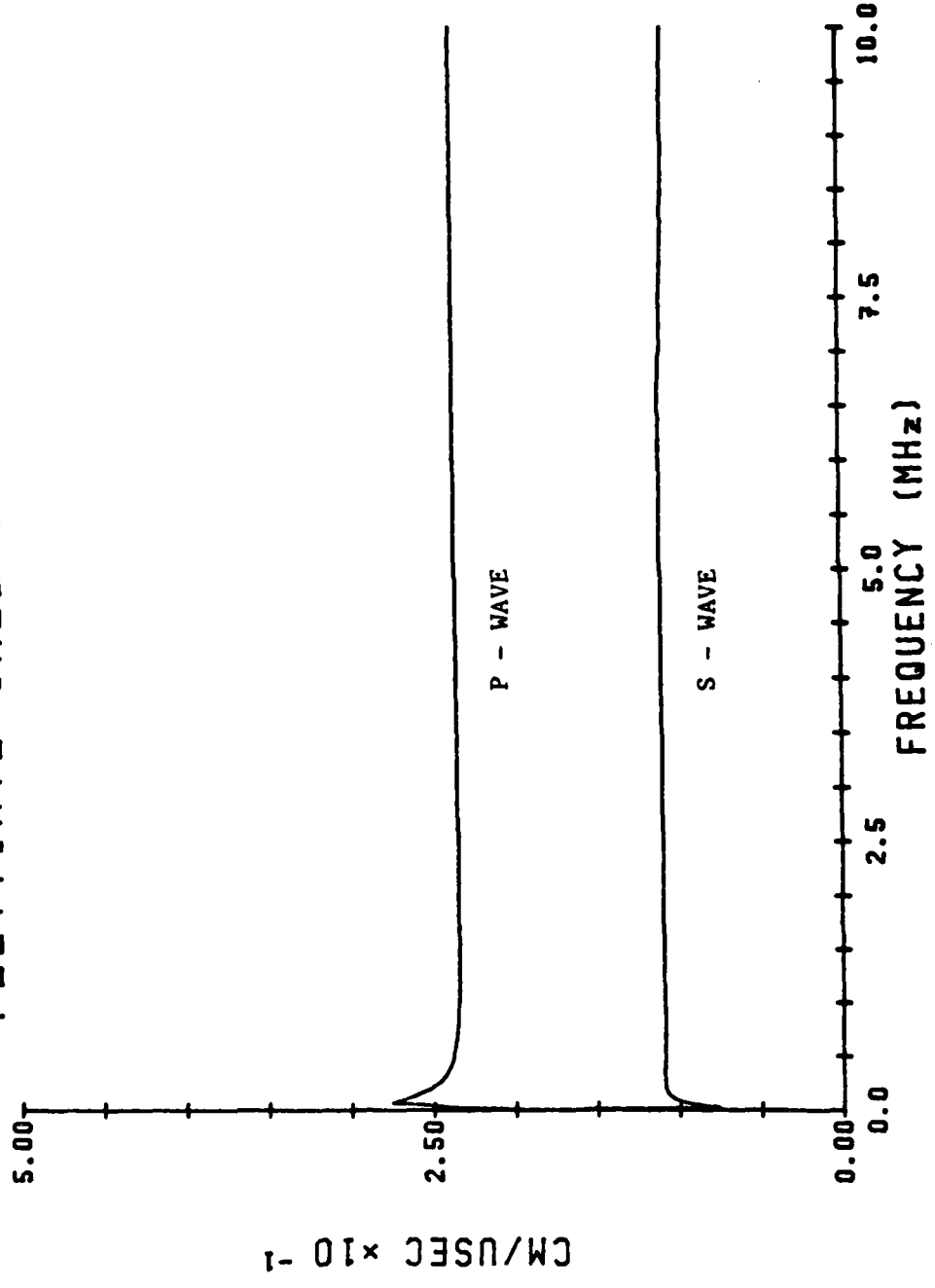

Figure 3. Phase Velocities - Specimen No. 12

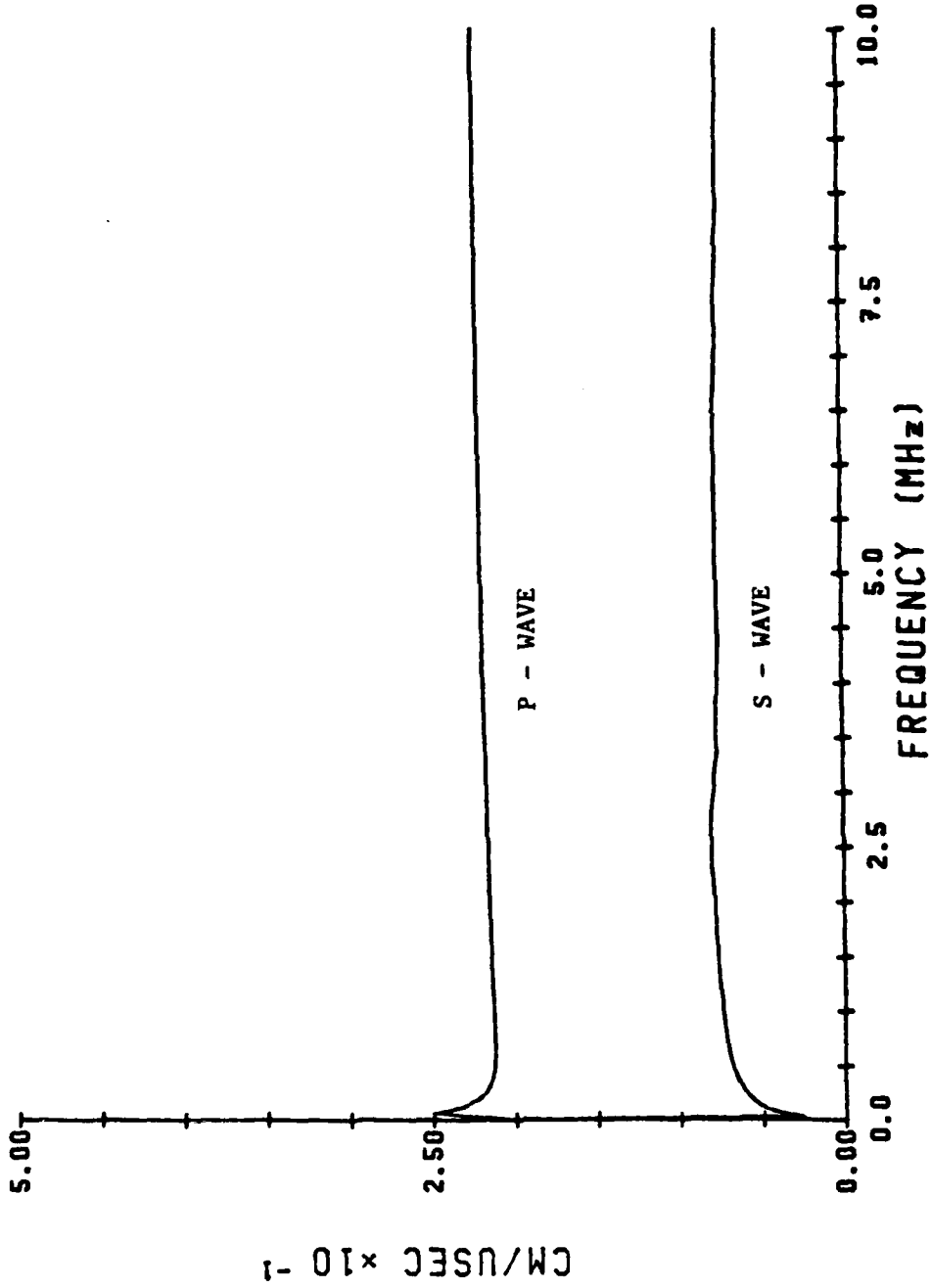

Figure 3. Phase Velocities - Specimen No. 13

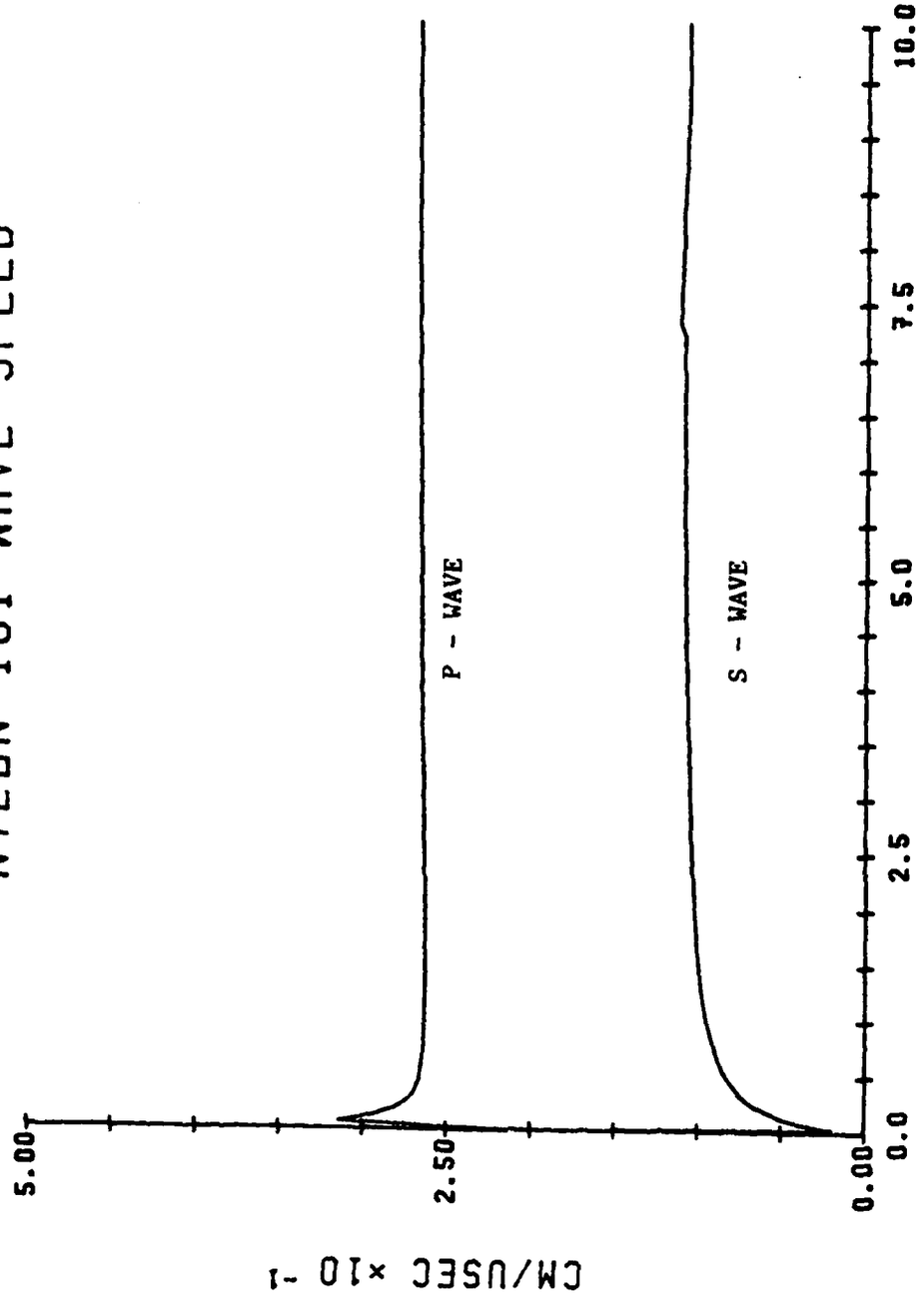

Figure 3. Phase Velocities - Specimen No. 14

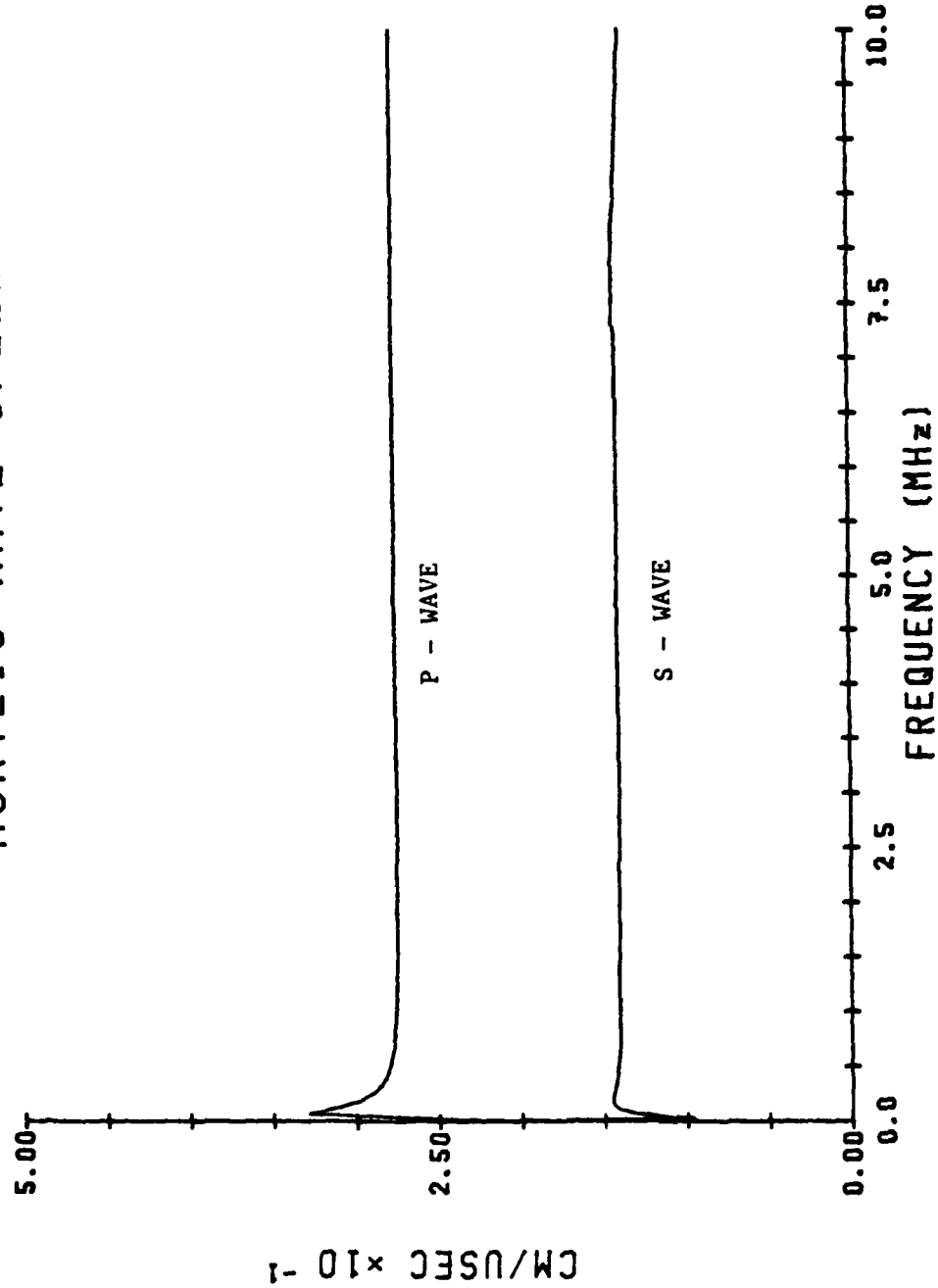

Figure 3. Phase Velocities - Specimen No. 15

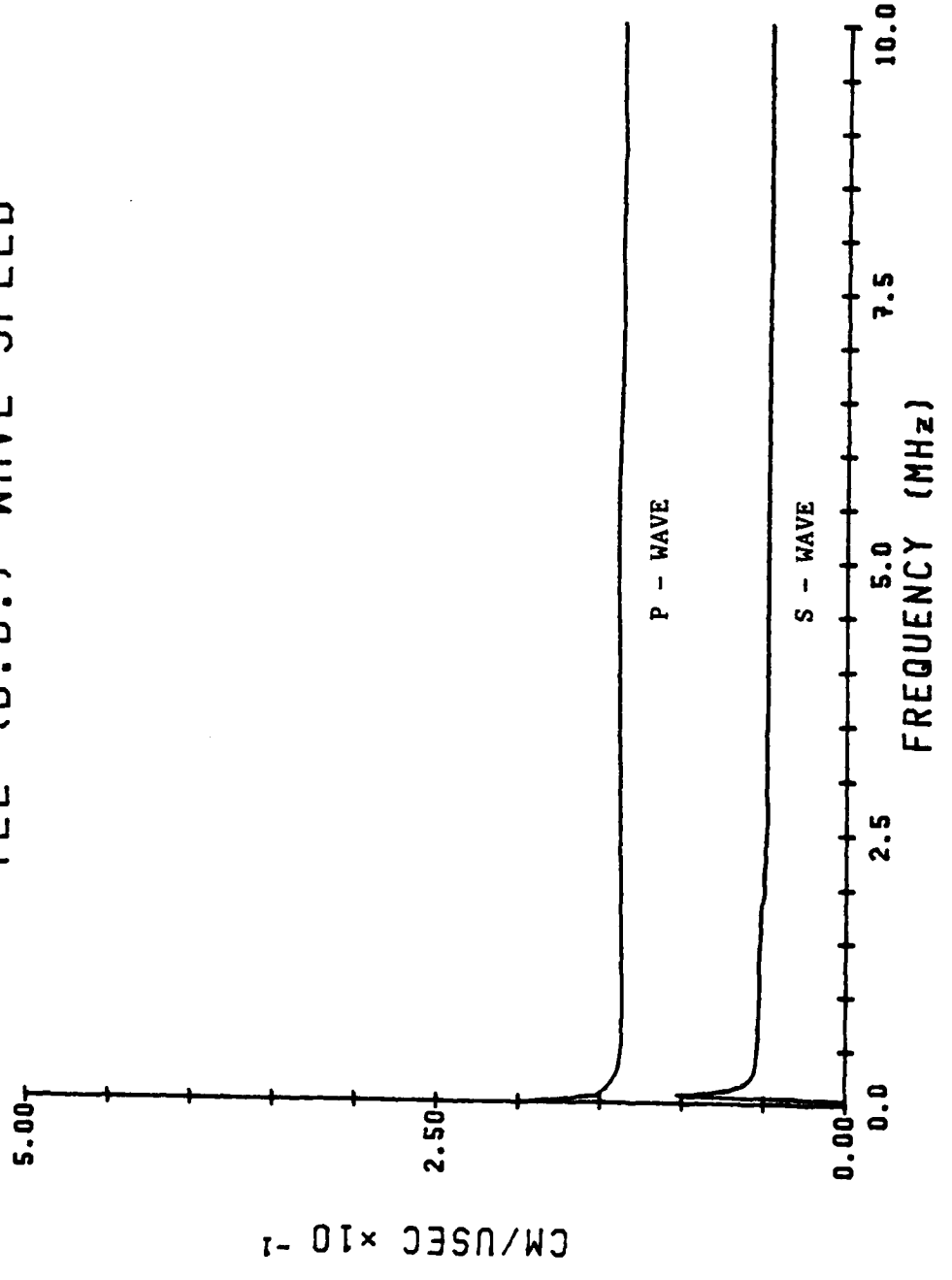

Figure 3. Phase Velocities - Specimen No. 16

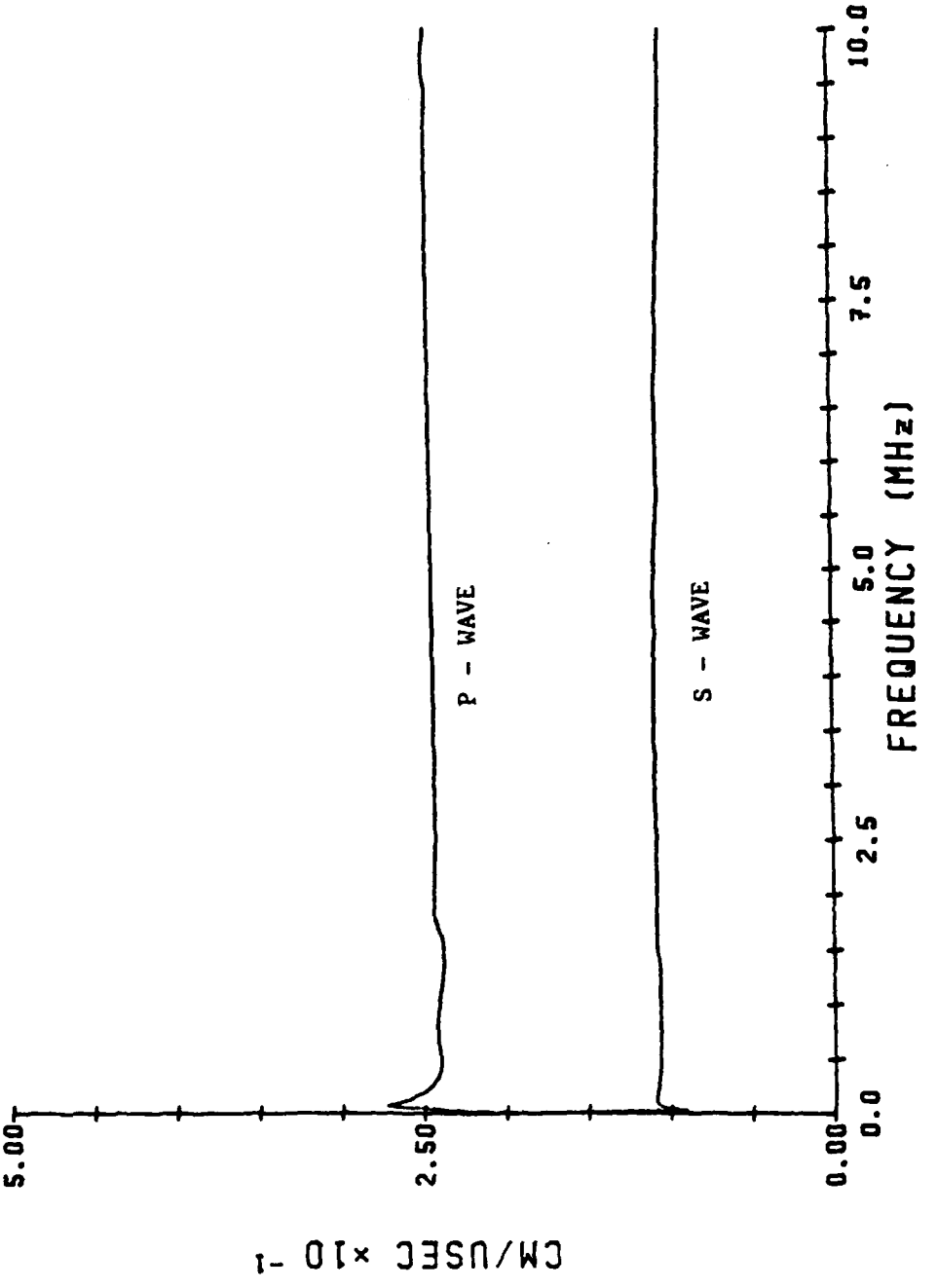

Figure 3. Phase Velocities - Specimen No. 17

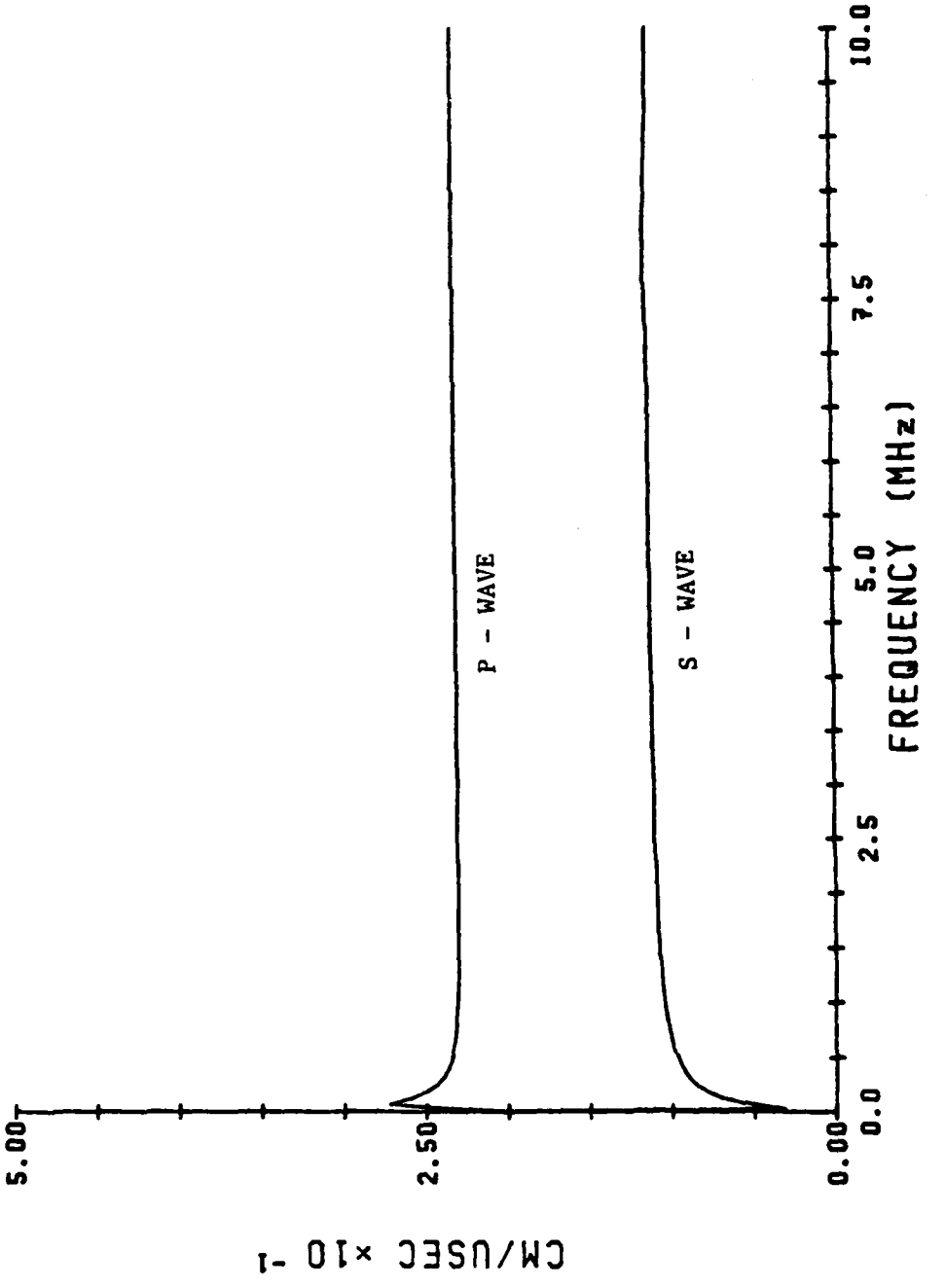

Figure 3. Phase Velocities - Specimen No. 18

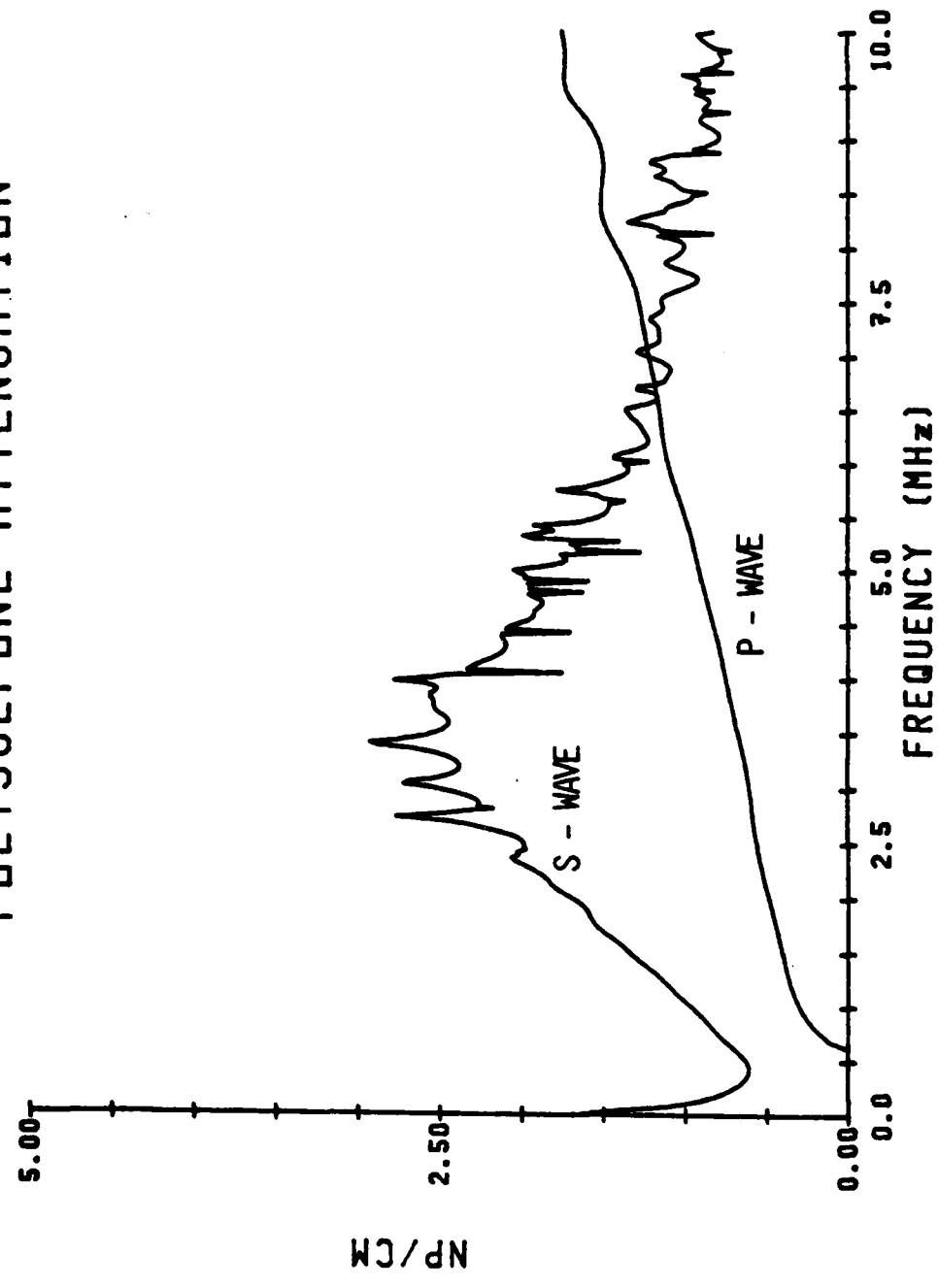

Figure 4. Attenuation Coefficients - Specimen No. 1

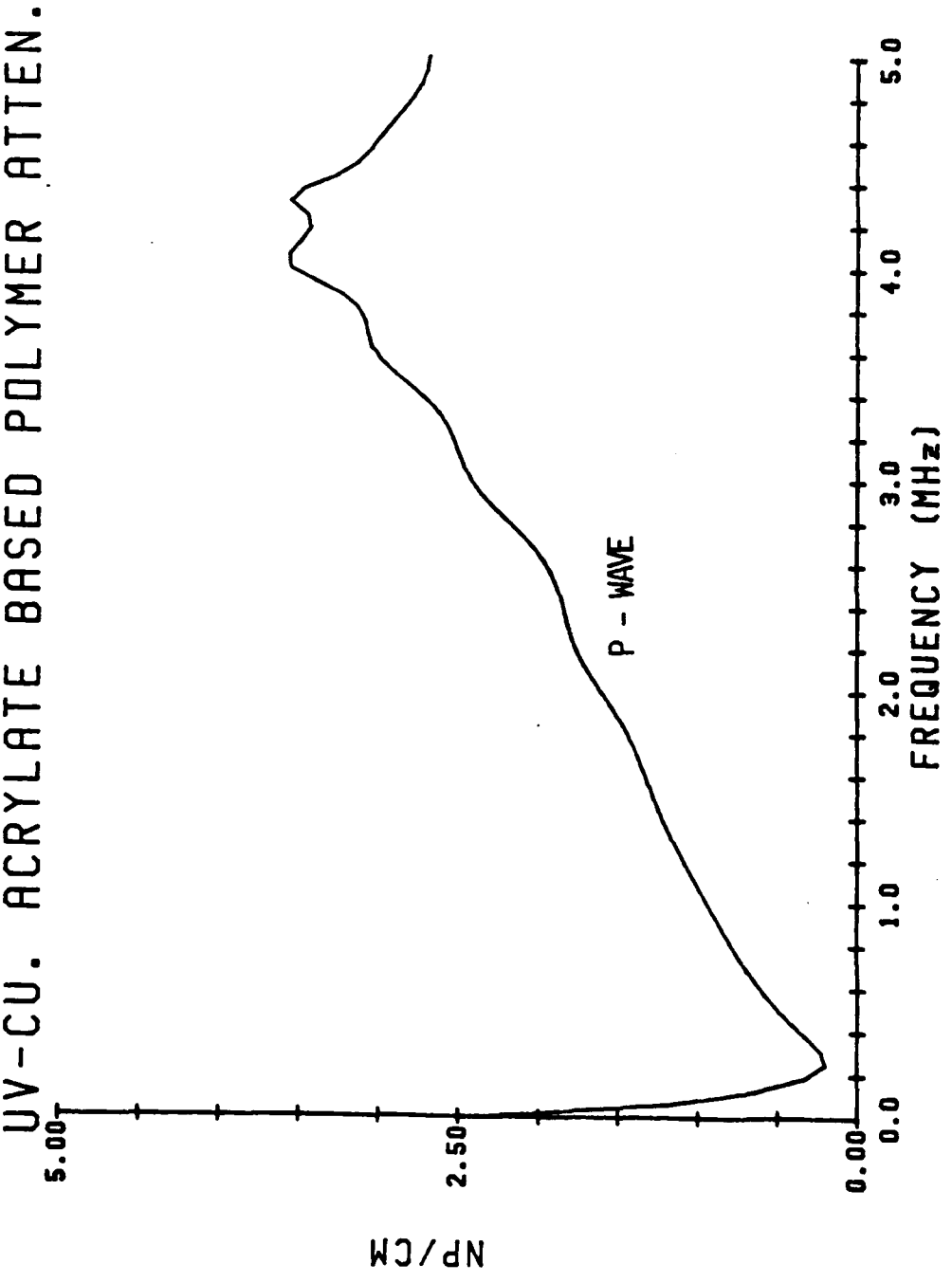

Figure 4. Attenuation Coefficients - Specimen No. 2

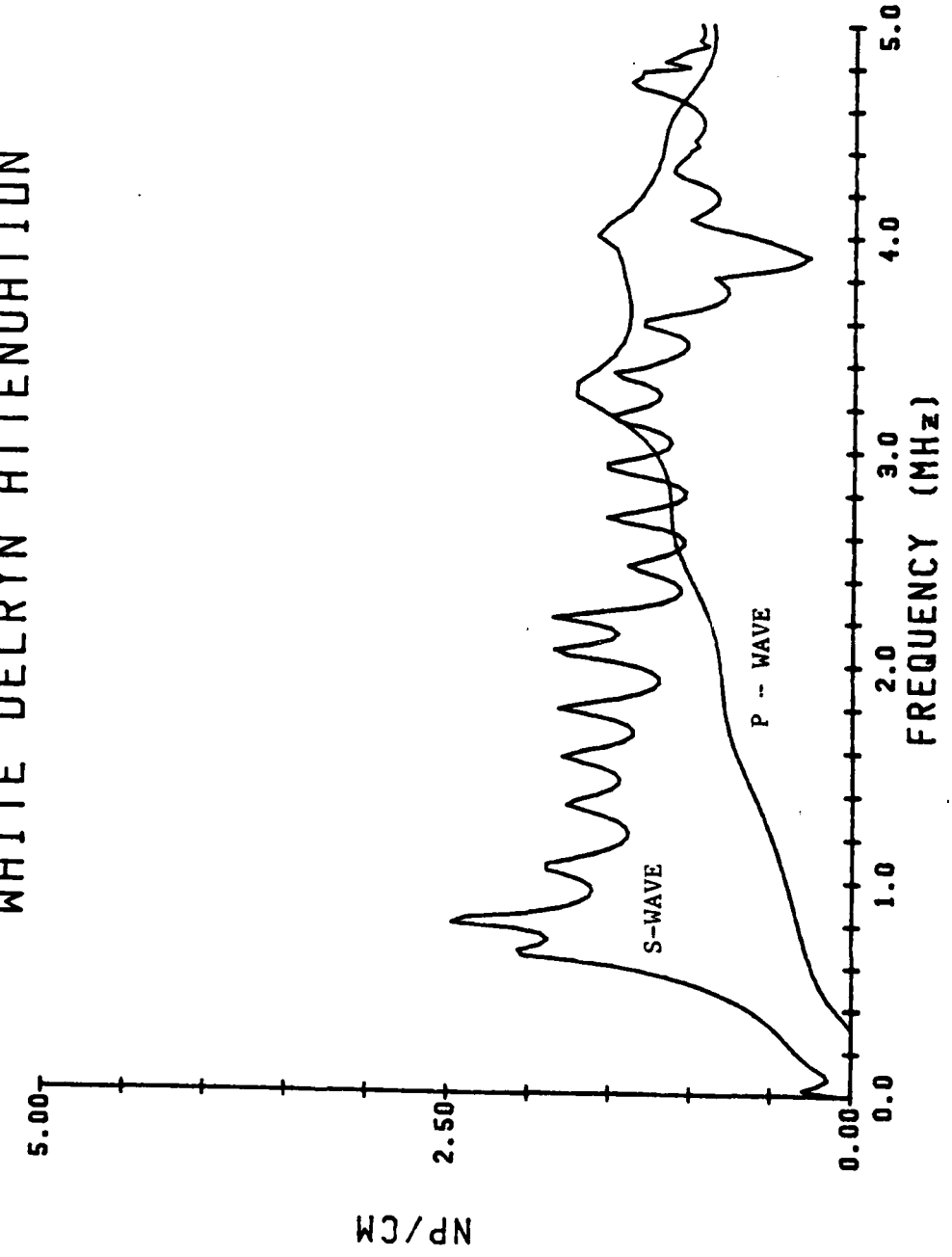

Figure 4. Attenuation Coefficients - Specimen No. 3

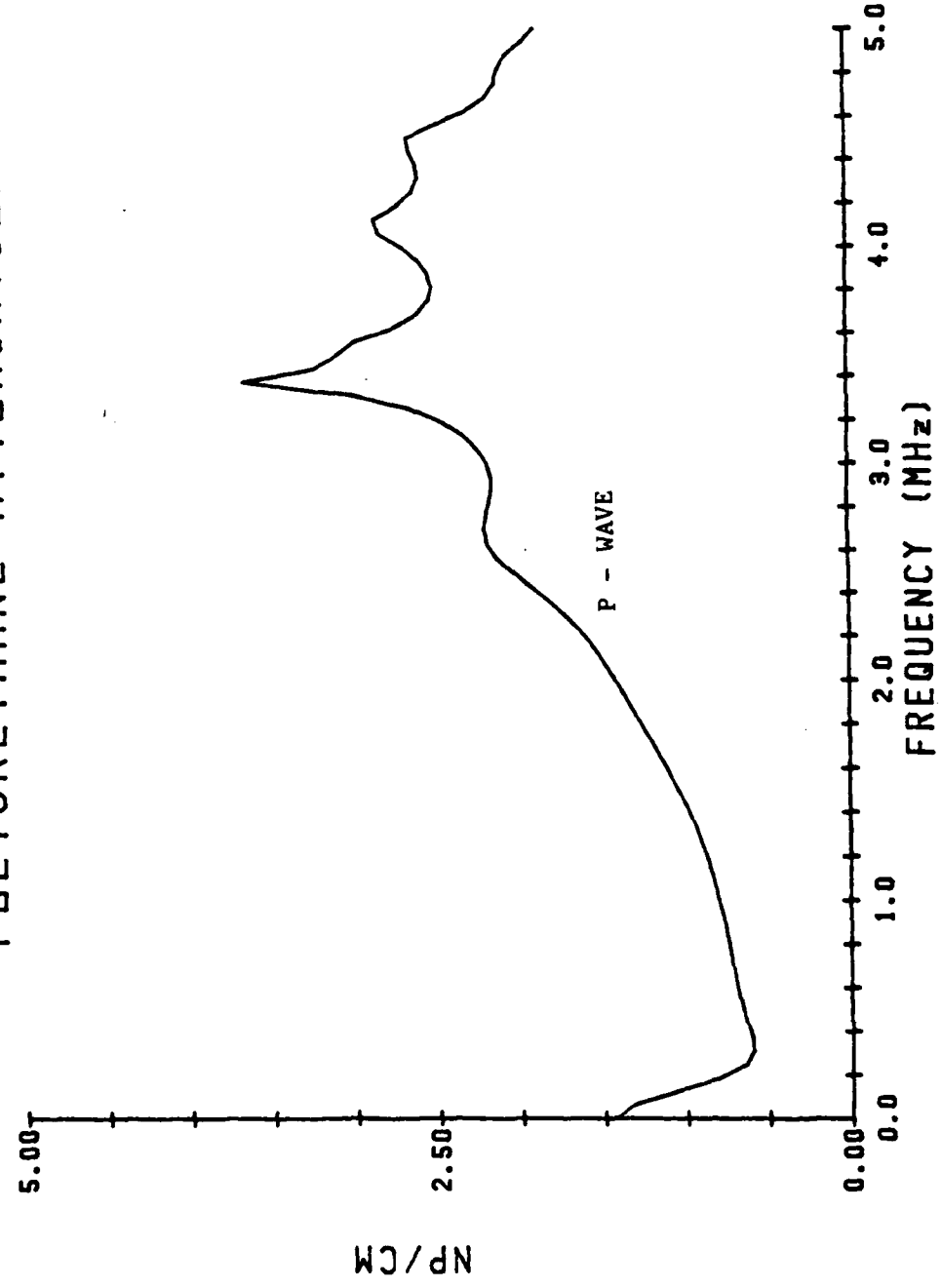

Figure 4. Attenuation Coefficients - Specimen No. 4

Figure 4. Attenuation Coefficients - Specimen No. 5

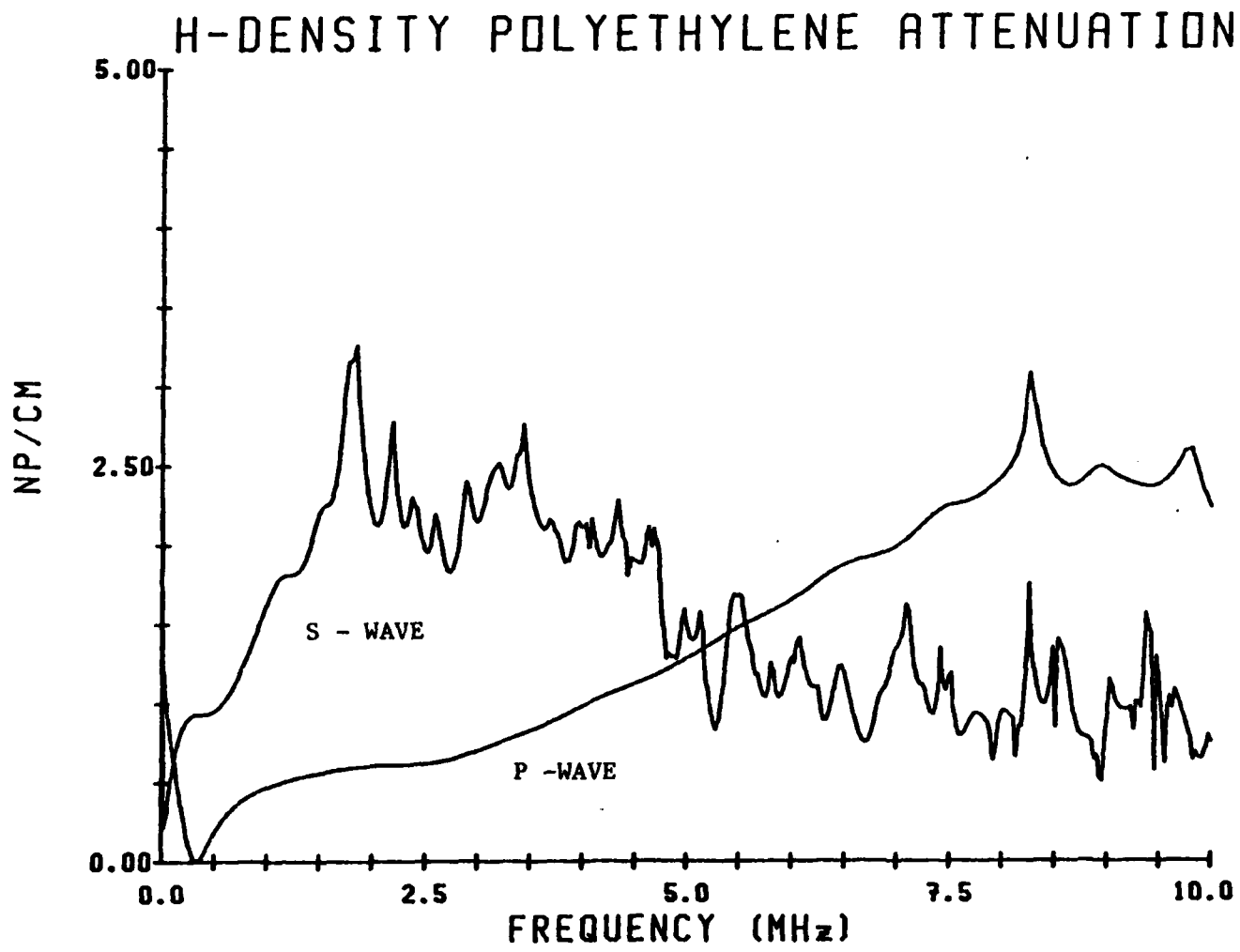

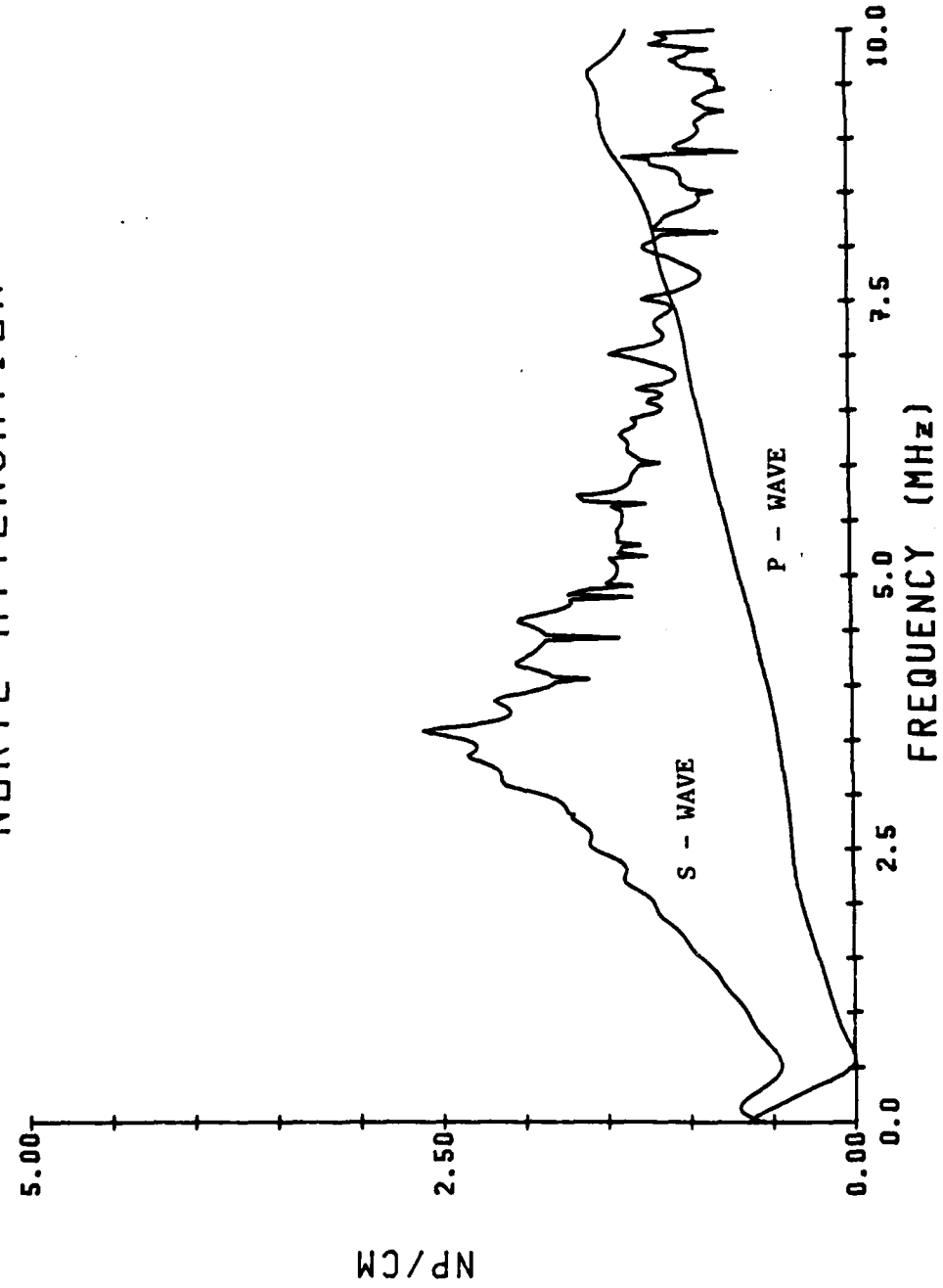

Figure 4. Attenuation Coefficients - Specimen No. 6

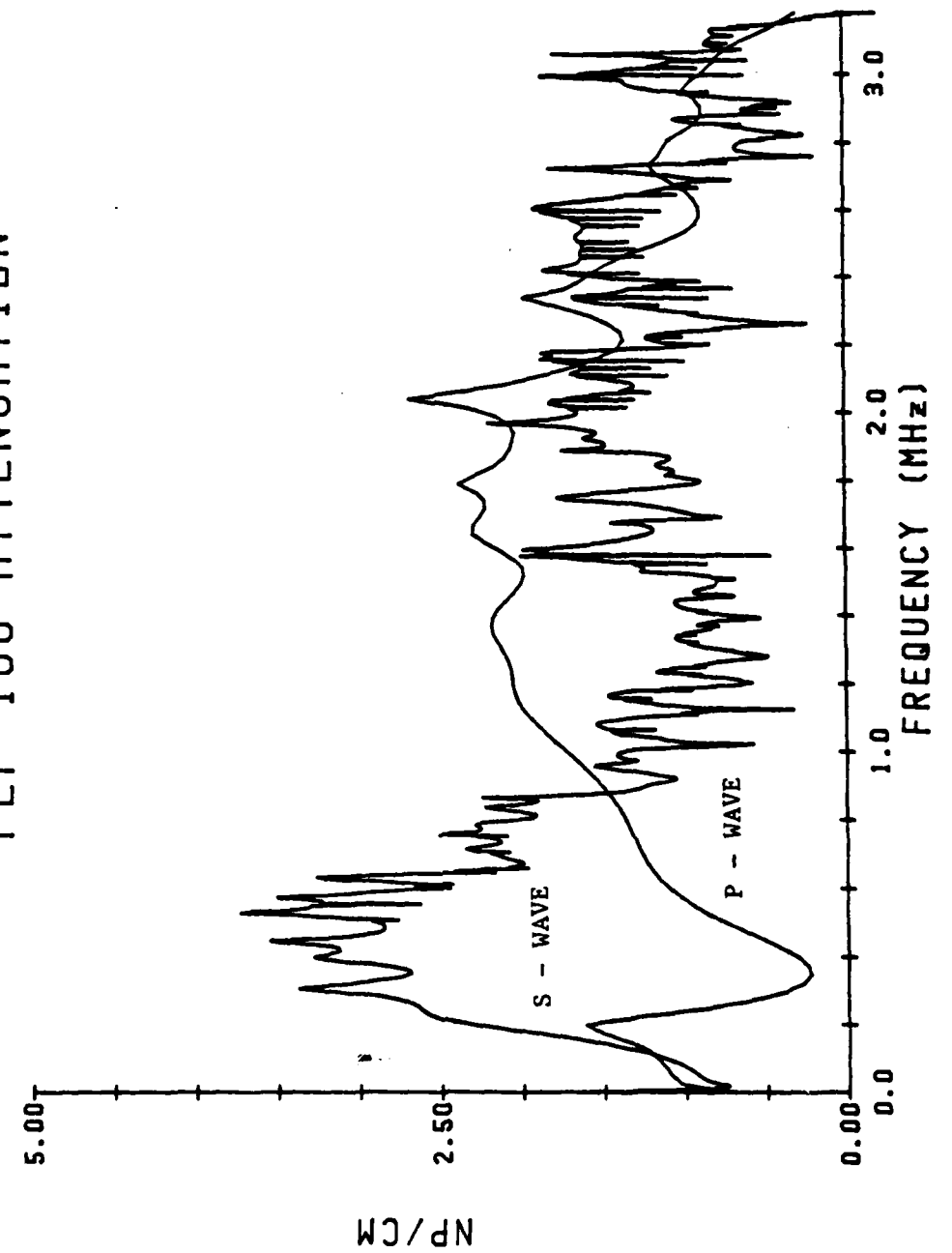

Figure 4. Attenuation Coefficients - Specimen No. 7

Figure 4. Attenuation Coefficients - Specimen No. 8

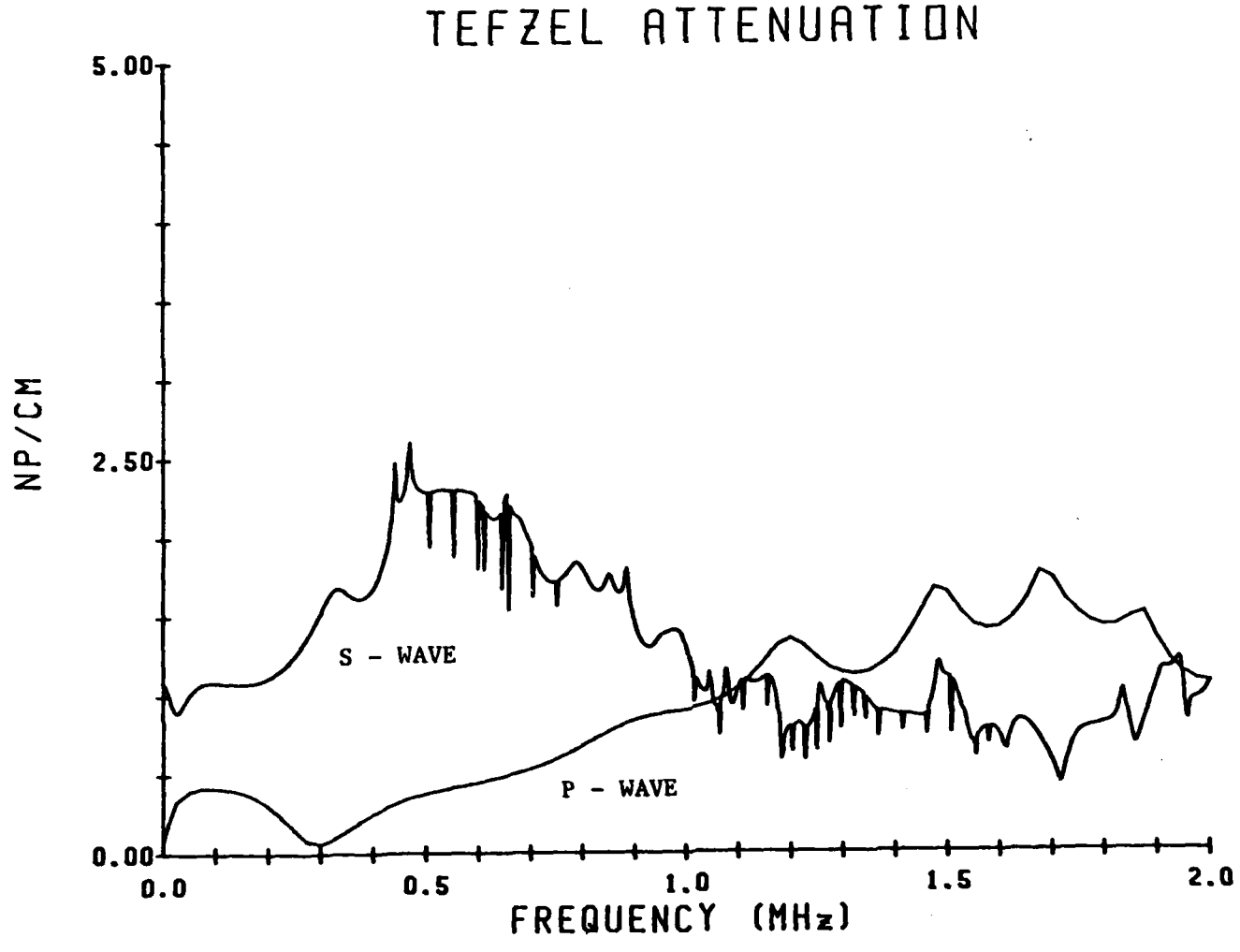

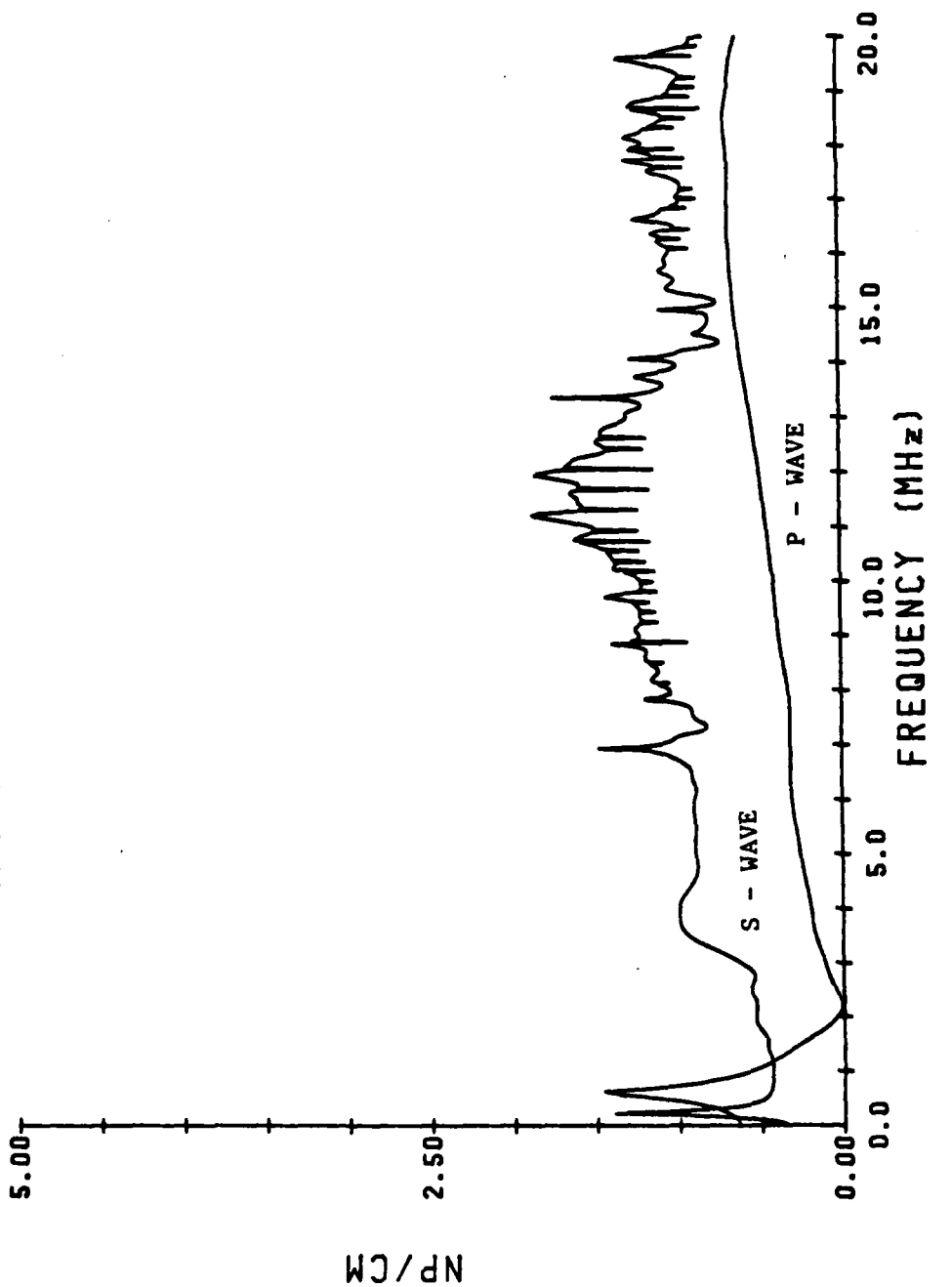

Figure 4. Attenuation Coefficients - Specimen No. 9

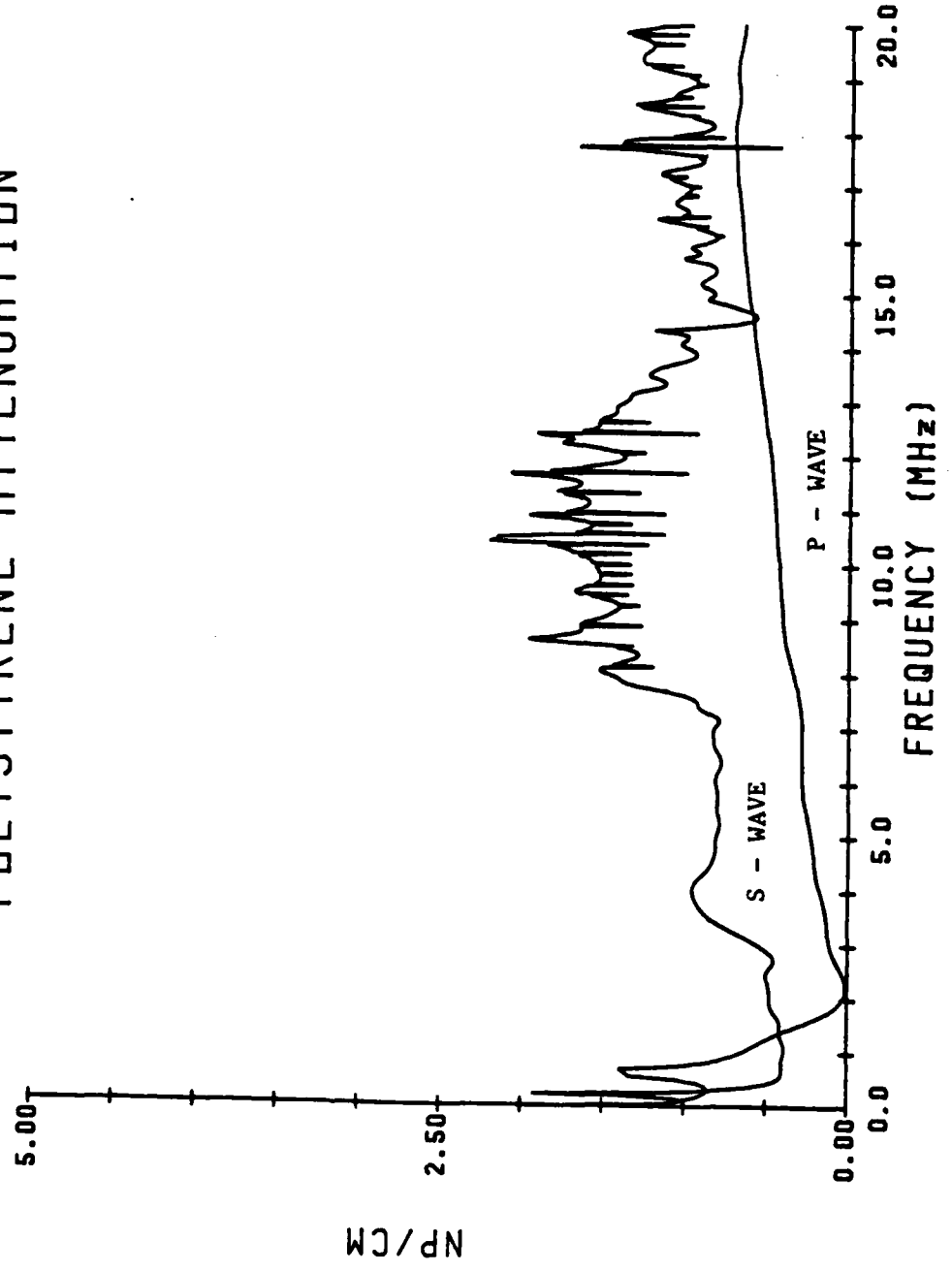

Figure 4. Attenuation Coefficients - Specimen No. 10

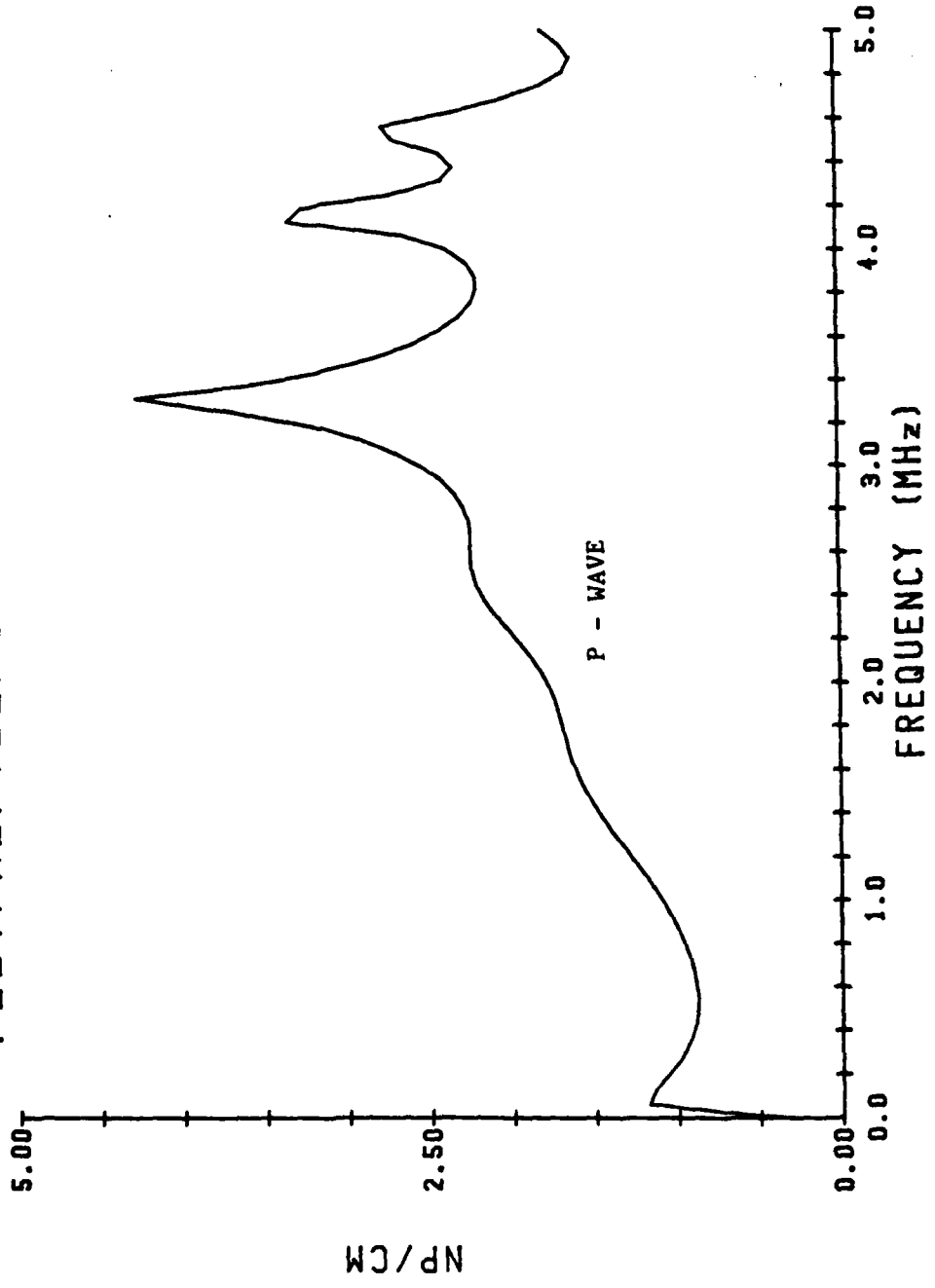

Figure 4. Attenuation Coefficients - Specimen No. 11

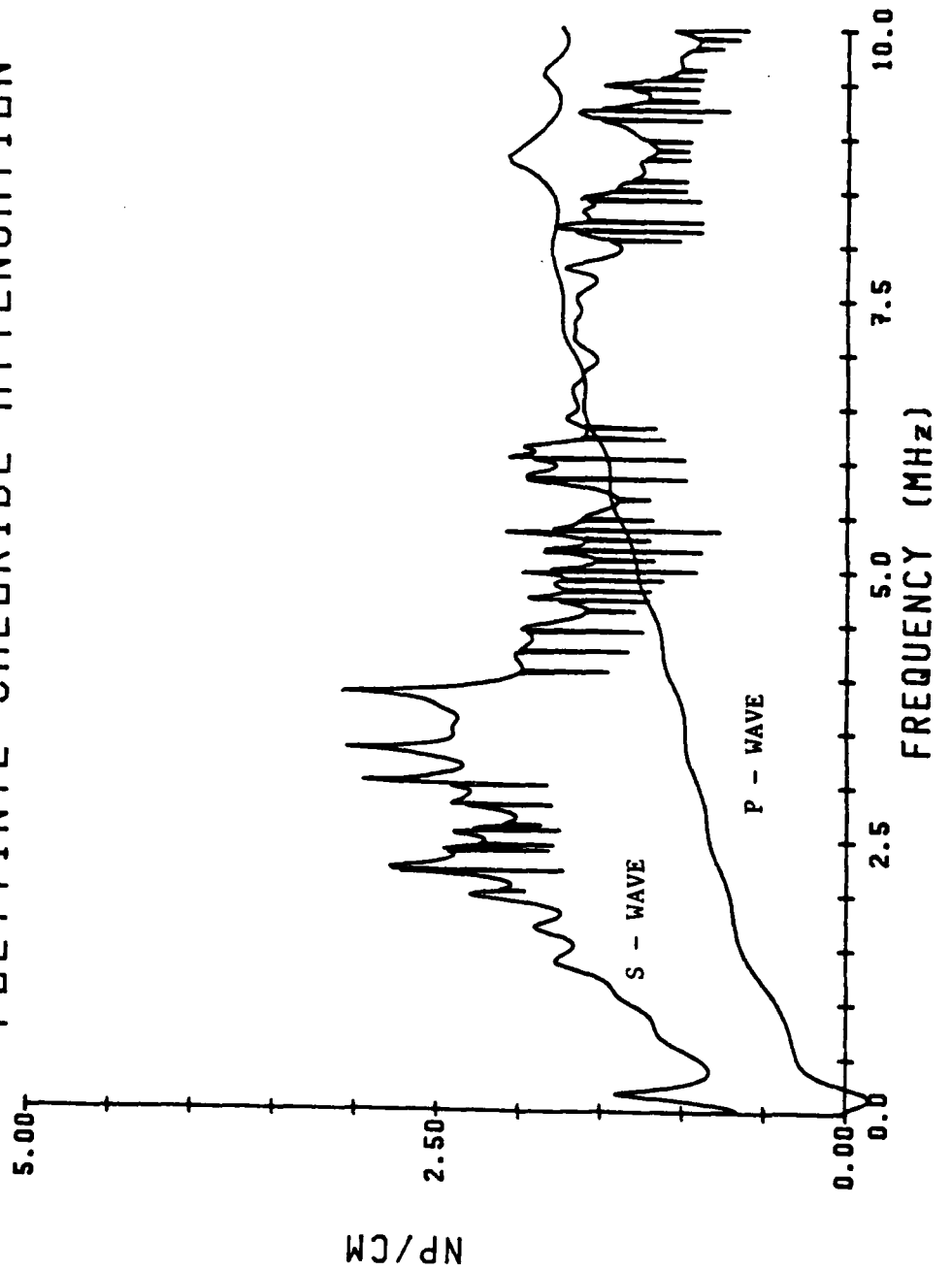

Figure 4. Attenuation Coefficients - Specimen No. 12

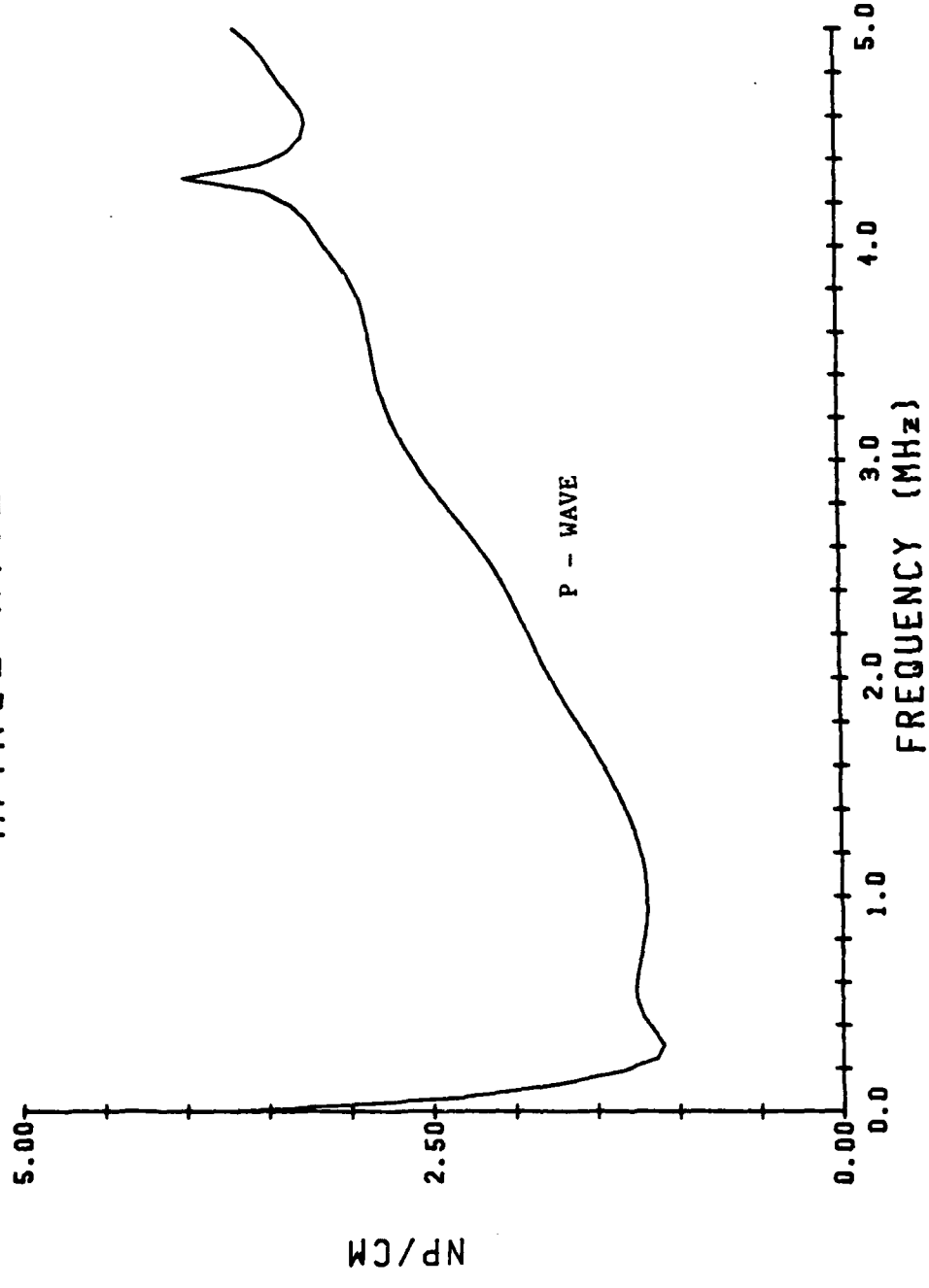

Figure 4. Attenuation Coefficients - Specimen No. 13

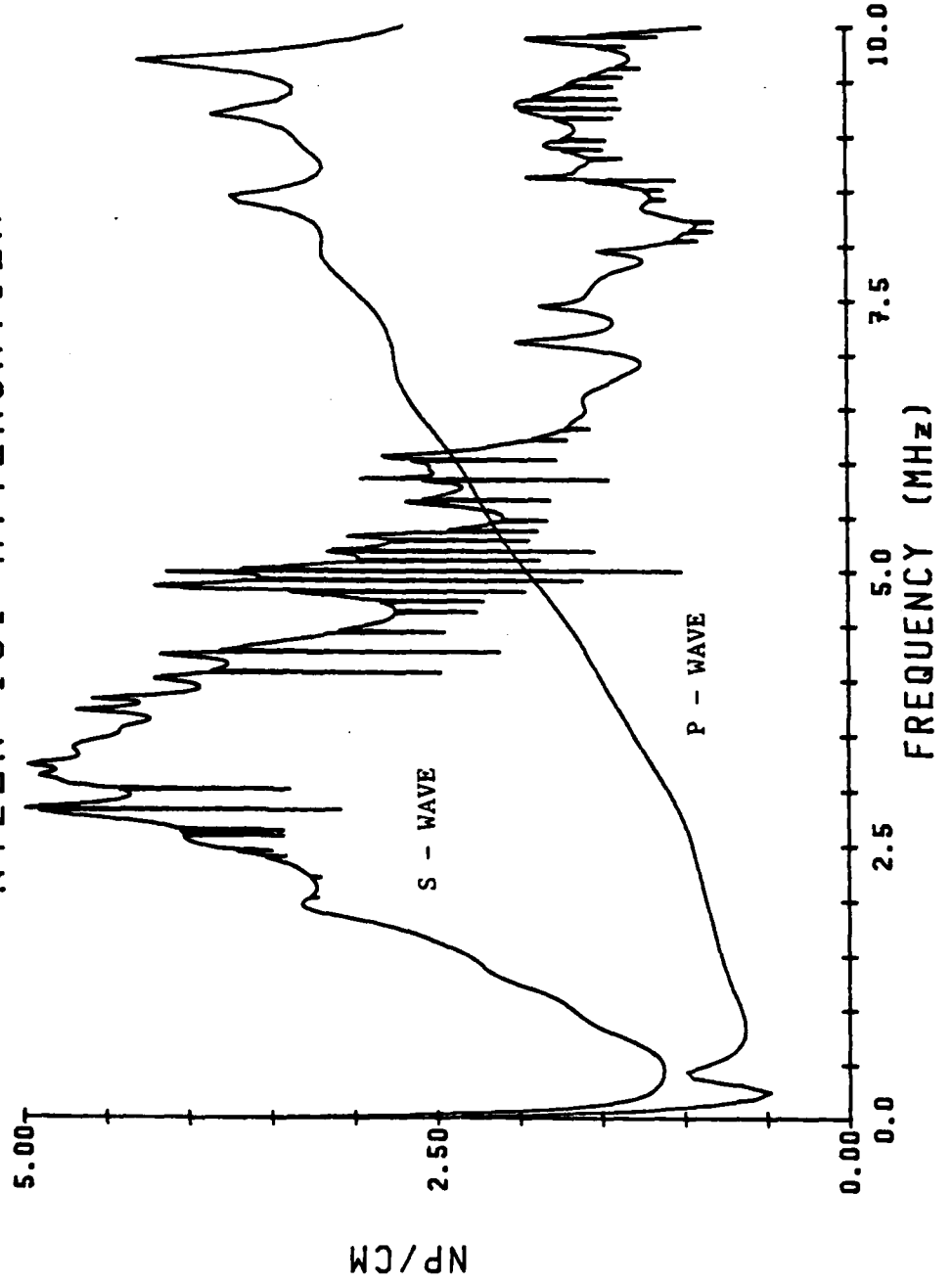

Figure 4. Attenuation Coefficients - Specimen No. 14

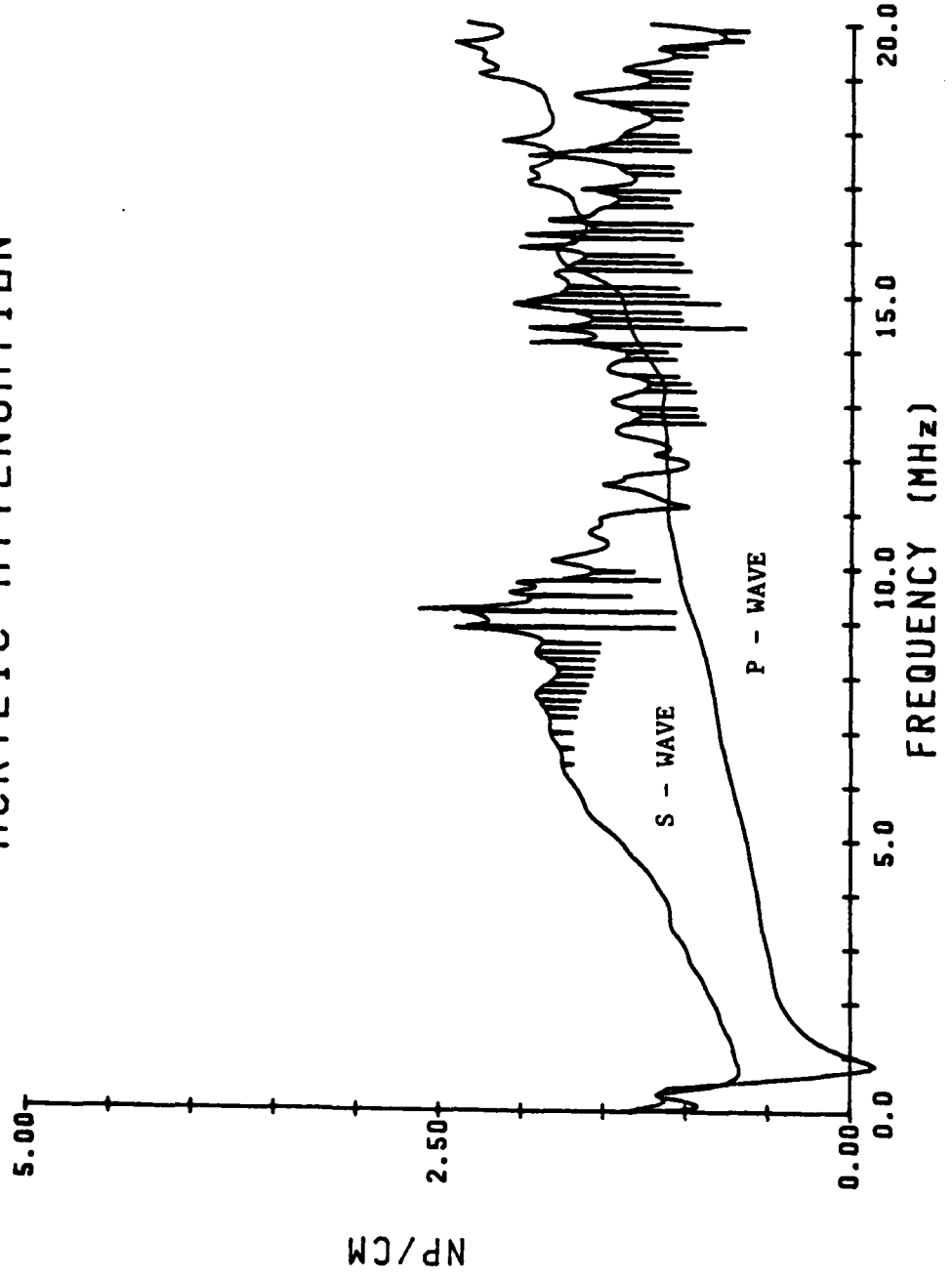

Figure 4. Attenuation Coefficients - Specimen No. 15

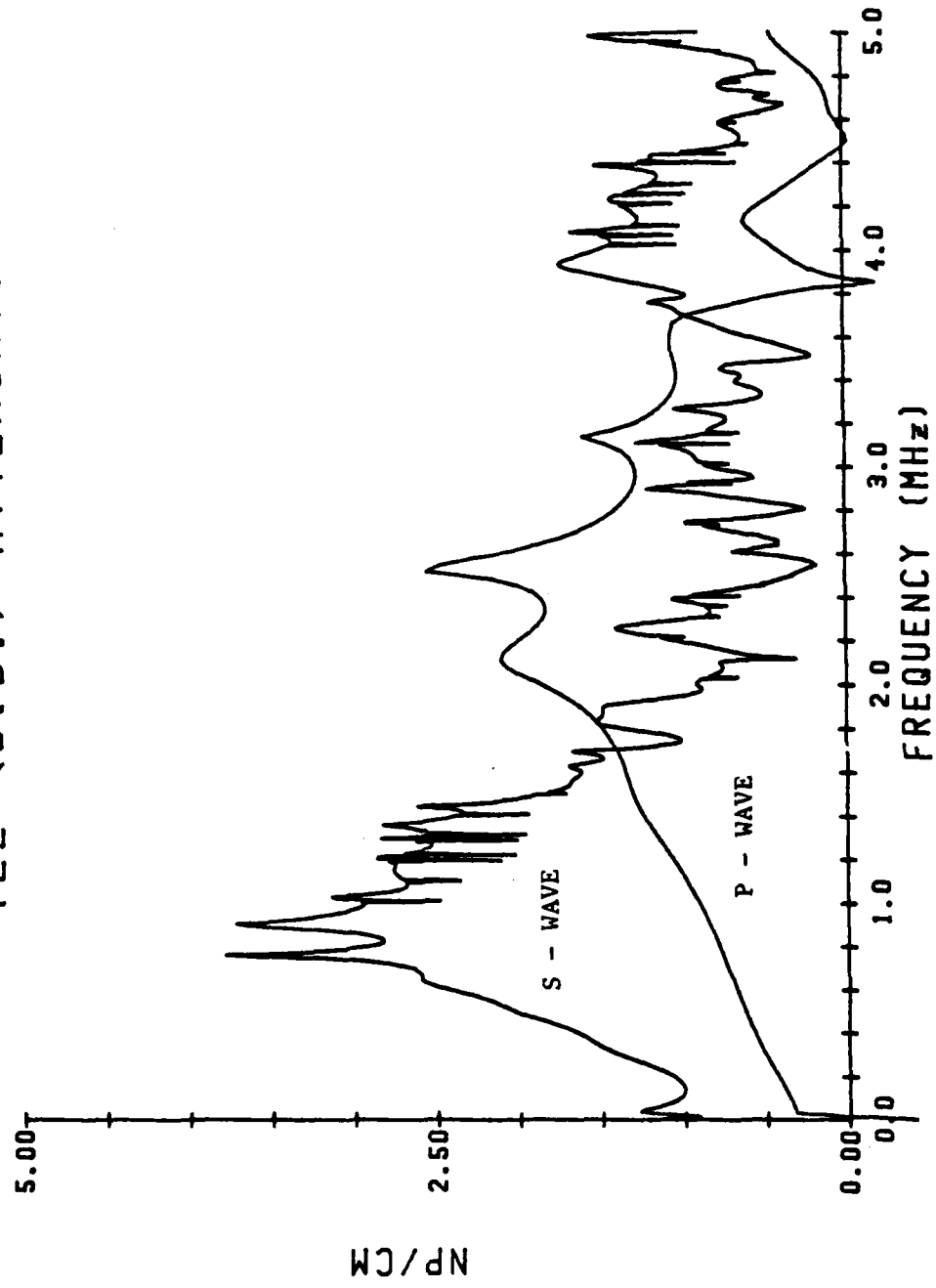

Figure 4. Attenuation Coefficients - Specimen No. 16

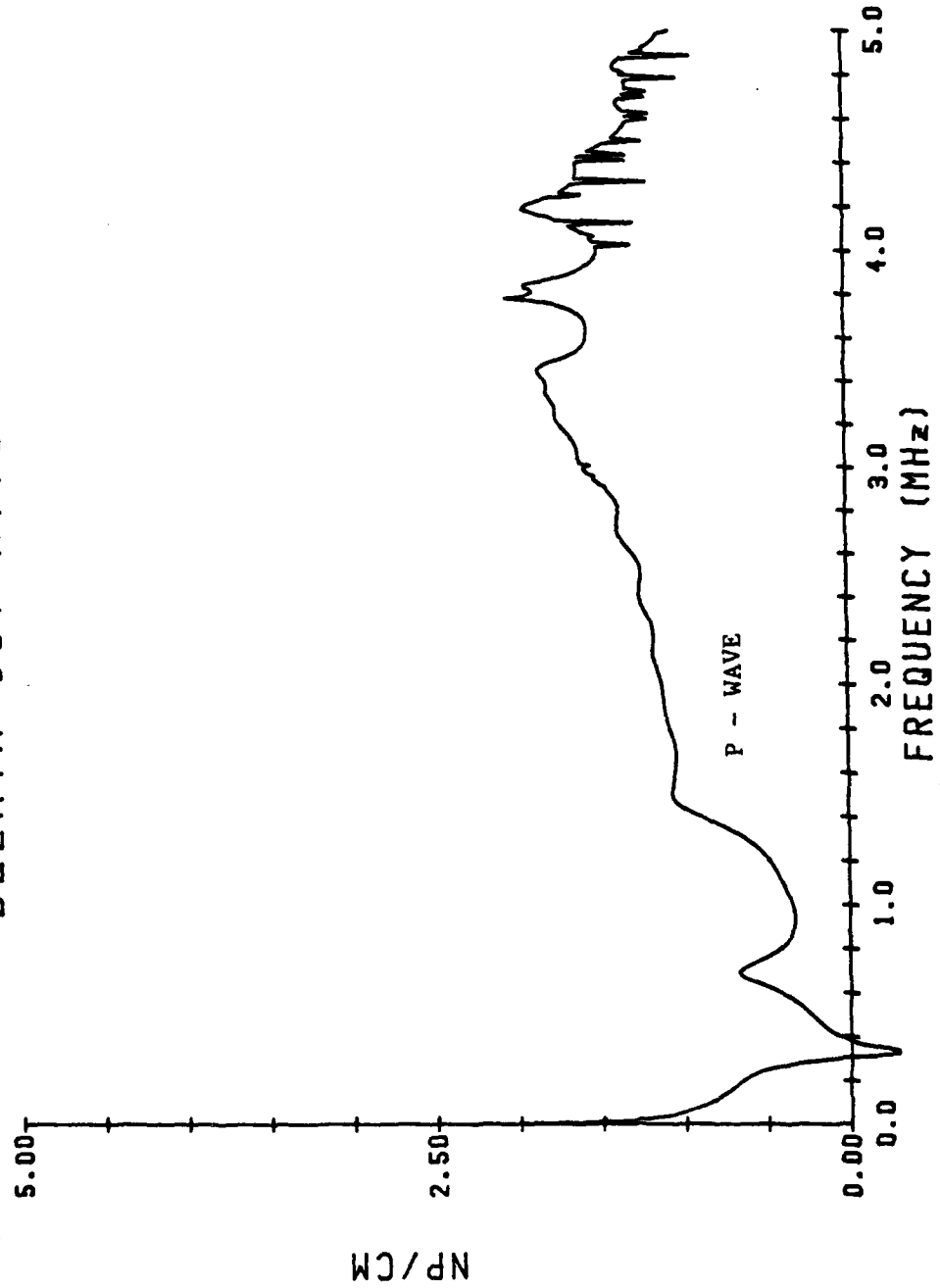

Figure 4. Attenuation Coefficients - Specimen No. 17

Figure 4. Attenuation Coefficients - Specimen No. 18

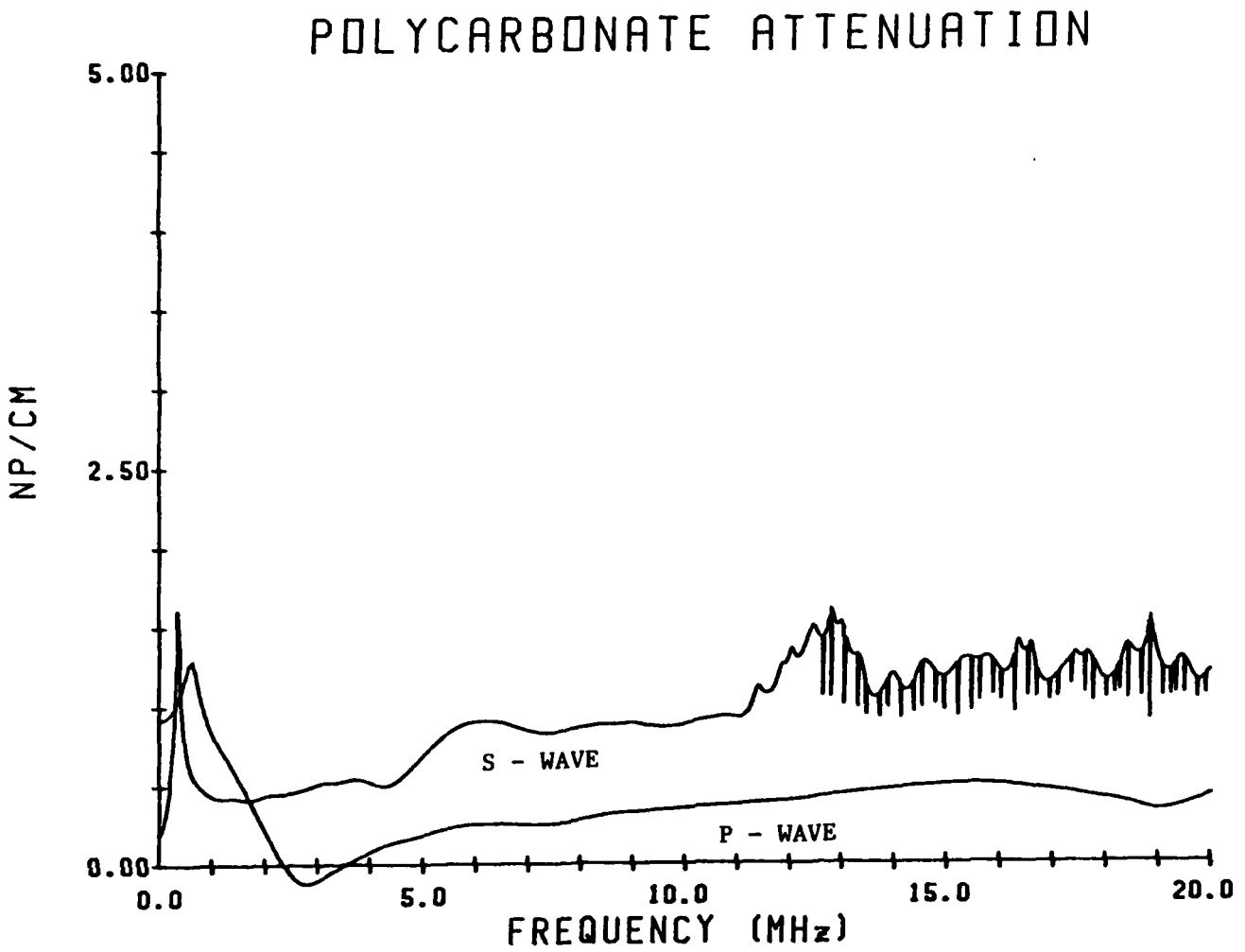

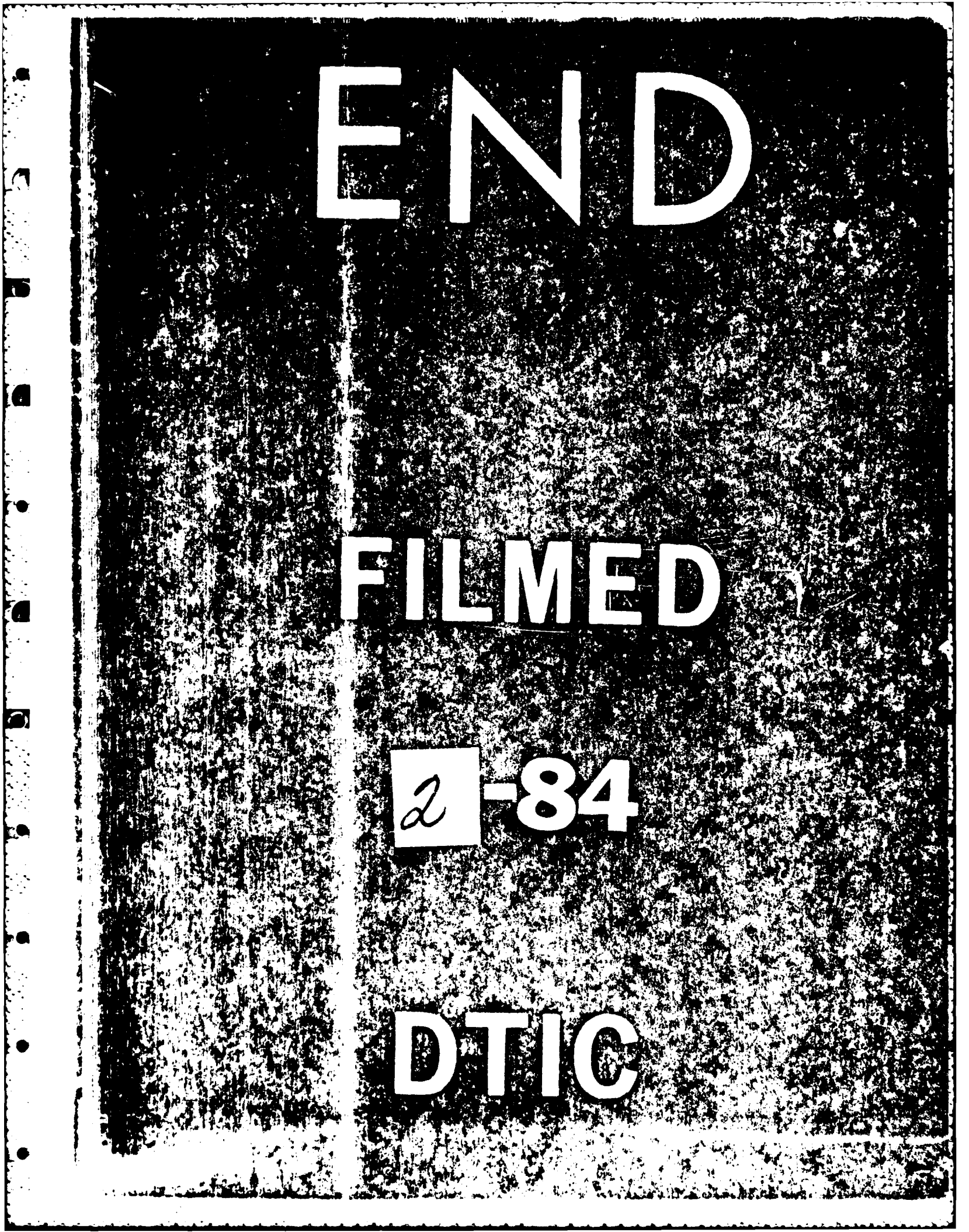
END
FILMED
2-84
DTIC